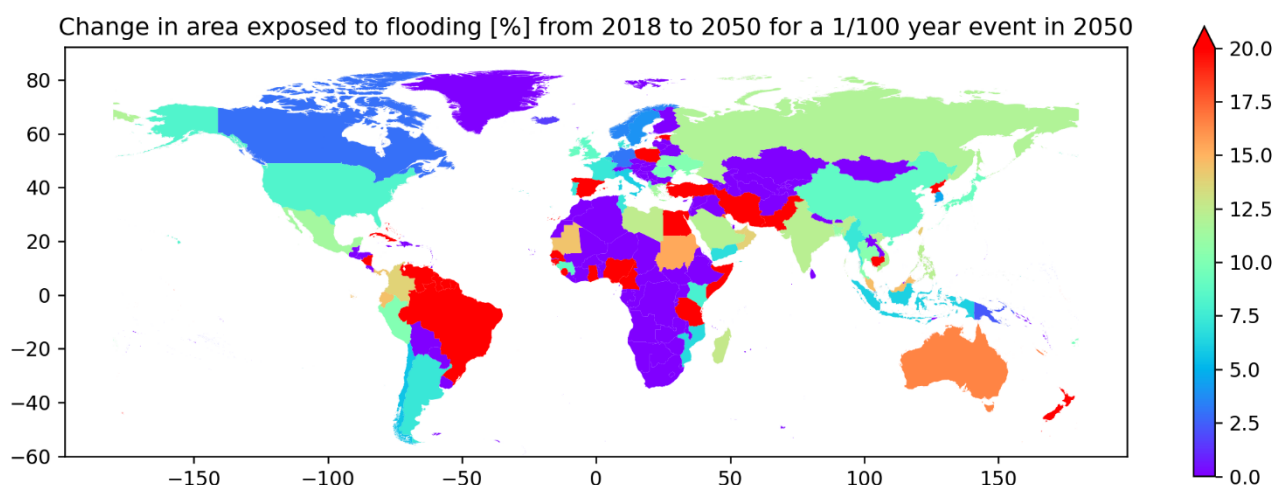
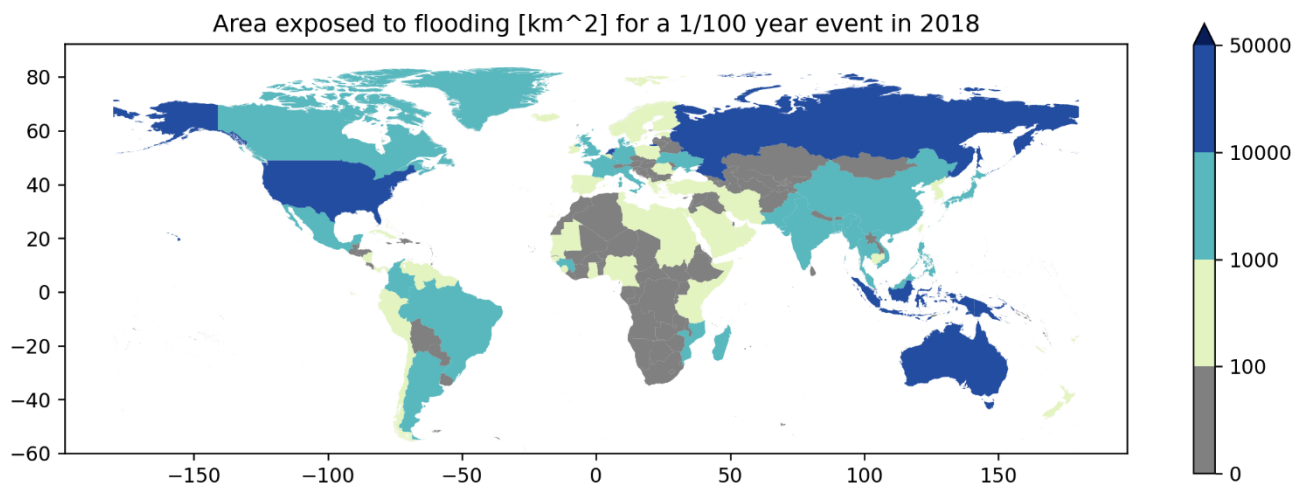


Planetary computer and Deltares global data

Flood Hazard Maps



Planetary computer and Deltares global data
Flood Hazard Maps

Summary

Coastal flooding is one of the most damaging hazards in coastal areas. Coastal flood risk is expected to increase under the pressures of Sea Level Rise (SLR), climate change and population growth. Mitigation of coastal flooding is essential for flood-prone coastal communities, especially in developing countries and small island states. Understanding potential flood extent on a global scale is important to identify hotspots of coastal flood risk and to help prioritize adaptation efforts.

Two data products have been developed in this project:

- 1 a global catalogue of coastal flood maps for major historical disasters; and
- 2 global maps of the change in flood prone areas from 2018 to 2050.

A bathtub inundation model that includes flood attenuation and roughness is used as the flood modeling tool. Historical extreme surge events between 1980 and 2018 are chosen based on the Surgedat database (Needham, 2013). Global coastal flood maps are simulated based on three DEMs (i.e. MERIT, NASADEM, LiDAR DTM) in combination with three spatial resolutions (i.e. 90m, 1km and 5km). Global flood maps are simulated based on coastal extreme water levels with given return periods. These coastal water levels are taken from the Deltares dataset of changes in extreme sea level under future climate change scenarios, which are based on global projections for a multi-model ensemble (i.e. High-Resolution Model Intercomparison Project of CMIP6). Return periods of water levels along the world's coastlines are calculated based on extreme sea levels derived from an ERA5 reanalysis (1979-2018). Spatial fields of sea level rise have been imposed, which were derived for the present-day situation (2018, end of the ERA5 climate reanalysis) and for the future situation (2050, based on the IPCC AR5 assessment for the RCP 8.5 scenario). The flood inundation models are computed on the Microsoft Azure cloud computing platform. Output flood maps are stored as NetCDF files.

Overall, this report provides detailed information about the global flood dataset that has been provided to Microsoft's Planetary Computer. Detailed information about the dataset is presented, including input data, flood modeling approach, high performance computing on Microsoft Azure, and details about the output flood maps. In addition, a discussion is provided about the limitations of the data and its recommended usage. Lastly, topics for future refinement of the flood maps are provided.

Contents

Summary	4	
1	Introduction	8
1.1	Motivation and objective	8
2	Input data	9
2.1	Digital Elevation Models (DEM)	9
2.1.1	MERIT	9
2.1.2	NASA DEM	9
2.1.3	LiDAR DTM	9
2.2	GTSMip6 water level	10
2.2.1	HighResMIP simulations	10
2.2.2	Tide and surge modeling (GTSMv3.0)	11
3	Methodology	12
3.1	Introduction	12
3.2	Model description	12
3.3	Model set-up in the cloud environment	13
3.3.1	Script updates	13
3.3.2	Pre-processing	13
3.3.2.1	DEM	13
3.3.2.2	Water mask	14
3.3.3	Run scheduler	15
3.3.4	Performance	15
3.4	Historical events	16
3.5	Global flood maps	16
4	Model validation	18
4.1	Validation against satellite images	18
4.1.1	Cyclone Nargis (2008)	18
4.1.2	Storm Xynthia (2010)	19
4.2	Validation against process-based models	21
4.2.1	Hurricane Ike (2008)	21
4.2.2	Hurricane Irma (2017)	22
5	Output flood maps	24
5.1	Flood maps for historic events	24
5.1.1	DEM product comparison	24
5.1.2	DEM resolution comparison (90m vs 1km)	26
5.1.3	Flood map results	27
5.2	Flood maps with return period	31
6	Limitation	37
7	Future work	39
Reference		41

Annex	44
A	45
B	52
C	58
C.1	Northwestern Europe
C.2	Gulf of Thailand
C.3	Bay of Bengal
	67

List of Acronyms

ALOS	Advanced Land Observing Satellite
ASTER	Advanced Spaceborne Thermal Emission and Reflection Radiometer
CMIP6	Coupled Model Intercomparison Project - Phase 6
DEM	Digital elevation model
DSM	Digital surface model
DTM	Digital terrain model
ERA5	Fifth global climate reanalysis produced by ECMWF
FLOPROS	Global database of FLOod PROtection Standards
GDEM	Global digital elevation models
GEBCO	General Bathymetric Chart of the Ocean
GLAS	Geoscience Laser Altimeter System
GLL_DTM	Global LiDAR Lowland DTM
GSWO	Global Surface Water Occurrence
GTSM	Global Tide and Surge Model
G1WBM	Global 1-second Water Body Map
HighResMIP	High Resolution Model Intercomparison Project (resolution of 50km and higher)
ICESat	Ice, Cloud and land Elevation satellite
IPCC	Intergovernmental Panel on Climate Change
LAT-MSL	Lowest Astronomical Tide – Mean Sea Level
LiDAR	Light Detection And Ranging
MERIT	Multi-Error-Removed Improved-Terrain
MSL	Mean Sea Level
RCP	Relative Concentration Pathway
SROCC	Special Report on the Oceans and the Cryosphere
SRTM	Shuttle Radar Topography Mission
SST	Sea Surface Temperature
TanDEM-X	TerraSAR-X add-on for Digital Elevation Measurement

1 Introduction

1.1 Motivation and objective

Global flooding caused by extreme sea levels can cause billions of dollars of damages annually. Climate change and sea-level rise is anticipated to lead to increases in the frequency of coastal flooding events. By 2100, potentially 20% of the global economy may be located within the 1 in 100-year flood zone (Kirezci et al., 2020). Prevention of disastrous impacts on the coastal communities would require large investments in emissions reduction as well as flood protection (Hinkel et al., 2014). A good understanding of which areas are prone to coastal flooding, and how this may change in the future will be instrumental in identifying appropriate mitigation and adaptation strategies. To address this need, global flood maps using state-of-the-art data are required.

Global flood maps can be used in several sectors. Within this project several potential users have been approached. A global catalogue of flood maps for major historical events can be utilized by the humanitarian community and development funding agencies. The flood maps for the mid-century can be used to predict changes in societal impacts of coastal flooding, which in turn may inform climate services, insurance companies, and global policy makers.

The objective of this project was defined as follows:

- Provide a global coastal flooding dataset, to help advance the understanding of areas prone to coastal flooding, and how this may change in the future;
- Understand how different digital elevation models (DEM) may impact the simulated flood extent.

2 Input data

There are two categories of input data required in this work:

- 1 Digital Elevation Models (DEM) as topographic data, and
- 2 Coastal water level as boundary conditions.

The sections below elaborate details of these data sources.

2.1 Digital Elevation Models (DEM)

2.1.1 MERIT

The Multi-Error-Removed Improved-Terrain (MERIT) is a global digital elevation model (DEM), which is freely available since 2017. This DEM has been developed by combining data from the Shuttle Radar Topography Mission, SRTM 3 DEM (below 60°N), with data from ALOS World 3D data at 30-meter resolution (above 60°N). The spatial resolution of MERIT is 90m, with an accuracy of ±12 m (Uuemaa et al., 2020, Yamazaki et al., 2017).

The MERIT DEM uses datapoints from the Viewfinder Panoramas DEM to fill the unobserved areas. Furthermore, the MERIT DEM has been post-processed to reduce errors by removing absolute bias, strip noise, speckle noise and vegetation bias. The absolute elevation bias is corrected using the ground control points from the ICESat laser altimeter. The strip noise is reduced with a two-dimensional Fourier transform filter. The speckle noise is removed by applying an adaptive smoothing algorithm, which is based on the relation between speckle noise and topography signals. The vegetation bias is corrected based on global tree density and height maps. The largest improvements of these error removal techniques have been reported in flat regions (Hawker et al., 2018, Yamazaki et al., 2017).

The MERIT DEM can be downloaded on the following link: http://hydro.iis.u-tokyo.ac.jp/~yamadai/MERIT_DEM/

2.1.2 NASA DEM

The NASADEM is a global DEM that is freely available since 2020. The NASADEM was developed with the objective to improve the height accuracy and data coverage of SRTM. NASADEM is a combination of SRTM and data from other satellite missions such as ICESat, GLAS, and ASTER. NASADEM has a resolution of 30m (NASA's Jet Propulsion Laboratory, n.d., Uuemaa, 2020, LP DAAC, 2020).

To provide global coverage, an SRTM mosaic software has been used to merge the improved SRTM DEMs, with refined ASTER, GDEM V2 DEMs and GLAS data. The elevation biases from the DEM have been corrected with the ground control points from the ICESat laser altimeter. Furthermore, this new free DEM provides additional products that include interferometric coherence, radar backscatter, radar incidence angle and radar backscatter image mosaic (NASA's Jet Propulsion Laboratory, n.d., Uuemaa, 2020, LP DAAC, 2020).

NASADEM can be downloaded on the following link:

https://cmr.earthdata.nasa.gov/search/concepts/C1546314043-LPDAAC_ECS.html

2.1.3 LiDAR DTM

Coastal flood risk assessments require accurate land elevation data in the form of digital terrain models (DTMs). Until recently, these DTMs only existed for limited parts of the world where airborne LiDAR altimetry data are available. This has resulted in high uncertainty in projections of coastal land area at risk of flooding and sea-level rise in most parts of the World. To help remedy this, a team led by Deltares has created and published the first global coastal lowland DTM that is derived from satellite LiDAR data (Vernimmen et al. 2020).

The global LiDAR lowland DTM (GLL_DTM_v1) at 0.05-degree resolution ($\sim 5 \times 5$ km) is created from ICESat-2 data collected between October 2018 and May 2020. It is accurate within 0.5 m for 83.4% of land area below 10 m above mean sea level (+MSL), with a root-mean-square error (RMSE) value of 0.54 m when compared to three local area DTMs for three major lowland areas: the Everglades, the Netherlands, and the Mekong Delta. This accuracy is far higher than that of four existing global digital elevation models (GDEMs), which are derived from satellite radar data and that are unable to penetrate vegetation. These GDEMs include, SRTM90, MERIT, CoastalDEM, and TanDEM-X. These latter GDEMs were found to be accurate within 0.5 m for 21.1%, 12.9%, 18.3%, and 37.9% of land below 10 m +MSL respectively, with corresponding RMSE values of 2.49 m, 1.88 m, 1.54 m, and 1.59 m respectively.

The recent availability of satellite LiDAR data presents a major and much-needed step forward for studies and policies requiring accurate elevation models. GLL_DTM_v1 is available in the public domain, and the resolution will be increased in later versions as more satellite LiDAR data become available. For the purpose of the study reported here, DTMs at ~ 1 km resolution were created for three large deltas in Asia: the Ganges-Brahmaputra-Meghna delta in Bangladesh and India, the Irrawaddy delta in Myanmar, and the Mekong delta in Vietnam. Additional ICESat-2 data up to September 2020 were used for these case studies.

2.2 GTSMip6 water level

Coastal water levels are the input data that are required as boundary conditions for flood inundation models. Coastal flooding in this study is driven by tide and storm surges (e.g. during a Tropical Cyclone event). The water level data required should also include sea level rise and climate change. Deltares computed a dataset of changes in extreme sea level under future climate change scenarios based on global projections for a multi-model ensemble consisting of five climate models. The dataset is produced by running the Global Tide and Surge Model version 3.0 (GTSM v3.0; Muis et al., 2020). The GTSM is a 2D hydrodynamic model with global coverage that incorporates tides, surges and mean sea-levels dynamically, using the newly available CMIP6 multi-model ensemble (Coupled Model Intercomparison Project Phase 6) as forcing. Specifically, the HighResMIP simulations (Haarsma et al., 2016) were used, which are high-resolution simulations with climate models with resolutions of at least 50 km in the atmosphere and 0.25° in the ocean, based on the Representative Concentration Pathway (RCP) 8.5. The enhanced resolution of this model ensemble has added value for the representation of climate extremes such as tropical cyclones (Roberts et al., 2020)

2.2.1 HighResMIP simulations

The main advantage of the HighResMIP simulations is the high spatial resolution of the models, as well as the temporal resolution that make it more suitable to look at extremes. The HighResMIP projections cover the period 1950-2050 for a set of climate models with a resolution higher than 50 km. The future simulations are based on RCP8.5. There are both coupled and atmosphere-only (i.e. SST-forced) simulations. An overview of the scenarios and epochs in the GTSMip6 simulation is given in Table 2-1. The experimental design of HighResMIP is explained in more detail at:

<https://www.primavera-h2020.eu/modelling/>.

Table 2-1 Overview scenarios and epochs in the GTSMip6 simulation

Simulation	Type	Period	Meteorological forcing	SLR scenarios
GTSMip6ER-A5	Climate reanalysis, baseline simulation	1979-2018	ERA5	IPCC SROCC ensemble mean
GTSMip6-hist	Historical simulation	1950-2014	Mix of SST-forced (HadGEM3GC31-HM, and GFDL-CMC192) and coupled (EC-Earth3P-HR,	IPCC SROCC ensemble mean

			CMCC-CM2-VHR4, and HadGEM3-GC31-HM) climate simulations	
GTSMip6-future	Future climate scenario based on RCP8.5	2015-2050	Mix of SST-forced (HadGEM3-GC31-HM, and • GFDL-CMC192) and coupled (ECEarth3P-HR, CMCC-CM2-VHR4, and HadGEM3-GC31-HM) climate simulations	IPCC SROCC ensemble mean

2.2.2

Tide and surge modeling (GTSMv3.0)

The Global Tide Surge Model (GTSM v3.0; Muis et al., 2020) is used to simulate the GTSMip6 water levels. The GTSMv3.0 is a depth-averaged hydrodynamic model with global coverage that dynamically simulates tides and storm surges. The GTSM v3.0 uses the unstructured Delft3DFM modeling suite (Kernkamp et al. 2011) and employs a variable resolution grid allowing for high accuracy at relatively low computational costs. It has an unprecedented high coastal resolution globally (2.5 km, 1.25km in Europe). The resolution decreases from the coast to the deep ocean to a maximum of 25km. Increased resolution has also been added in the deep ocean with steep topography areas to enable the dissipation of barotropic energy through the generation of internal tides. The bathymetry used in GTSM v3.0 consists of a combination of the EMODnet high-resolution (250m) bathymetry for Europe (<http://www.emodnet.eu/bathymetry>) corrected for LAT-MSL differences and the General Bathymetric Chart of the Ocean 2014 (GEBCO 2014, <https://www.gebco.net/>) with a 30 arc seconds resolution. The vertical reference of the model is mean sea level, given that the bathymetric data is referenced to that vertical datum.

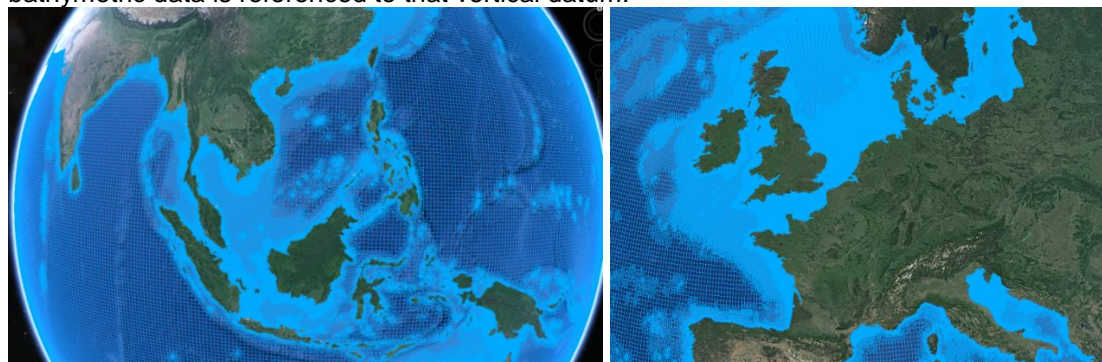


Figure 2-1 Model grid of GTSM in Southeast Asia and Europe

The global model does not have open boundaries and therefore is purely forced by the tide-generating forces (tidal constituents, including self-attraction and loading) and external forcing fields (e.g. winds, surface pressure). In terms of calibration, the model uniform bottom friction coefficient and internal wave drag coefficient have been tuned to match observed total rates of energy dissipation and show spatial energy dissipation distributions that are in good agreement with observed rates in Egbert and Ray (2001). For surges, the relation by Charnock (1955) to model the wind stress at the ocean surface is used, and the user-defined drag coefficient has also been tuned during the calibration process.

3 Methodology

3.1 Introduction

Two data products are developed in this project:

- 1 a global catalogue of flood maps for major historical disasters; and
- 2 global maps of the change in flood prone areas from 1950 to 2050.

To estimate coastal hazard, extreme sea levels derived from simulations with the next generation GTSM v3.0 were used. A dataset of historical water levels based on the ERA5 climate reanalysis (Muis et al., 2020) is also used. From a comprehensive literature review and online search, major historical coastal flood events were selected, and the corresponding water levels were extracted (see details in section 3.4). The selected events cover all continents. In addition, mid-21st century projections of extreme sea levels were produced by forcing the GTSM model with the latest climate models. Based on these time-series, various return periods of extreme sea levels were calculated based on 30-year time slices (1951-1980, 1985-2014, and 2021-2050). These can be used to assess how the flood hazard may change for the mid 21st century. Details are elaborated in section 3.5.

A GIS-based inundation routine was applied, similar to the approach in Vafeidis et al. (2018). The method uses GTSM's extreme sea levels and DEM as input and assumes that areas that are hydraulically connected to a given extreme sea level are completely inundated (Aqueduct Technical Note, 2020). The analysis does not include flood protection. For the historical events, the dataset has been validated with available flood maps from satellite measurements and available modeling results. The quality of the flood maps is largely determined by the quality of the DEM used. The sensitivity of using different DEMs and the trade-offs between high resolution and accuracy was assessed. SRTM-based DEMs (i.e. MERIT, NASA DEM) at the resolution of 90m and 1km were compared with the LiDAR DTM with resolution of 5km globally. The LiDAR DTM is also available at three deltas in Southeast Asia with 1km resolution.

The flood simulations are run on the Azure cloud. The output water levels require ~30 GB of storage. The output of one 1 km resolution map is ~14 MB, whereas the 90m resolution map is ~900MB.

3.2 Model description

Inundation maps of flood depth are produced using a geographic information system-based inundation model that includes water level attenuation. At the coastline, the model is forced by extreme water levels containing surge and tide from GTSMip6 (see Section 2.2). The water level at the coastline is extended landwards to all areas that are hydrodynamically connected to the coast following a 'bathtub' like approach that calculates the flood depth as the difference between the water level and the topography. Unlike a simple 'bathtub' model, this model attenuates the water level over land with a maximum attenuation factor of 0.5 m km⁻¹ consistent with other studies (Vafeidis et al., 2018). The attenuation factor simulates the dampening of the flood levels due to the roughness over land, and it is applied via the so-called water mask file (see section 3.3.2.2 water mask). The attenuation factor has been linearly scaled to account for spatial variation in roughness based on the proportion of permanent water features in each model grid cell (Haer, 2018). Specifically, the attenuation factor would range from 0.0 m km⁻¹ for cells in rivers and lakes where the percentage of permanent water is 100% to the maximum value of 0.5 m km⁻¹ for cells that exclusively contain land. The percentage of permanent water per grid cell were derived from global surface water occurrence maps for the period from 1984 to 2019 with a resolution of 30 m (Pekel et al., 2016).

The model does not account for the compound effects of waves, rainfall and river discharge on coastal flooding. It also does not include the mitigating effect of coastal flood protection. Flood extents must thus be interpreted as the area that is *potentially* exposed to flooding without coastal protection.

3.3 Model set-up in the cloud environment

3.3.1 Script updates

The model described in section 3.2 is wrapped within a Python script that also handles all the required pre- and postprocessing steps, such as finding the relevant coastal sections and matching those with the output of the GTSM model. The Python script also stitches all tiled GeoTIFF output files together into a single NetCDF file. Besides this, the script also handles user input (through both a user settings file and command line arguments) and logging. The original scripts have been used in a number of studies (e.g. Haer et al., 2018; Tiggeloven et al., 2019) and the Aqueduct Floods tool of the World Resource Institute (WRI), available at <https://www.wri.org/aqueduct> (Ward et al., 2020). The scripts are hosted on a public repository (<https://github.com/Deltares/aqueduct-coastal-flooding>).

The geospatial processing within the scripts is handled with the PCRaster Python library (<https://pcraster.geo.uu.nl/>), which contains a large set of relevant spatio-temporal functions. The original scripts referred to above used PCRaster version 4.1.0, which required Python 2.7 and did not yet support multicore CPU processing. While this is not an issue when running the model at the original 1 km scale, it could become problematic when investigating multiple scenario's or return periods at high resolution (i.e. 90 m). As such, the scripts have been converted to the most recent versions of PCRaster and Python (4.3 and 3.8 respectively), which do support multicore CPU processing. The updated scripts have been added to a new branch (dubbed 'py38') at the previously mentioned repository.

In addition to this, several conceptual improvements have been added, which ensures proper handling of all individual tiles. During processing additional area is added on all sides of each tile (overlap), the amount of which is set by the user in the settings file. This overlap exists to make sure that the inundation is not artificially stopped when it reaches a tile edge. However, especially at higher resolutions, the tile size and/or overlap would have to be set very high to ensure this does not happen, which negatively impacts computation speed up to a point that would make running all required scenario's and return periods impossible within the constraints of the project. Therefore, a new (post)processing was introduced that does not just stitch together all individual tiles but also takes the data within the overlap of each tile into account, taking the maximum inundation at each pixel. This allows the tile settings to be kept to a proper size while also producing results that are (nearly) completely devoid of edge-effects. At the same time, this incorporates the water mask (see Section 3.3.2.2) by masking out (inundated) pixels over permanent water. On top of this a caching mechanism has been added, that keeps the intermediate outputs that are the same for multiple scenarios, such as the mapping of border conditions to the coast and the adjusted elevation map. When running on a 64-core machine in Azure (i.e. Standard_M64ds_v2), runtime for subsequent scenarios improved from 24h to 6h.

3.3.2 Pre-processing

3.3.2.1 DEM

Different DEMs are used to assess their impact on the coastal flood inundation. The pre-processing steps needed to create the MERIT and NASA DEMs at two resolutions (1km and 90m) are described here. The objectives of the pre-processing steps are to create global GeoTIFF DEM files at 1km and 90m resolution from the MERIT and NASA DEM source files.

For MERIT DEM, the source data is the global NetCDF dataset made available by the Japan Agency for Marine-Earth Science and Technology. The terrain elevation data has a resolution of approximately 90m at the equator, and covers land areas between 90N-60S, referenced to EGM96 geoid.

See also: http://hydro.iis.u-tokyo.ac.jp/~yamadai/MERIT_DEM/

To convert the global MERIT 90m resolution NetCDF data to a global 90m resolution GeoTIFF, the GDAL translator library for raster and vector geospatial data formats was used. The resultant 90m resolution MERIT GeoTIFF file was used in the 90m resolution simulation presented in this report.

See also: <https://gdal.org/>

The 90m resolution MERIT GeoTIFF was then resampled to 1km using GDAL. The resampling was done by computing the average of pixel dimensions within the source rasters and stitching these together to form the global 1km resolution MERIT DEM GeoTIFF.

For the NASA DEM the source data are 30m resolution NetCDF data available on Microsoft Azure. The global 30m resolution NetCDF data are separated into 14520 individual NetCDF files, or tiles, and are organized along discrete longitudes and latitudes. The same pre-processing steps were applied to generate two global GeoTIFF files, one at the 1km target resolution and another at the 90m target resolution.

Firstly, each of the 30m resolution NetCDF files was converted to a GeoTIFF file using the GDAL translator library. Then, to create global NASA DEM GeoTIFF files at 1km and 90m resolution, the 30m resolution GeoTIFF files were used to create a virtual dataset (using the gdalbuildvrt function).

See also: <https://gdal.org/programs/gdalbuildvrt.html>.

During this step the 30m GeoTIFF files were resampled to the target resolution (1km and 90m) by computing the average of pixel dimensions within the set of source rasters and the longitudinal and latitudinal extent was adjusted to match that of the MERIT DEM.

Next, the virtual dataset was translated to one global GeoTIFF file using the GDAL's translate function. Following this step, to ensure that the longitudinal and latitudinal extent of the MERIT and NASA DEMs remains consistent, the resultant global NASA DEM GeoTIFF was reprojected to the MERIT DEM using GDAL's gdalwarp utility.

Finally, an additional pre-processing step is needed before the NASA DEM can be used in the coastal inundation model. This is due to the fact that the NASA DEM includes zero values over the sea or ocean (just like the SRTM DEM it is based on). These zero values have been removed (masked out) in the MERIT DEM. Therefore, the pixels which are masked out in the MERIT DEM are also masked out in the NASA DEM using GDAL's gdal_calc function.

Reprojecting the NASA DEM to the MERIT DEM extent and masking ocean and sea data according to the MERIT DEM allows for the same water mask to be used in the simulations and their results can more easily be compared with each other.

3.3.2.2 Water mask

The inundation model includes an attenuation factor that simulates the dampening of the flood levels due to roughness over land. This feature of the model requires a water mask. In the absence of a water mask the model does not account for reduced roughness over permanent water bodies, and thus underestimates the potential inland inundation extent particularly in low-lying delta regions, as explained in section 3.2.

Here, the water mask is derived from Global Surface Water Occurrence data (Pekel et al., 2016).

See also: <https://global-surface-water.appspot.com/download>.

The Global Surface Water Occurrence shows where surface water occurred between 1984 and 2019 and provides information concerning overall water dynamics. This product captures both the intra and inter-annual variability and changes. The data has a spatial resolution of 0.00025° (approximately 30m).

To generate two global water mask GeoTIFF files at the two target resolutions (1km and 90m), the 30m resolution water occurrence data is used. Firstly, the tiled GeoTIFF data was masked. All pixels where water occurred more than 50% of the time were set to 1 and all pixels where water occurred less than 50% of the time were set to 0. This was done using the GDAL translator library for raster and vector geospatial data formats (<https://gdal.org/>). The water mask GeoTIFFs were then resampled to the target resolution by computing the average of pixel dimensions within the source rasters and stitching these together to form the two global water mask GeoTIFF files at the two target resolutions (1km and 90m).

In order to use the water mask with the MERIT and NASA DEM simulations, the water mask is reprojected onto the MERIT DEM grid in the same way that the NASA DEM was reprojected to the MERIT DEM.

3.3.3

Run scheduler

A tailor-made script has been set up in python to generate a series of model runs with varying input data. The script is started locally on the computational node after a manual log in. The script prepares a folder for each run with a correct initialization file, which includes the paths to the desired DEM, reference level offset file and optionally a water mask file in the blob storage. The blob storage is a scalable and secure object storage to store our input and output data in Microsoft Azure. Additionally, the tiling settings are specified. For the first run, the size in pixels of the tiles and the overlap are specified. Consecutive runs use the generated json-file with the tiling information to reduce the start-up time. Other settings in the initialization file are fixed.

Subsequently, the run is started by calling upon the main script of the inundation model and supplying it with the boundary conditions with return levels and with a sea level rise map. The model distributes the tiles over all but one computational core, until all tiles are calculated. When the run is finished, the output data is moved to the blob storage to free up space on the computational node for the next run in the series.

3.3.4

Performance

The computational nodes used on Azure are the so-called compute optimized nodes. Three types of VMs were used within the project: Standard_H16 (16 vCPUs, 112GiB RAM), Standard_M32dms_v2 (32 vCPUs, 875GiB RAM), and Standard_M64ds_v2 (64 vCPUs, 1024GiB RAM). For the DEMs with a resolution of 1km and a good distribution of the tiles, the runtime on Standards_H16 VMs is manageable. For the 90m runs it was necessary to scale up to 64 core machines, namely the M64ds_v2 type, with 1TB of memory, of which 6 instances were used to speed up the simulation. Moreover, Standard_M32dms_v2 were also used to speed up the 1km runs. Model performance for the different DEMs per global simulation is given in Table 3-1 and CPU usage is depicted in Figure 3-1 and Figure 3-2.

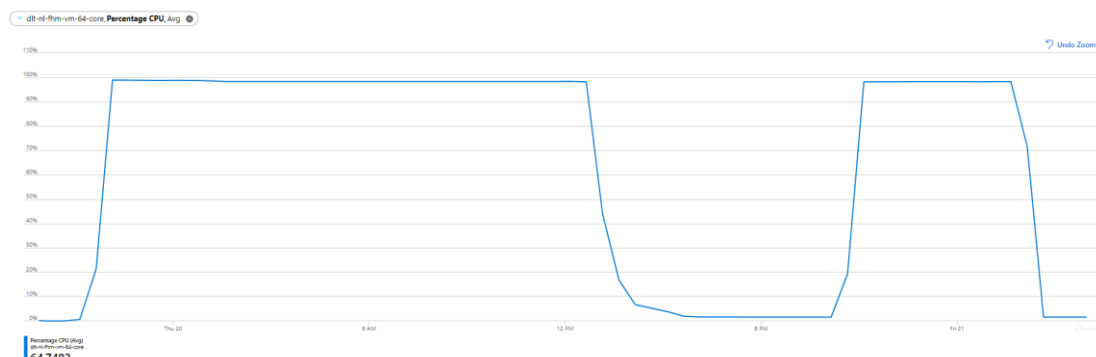


Figure 3-1 CPU usage for two consecutive model runs with NASADEM 90m on a Standard_M64ds_v2 machine. The second (and other consecutive runs) are faster because they use the cache produced during the first run.

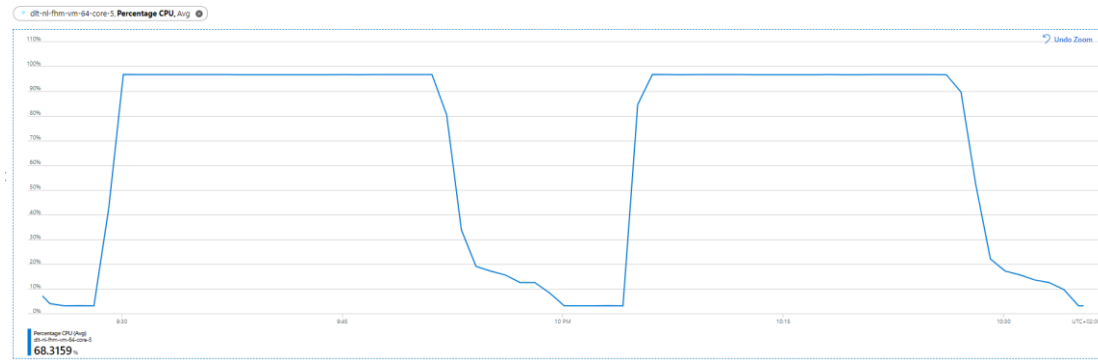


Figure 3-2 CPU for two consecutive model runs with MERITDEM 1km on a Standard_M32dms_v2 machine.

Table 3-1 Model run times for different DEMs per global simulation

DEM	resolution	run time (including tiling)	VM
MERIT	1km	~30 m	Standard_M32dms_v2
MERIT	90m	~20 h (first run) + 6 h per consecutive run	Standard_M64ds_v2
NASA	1km	~ 25 m	Standard_M64ds_v2
NASA	90m	~20 h (first run) + 6 h per consecutive run	Standard_M64ds_v2
LIDAR	5km	~7 m	Standard_H16

3.4 Historical events

To estimate coastal hazard, extreme sea levels are used that are derived from simulations with the next generation GTSM v3.0. In order to identify the major surge events between 1980 and 2018, a dataset of historical extreme surge events from the Surgedat database (Needham, 2013) was used. As this database focuses primarily on tropical-cyclone generated storm surges, the database with major storm events from the literature that resulted in coastal flooding (e.g. Xynthia in France in 2010) has been appended to the database. The peak water level for each event was defined as the maximum water level in the GTSM ERA5 reanalysis simulation for the month the event happened in. The list of simulated historic events is provided in Appendix A.

3.5 Global flood maps

There are various ways to look at the global flood maps under sea level rise and climate change. The dataset provided in phase one of the project can be used to understand how future coastal flood inundation will change due to sea level rise only. The baseline simulations (ERA5 reanalysis run, Table 2-1) have been post-processed by removing annual mean sea level, such that no sea level rise is included. Sea level rise is then added to the post-processed baseline simulation (without sea level rise) in order to compute flood maps. Lastly the two maps are compared, and the changes of flood extent are presented (see section 5.3).

The hydrodynamic forcing on the boundaries is produced with GTSM v3.0 with atmospheric forcing from the present-day climate from the ERA5 climate reanalysis. Based on an extreme value analysis, return levels along the world's coastlines are computed for return periods of 2, 5, 10, 25, 50, 100 and 250 years. Spatial fields of sea level rise are used for the present-day situation (2018, end of the ERA5 climate reanalysis) and the future situation (2050, based on the IPCC AR5 assessment (Church et al. 2013) for the RCP 8.5 scenario).

The global flood maps are computed for the various return periods of extreme sea levels in combination with the two sea level rise situations. These were used to assess how the flood hazard may change for the mid-century. Specifically, they are calculated based on combinations of three DEMs and resolutions.

Both 90m and 1km resolution maps are available for MERIT and NASA DEM, whereas 5km resolution maps are available globally for LiDAR DTM (Table 3-2).

Table 3-2 Overview of global flood maps

DEM	Resolution	Original datum	Return period (yr)	Periods	Number of runs
MERIT	1km, 90m	EGM96	0, 2, 5, 10, 25, 50, 100, 250	2018 (Present day)/2050 (+ SLR)	16
NASA	1km, 90m	EGM96	0, 2, 5, 10, 25, 50, 100, 250	2018 (Present day)/2050 (+ SLR)	16
LIDAR	5km	MSL	0, 2, 5, 10, 25, 50, 100, 250	2018 (Present day)/2050 (+ SLR)	16

4 Model validation

To validate our global modeling approach, the results for selected historical events were compared either against satellite images of observed flood extent or against flood maps generated with process-based models. The main purpose of this study was to compute the extent of coastal flooding, so the validation is focused on the flood extent not flood depth.

Process-based models solve the physical equations of water flow and can thus accurately simulate the flooding during a storm event. The disadvantage of these models is that they are computationally expensive and are often only applied to small areas. Process-based models simulate the main processes that contribute to coastal flooding, but they do not include all processes due to their underlying assumptions of the model physics. Their performance is furthermore limited by the quality of input data. Process-based models provide a reasonable but not perfect representation of the actual historic event.

Satellite images are not always available for the peak of the storm event and the images can be compromised by cloud cover. The satellite images do however provide information about the actual flood event, but must be correctly pre-processed to identify areas covered by water in the image.

4.1 Validation against satellite images

4.1.1 Cyclone Nargis (2008)

Tropical cyclone Nargis was rated a category 4 storm on the Saffir–Simpson Hurricane Scale and made landfall on Myanmar's coastline on the 2nd of May 2008 (Fritz et al. 2009). Flood inundation reached up to 50km inland due to the peak storm surge exceeding 5m and storm waves of 2m and higher. Sustained wind speeds were over 210 km/h, gusting up to 260 km/h. The peak surge level simulated by GTSM was 4.84m.

Nargis was the worst natural disaster on record in Myanmar. The storm caused more than 138,000 fatalities, which is the highest death count due to a cyclone worldwide since the Bhola cyclone in 1970 with up to 500,000 fatalities. The damages caused by Nargis amounted to over \$10 billion, which made it the costliest cyclone ever recorded in the Indian Ocean.

Figure 4-1 provides a comparison between the satellite derived flood extent of Nargis (top panel) and the flood depths simulated by the bathtub model (bottom panel). The model shows extensive flood extent on the eastern side of the delta. GTSM correctly simulates high surge and tide levels of up to 5 meters, which are used by the bathtub model around the Irrawaddy river mouth and in the surroundings of Yangon. This corresponds well with the satellite observations of the event as shown in Figure 4-1. Overall the flood extent calculated with the bathtub model provides similar results to the observed satellite imagery. The coastline of Myanmar is characterized by multiple river deltas that allow flood waters to reach far inland. On these river deltas, the bathtub model predicts larger flood extents than observed, whereas in the eastern side of Yangon less flood extent is estimated. The reasons for this might be that Nargis was an event characterized by heavy precipitation, which can cause additional inland flooding. Precipitation is not included in the GTSM model simulations. More information regarding this limitation of the bathtub model can be found in section 3.2 and section 6.

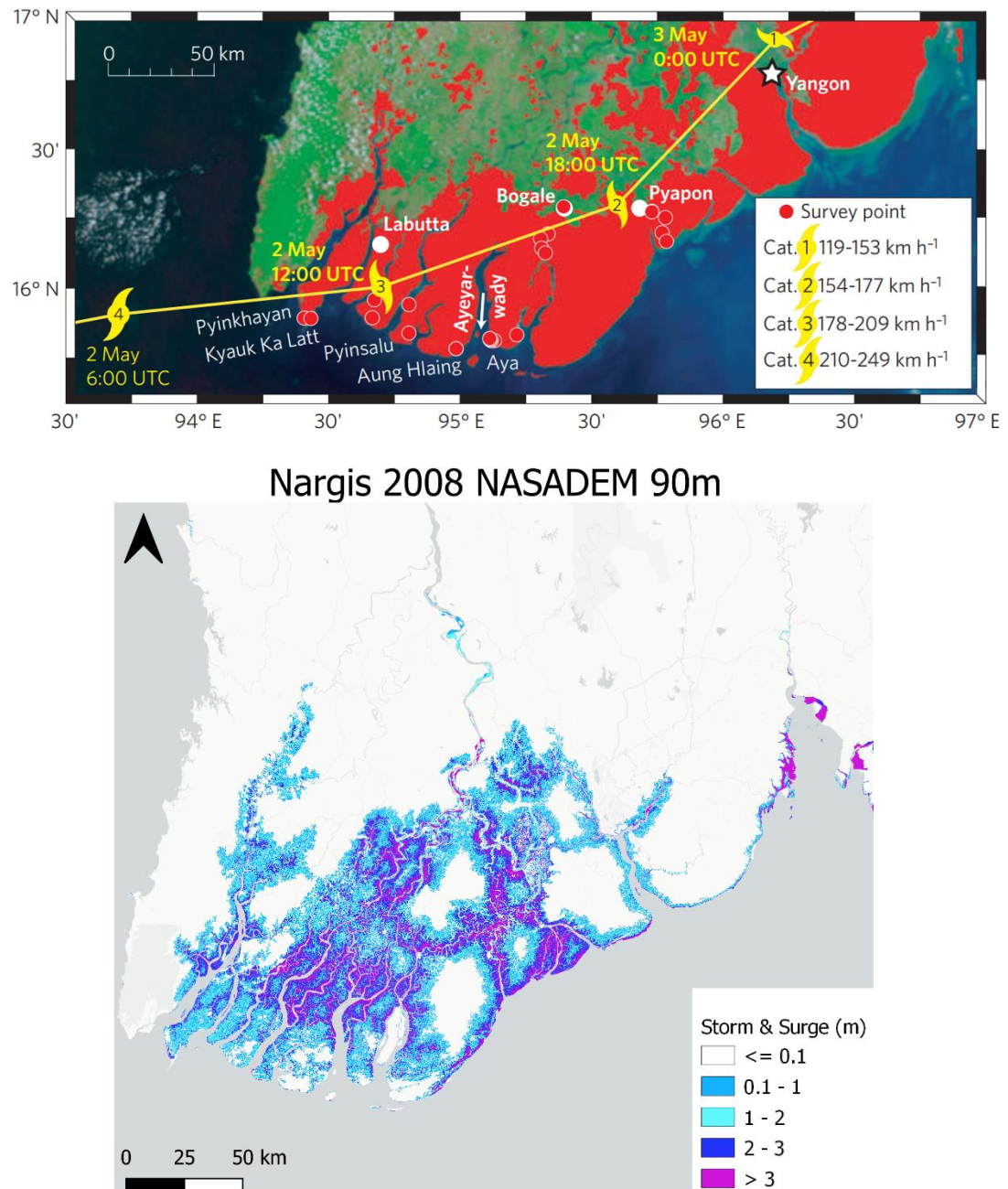


Figure 4-1. Satellite observation of the flood extent during Nargis (upper panel, Fritz et al. 2010) and results of the bathtub model using the NASADEM 90m (lower panel).

4.1.2

Storm Xynthia (2010)

Xynthia made landfall on the French Atlantic coast on the 27th of February 2010, with wind speeds of approximately 95km/h. During this event, large water levels were caused due to the combination of a storm surge of 1.6m, with a high tide of approximately 2.75m. The highest water level was measured in La Rochelle, at 4.5m. This caused a flood with a return period of around 100 years, which caused significant damage along the French coast. The storm caused 47 fatalities, and the damage caused impacted the fisheries, agriculture, infrastructure and the tourist industries (Kolen et al., 2010).

In Figure 4-2 the modelled flood extent in the coastal areas shows good agreement with the observed flood extent. Along the coast, water levels of approximately 4m are observed. Flood depths of around 4 m are modelled along the coast, which is in line with observed peak surge levels of 4.5 m in La Rochelle.

Further inland the simulated flood extent is underestimated by the bathtub model. This mismatch of the flood extent is most likely caused by the omission of inland flooding in this bathtub model. More information regarding the limitation of the bathtub model can be found in Section 6.

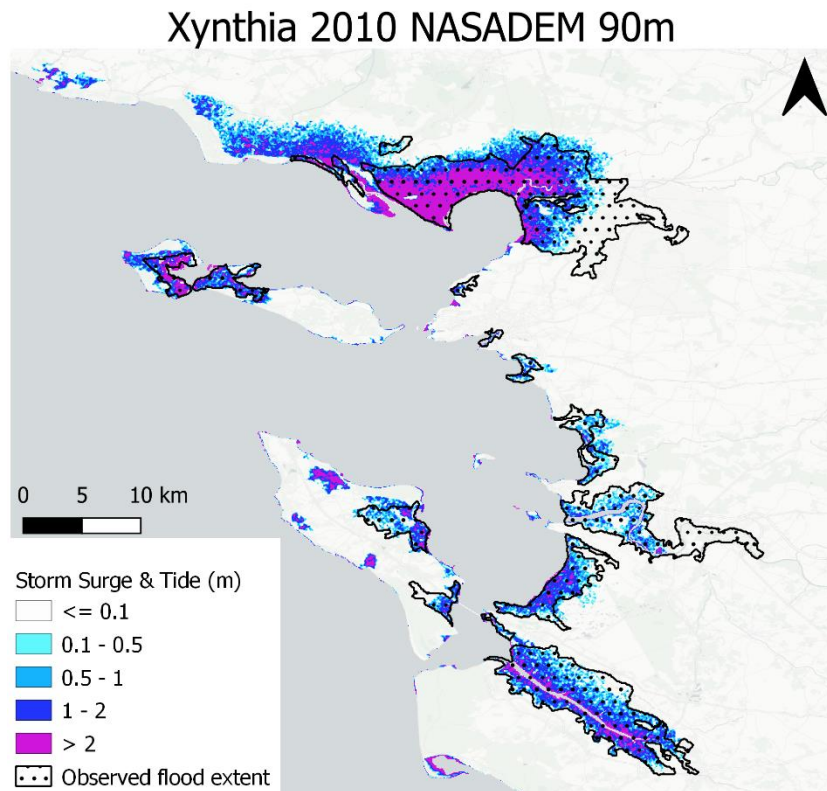


Figure 4-2 Flood extent and depth derived from the inundation model based on NASA 90m DEM, together with the observed flood extent for Xynthia 2010.

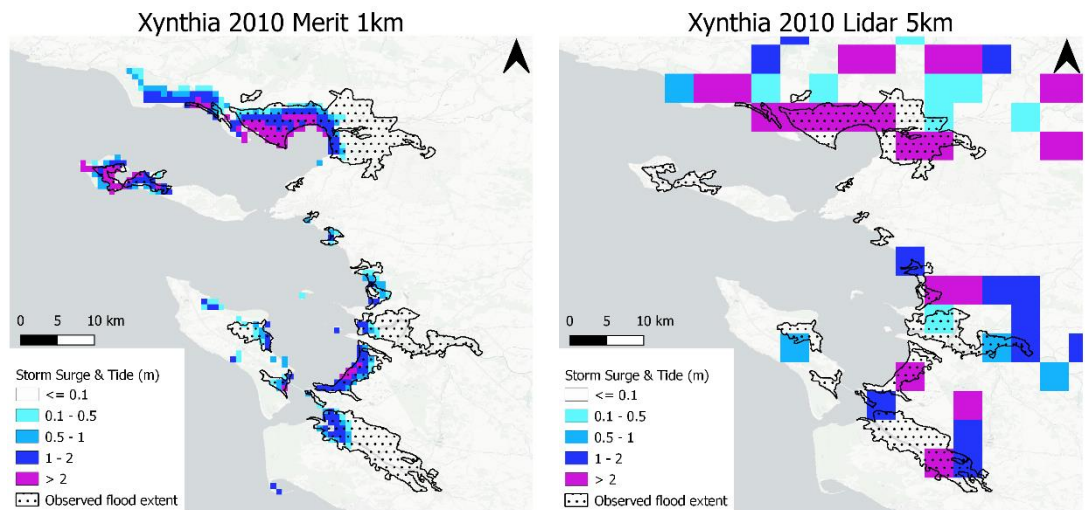


Figure 4-3 Flood extent and depth derived from the inundation model for Xynthia 2010. Left panel: model results with Merit DEM 1km; Right panel: Lidar DEM 5km

4.2 Validation against process-based models

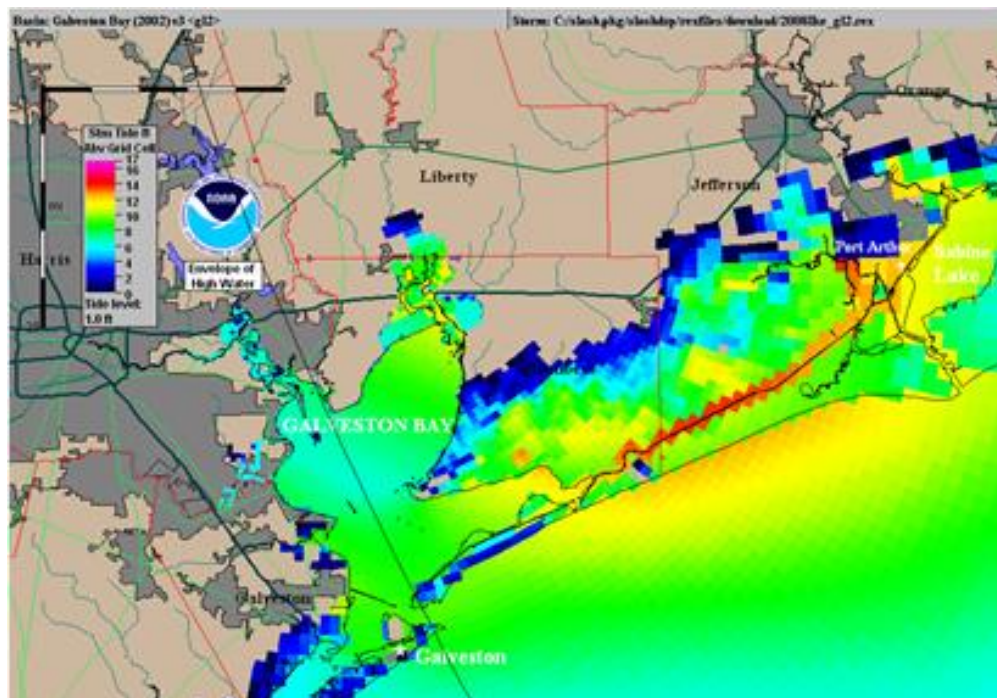
4.2.1 Hurricane Ike (2008)

Hurricane Ike made landfall on the Texan coast on the 13th of September 2008 with sustained windspeeds of 180 km/h. It was categorized as a Category 2 storm on the Saffir–Simpson Hurricane Scale. The maximum surge was measured in Chambers County, at 5.3m. Hurricane Ike produced significant damage along the coast of Texas and Louisiana (Hope et al., 2013, National Weather Service n.d.).

Figure 4-4 presents a comparison of the flood extent and water depth as calculated by NOAA's SLOSH model and by the bathtub model. The flood extent results of the bathtub model provide similar predictions compared to the SLOSH model, with flood extents that become more pronounced in the coastline between Galveston Bay and Sabine Lake. More information regarding the limitation of the bathtub model can be found in Section 6.

Along the coastline east of Galveston Bay, flood depths of around 14 feet are predicted by both models. On the west side of Galveston Bay, the flood depths are lower: less than 5 feet for both models.

Notice that the bathtub results present a line pattern in the results, especially noticeable in the right side of the figure. This pattern is inherent in the NASADEM, and was not caused by the bathtub model.



Ike 2008 NASADEM 90m

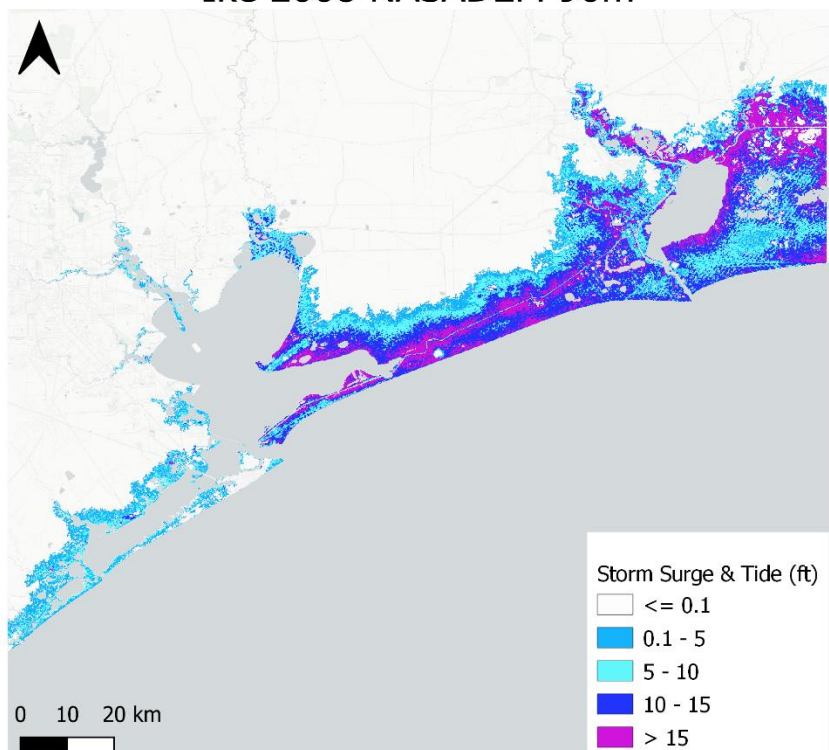


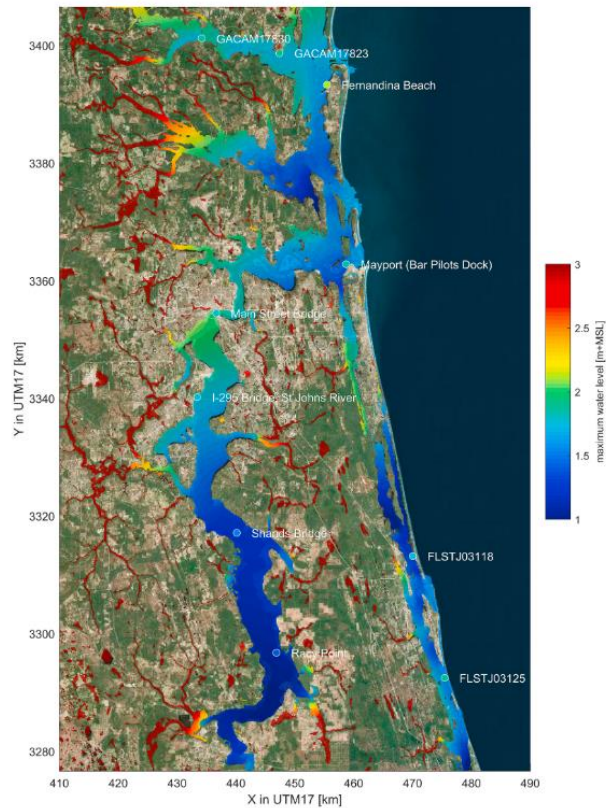
Figure 4-4. Top: simulated storm surge level above grid cell in feet and flood extent (with the process-based model SLOSH by NOAA) (National Hurricane Center and Central Pacific Hurricane Center (n.d.)) and bottom: simulated flood depth in feet and extent in km with the bathtub model.

4.2.2 Hurricane Irma (2017)

Hurricane Irma made landfall in Florida on 10 September 2017 with sustained windspeeds of 210 km/h. It was categorized as a Category 4 storm on the Saffir–Simpson Hurricane Scale. Hurricane Irma caused one direct death, and 33 indirect deaths in South Florida. In Collier County, at least 88 structures were destroyed, and 1500 structures had major damages. The costs of Hurricane Irma were tremendous. Collier County and Palm Beach County each reported losses of more than \$300 million due to damages (National Weather Service).

Figure 4-5 presents a comparison between the results of the bathtub model and SFINCS model (Leijnse et al., 2020). Through visual inspection the flood extent along the coast seems to follow a similar pattern compared to the flood extent presented in the top panel, although further inland flood extent is underestimated by the bathtub model in comparison with SFINCS model.

The bathtub model results seem to provide larger water depths in certain locations, in comparison with SFINCS results. At some locations along the coast and inland channels, the bathtub model results suggest water depths of more than 3m, while in the SFINCS model those locations seem to have depths between 1.5 and 2 m. While the bathtub model predicts a decrease in flood depths further inland, SFINCS presents larger water depths. This could be caused by the simplification of the attenuation of the flood levels over land in the bathtub model, whereas SFINCS models the physical processes.



Irma 2017 NASADEM 90m

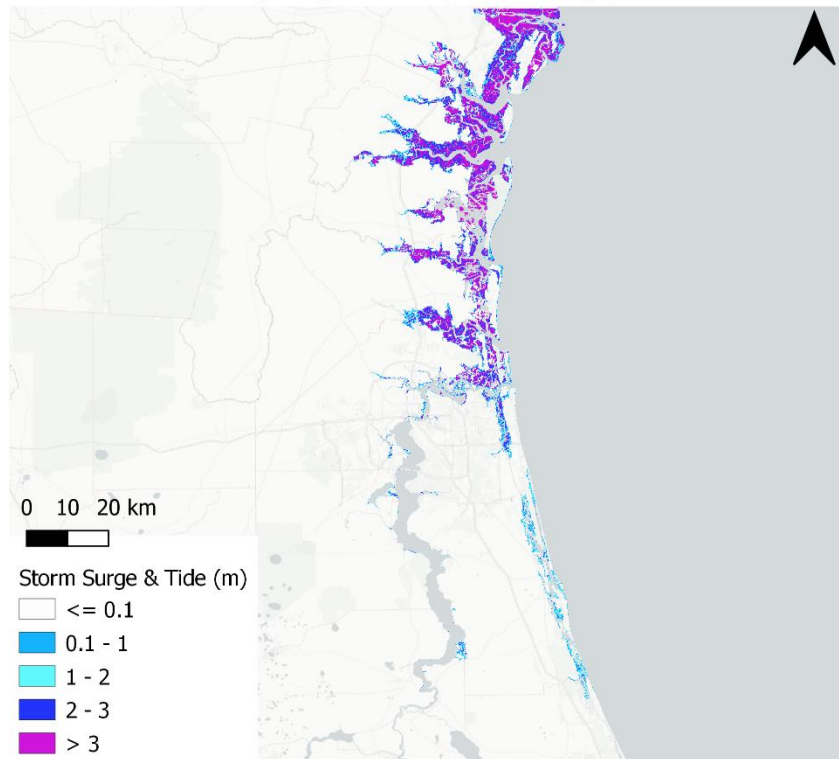


Figure 4-5 Simulated storm surge model from SFINCS model (upper panel); simulated flood depth and extent by the bathtub model (lower panel).

5 Output flood maps

5.1 Flood maps for historic events

The model has been run for 186 historic flood events that have occurred globally during the last 40 years. The results are presented in the following sections.

Figure 5-1, 5-2 and 5-3 display the inundation model results for a selection of events, when using different digital elevation models:

- NASADEM at 90m resolution
- MERIT at 90m resolution
- NASADEM at 1km resolution
- MERIT at 1km resolution
- LiDAR at 1km resolution
- LiDAR at 5km resolution

Note that the LiDAR DTM at 1km is a refined DTM that is only available for a limited number of historical events (see Section 2.1.3).

5.1.1 DEM product comparison

The DEMs mentioned above have been briefly described in Section 2.1. This section describes their differences in terms relevant for flood inundation modeling, to help understand the differences in flood maps. The focus areas are where the LiDAR DTM is available at 1km, so that a comparison at equal spatial resolution is possible.

Figure 5-1 shows the different DEMs over the Mekong delta. In general, MERIT has the highest elevation, while NASADEM has the lowest elevation for this region. However, the LiDAR DTM has the highest accuracy when compared to the locally created DTM benchmark, which suggests that MERIT contains overestimations while NASADEM contains underestimations. Additionally, the diagonal striping pattern (strip noise), which originates from the base SRTM DEM, is still present in the NASADEM. The SRTM-based DEMs have streams and channels better incorporated than the LiDAR DTM, because their original resolution is much higher and allows more detailed features to be included. However, it can also be seen that elevation along the banks of these streams is higher than their surroundings, which is probably related to the fact that absolute bias due to urban buildings, or man-made features in general, have not been corrected and/or not all vegetation bias has been corrected.

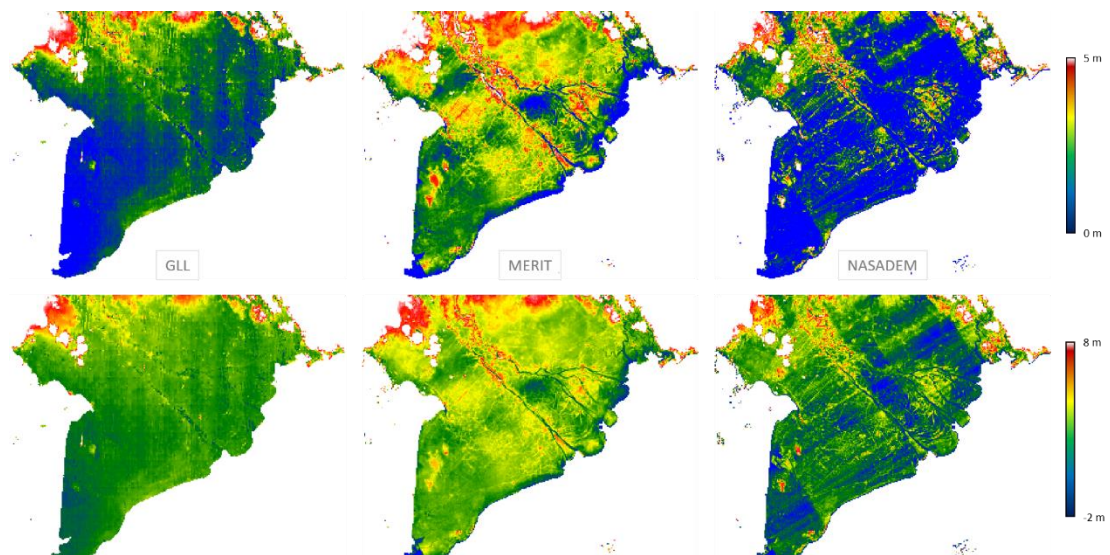


Figure 5-1: Comparison of DEMs at 1km over Mekong delta with two different minimum/maximum values for visualization (left: LiDAR DTM, middle: MERIT, right: NASADEM)

Figure 5-2 shows the difference between both SRTM-based DEMs and the LiDAR DTM (calculated as DEM-DTM). This again shows that generally MERIT overestimates (yellow to red areas) and NASADEM underestimates (blue to green areas) when compared to this DTM. It also reveals the strip noise in NASADEM (and the fact that this error has been removed in MERIT).

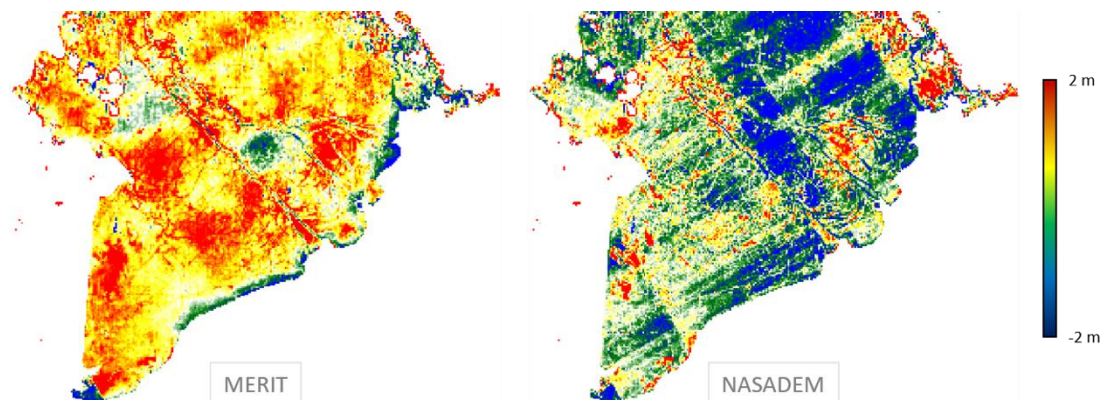


Figure 5-2: Difference between MERIT, NASADEM and LiDAR DTM at 1km over the Mekong delta

A similar analysis and figures have been created for the Ganges-Brahmaputra-Meghna delta in Bangladesh (Figure 5-3, Figure 5-4). This reveals a slightly different picture from that of the Mekong delta. First, while MERIT still has overestimations compared to the LiDAR DTM, NASADEM does not seem to be lower in general, instead showing more variability (some areas with lower, other areas with higher elevation). One area that clearly stands out is the Sundarbans mangrove forest (highlighted in each figure with a dashed box), especially in NASADEM. The higher elevations nearly perfectly match the outline of this protected forest, which seems to imply that vegetation bias correction was insufficient here. In contrast, the areas outside of it are lower than the LiDAR DTM, which could indicate overfitting/overestimation of the bias correction there. This is less of an issue in MERIT. Similarly, as seen in the Mekong delta, rivers and streams are better incorporated in MERIT and NASADEM. This area also reveals a potential inconsistency issue with the water mask; the LiDAR DTM already includes a water mask, which is different from the water mask used in this study (and the previously carried out Aqueduct related studies mentioned earlier). With all flood maps being updated with the same water mask, and the effect of (permanent) water areas far greater in the higher resolution DEMs (for which the LiDAR DTM is not available, see also next sections of this chapter), this issue is probably neglectable.

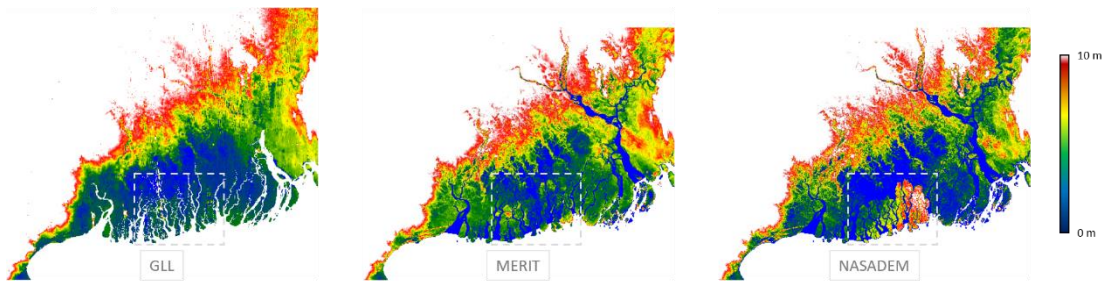


Figure 5-3: Comparison of DEMs at 1km over Ganges-Brahmaputra-Meghna delta in Bangladesh

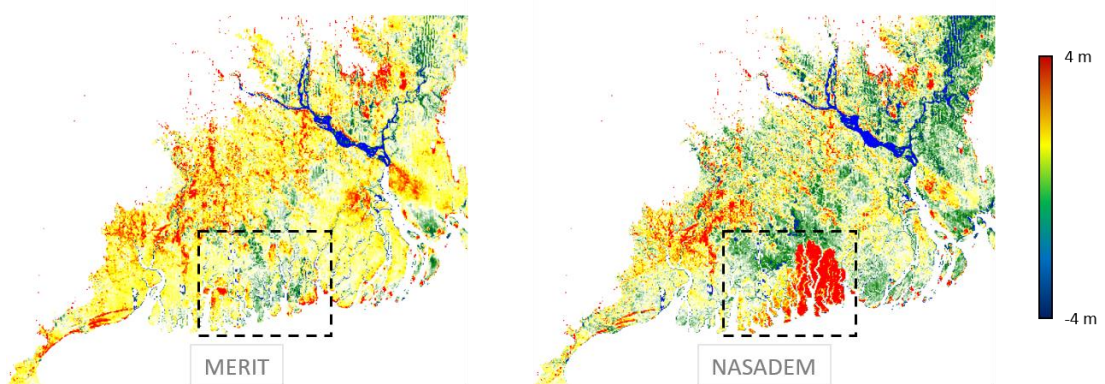


Figure 5-4: Difference between MERIT, NASADEM and LIDAR DTM at 1km over Ganges-Brahmaputra-Meghna delta in Bangladesh

It can be expected that the differences in DEMs described here will propagate to the inundation modeling, although it should be noted that these differences will vary for other regions across the globe. General take-aways, which probably hold for any region, are: (1) LiDAR DTM is probably the most accurate in terms of absolute elevation values, at the spatial resolution for which it is available, (2) rivers, streams and other detailed features are better included in MERIT and NASADEM, also at 1km, because they are based on higher resolution data, (3) strip noise is still present in NASADEM. Finally, it seems that NASADEM can contain somewhat extreme (bias) corrections, which can lead to over- and underestimations of “true” elevation, although it cannot be claimed this is the case globally from the two cases analyzed here.

5.1.2

DEM resolution comparison (90m vs 1km)

As hydraulic connectivity is included in the inundation model, water will flow across streams, rivers, lakes and other permanent water features when present, which are better represented in MERIT and NASADEM (see Section 5.1.1) and of course better represented at their higher resolution 90m versions. Their 1km versions are created by averaging higher resolution pixels, which means that water features less than a kilometer wide might not be included in the water mask and/or will see their elevation increase in the DEM due to inclusion of neighboring land pixels. This is illustrated in Figure 5-5, from which it can be seen that the 90m version contains far more water features, which are better connected and penetrate further inland. This will allow water to travel further inland as well and reach potentially low-lying areas which will then be inundated. Assuming that the (permanent) water mask is correct and that elevation is accurate as well, this should better match reality, which implies that, at least with the current setup, flood maps at 90m are more accurate and more in line with reality than their counterparts at 1km.

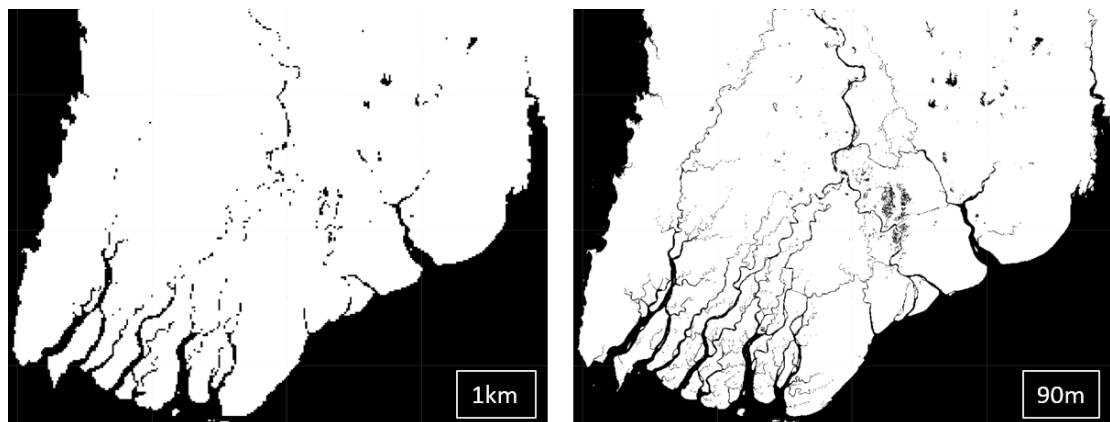


Figure 5-5: water mask over Irrawaddy delta in Myanmar at 1km (left) and 90m (right)

There are other factors that also play a role. Especially in South-East Asia (the only regions for which the LiDAR DTM is available at 1km instead of the globally available 5km), areas directly at the coast are often natural mangrove forests, which might not be properly (bias) corrected for canopy heights in the DEMs. As such, direct coastal flooding might be less than happens in reality, especially when derived with MERIT and NASADEM. In contrast, when water can further travel inland (at 90m resolution), it can reach non-mangrove areas with lower elevation and cause inundation there. This lower elevation can be inaccurate due to lack of more accurate data (e.g. vegetation, or at least thick, high canopies), but also because of overfitting/overestimation of bias correction (as might be the case in Bangladesh for NASADEM, see Section 5.1.1).

5.1.3

Flood map results

By performing a visual inspection, it can be observed that the 90m NASADEM and MERIT produce similar results regarding the flood extents and depths, with the NASADEM resulting in both, largest flood depths and extents. In comparison with the same DEMs at 1km, the 90m resolution results in significantly larger inland flooding. This is most likely due to the better representation of streams and rivers. Because hydraulic connectivity is included in the model, water can flow across (permanent) waterstreams/rivers when present. Because the NASA and MERIT DEMs at 1km resolution are the result of upscaling from 90m resolution, this water flow across water bodies also holds up to a certain extent. There are two flood events for which the 1km LiDAR DTM is available, A comparison of the results at 1km LiDAR with the other DEMs at 1km show a larger flood extent and water depths for Mala (Figure 5-7), and lower for Sidr (Figure 5-8). Due to the coarseness of the LiDAR 5km DTM, flooding in certain locations is neglected by the inundation model, or does not provide a sufficiently accurate flood extent compared to the 1km and 90m maps.

A comparison of the flood extent for all events, DEMs and the LiDAR DTM is provided in Annex B. For example, Figure 5-6 provides a summary of the total flooded area (in km²) for Storm Xynthia (also presented in Annex B). The area is calculated for the observed flood extent, as well as for the flood extent derived from the flood maps derived from the 5km LiDAR DTM, 1km and 90m NASADEM, and 1km and 90m MERIT DEM. The flood extent NASADEM at 90m resolution shows the best agreement with the observed flood extent. NASADEM at 1km and MERIT at 90m underestimate the flood extent by approximately 50 km², and MERIT 90m by approximately 100 km². The 5km LiDAR DTM overestimates the flooded area by a large margin of approximately 200%. The reason for the poor performance of the flood map derived with the 5km LiDAR DTM could be due to the coarseness of the grid with respect to the size of the study area, which does not define the flood extent very accurately (see Figure 4-3).

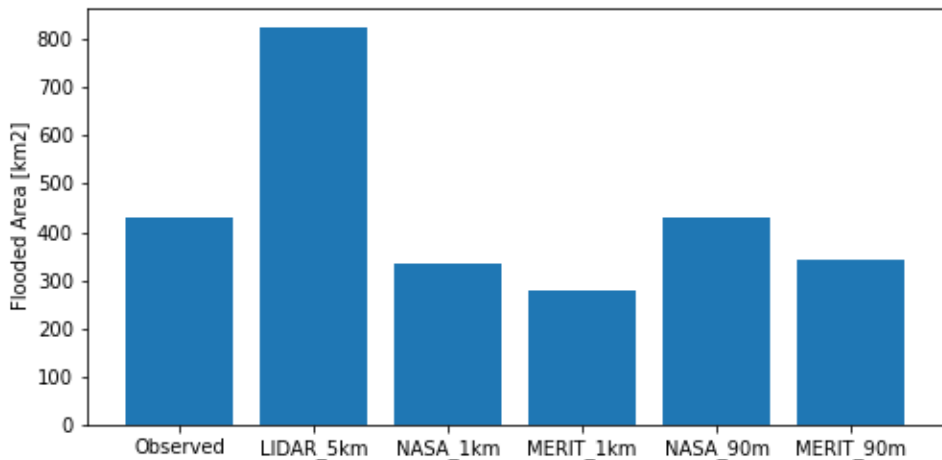


Figure 5-6 Flooded area in km² for the Xynthia event in 2010 for observations and model results for different DEMs

Tropical cyclone Mala (Myanmar, 2006)

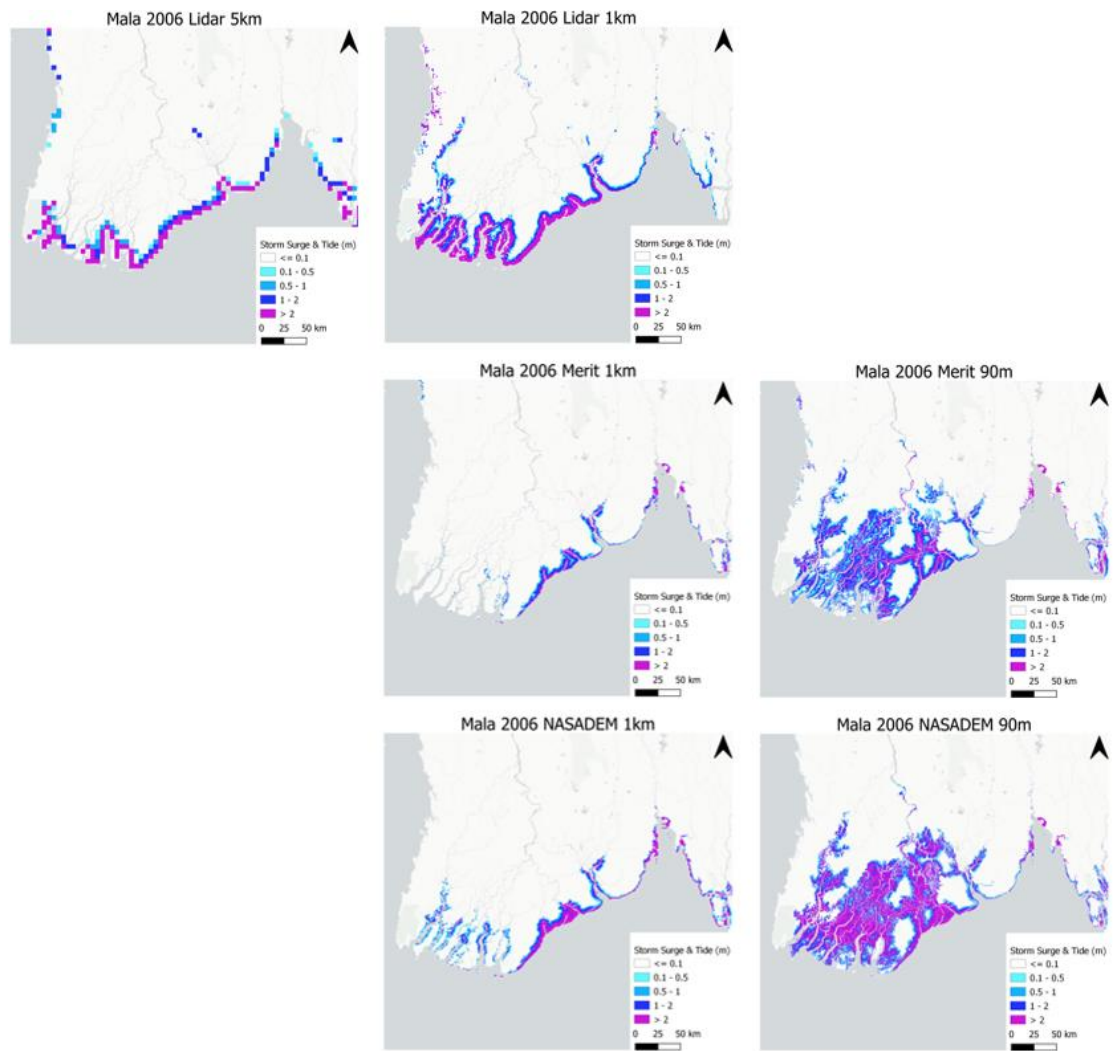


Figure 5-5 Inundation depth and extent for the Mala event in 2006, output of the model runs with four different DEMs with varying resolution.

Tropical cyclone Sidr (Bangladesh, 2007)

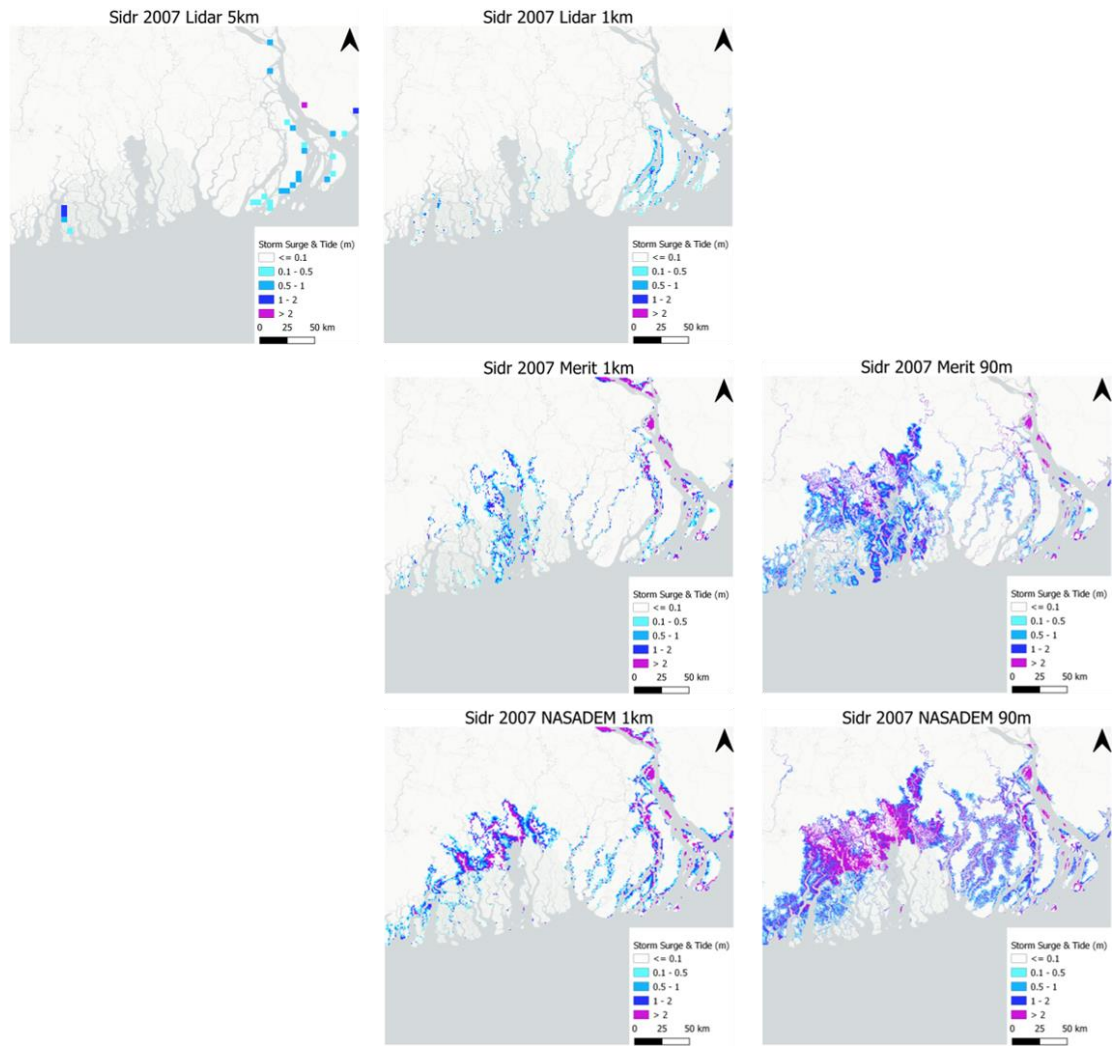


Figure 5-6 Inundation depth and extent for the Sidr event in 2007, output of the model runs with four different DEMs with varying resolution.

Storm Xynthia (France, 2010)

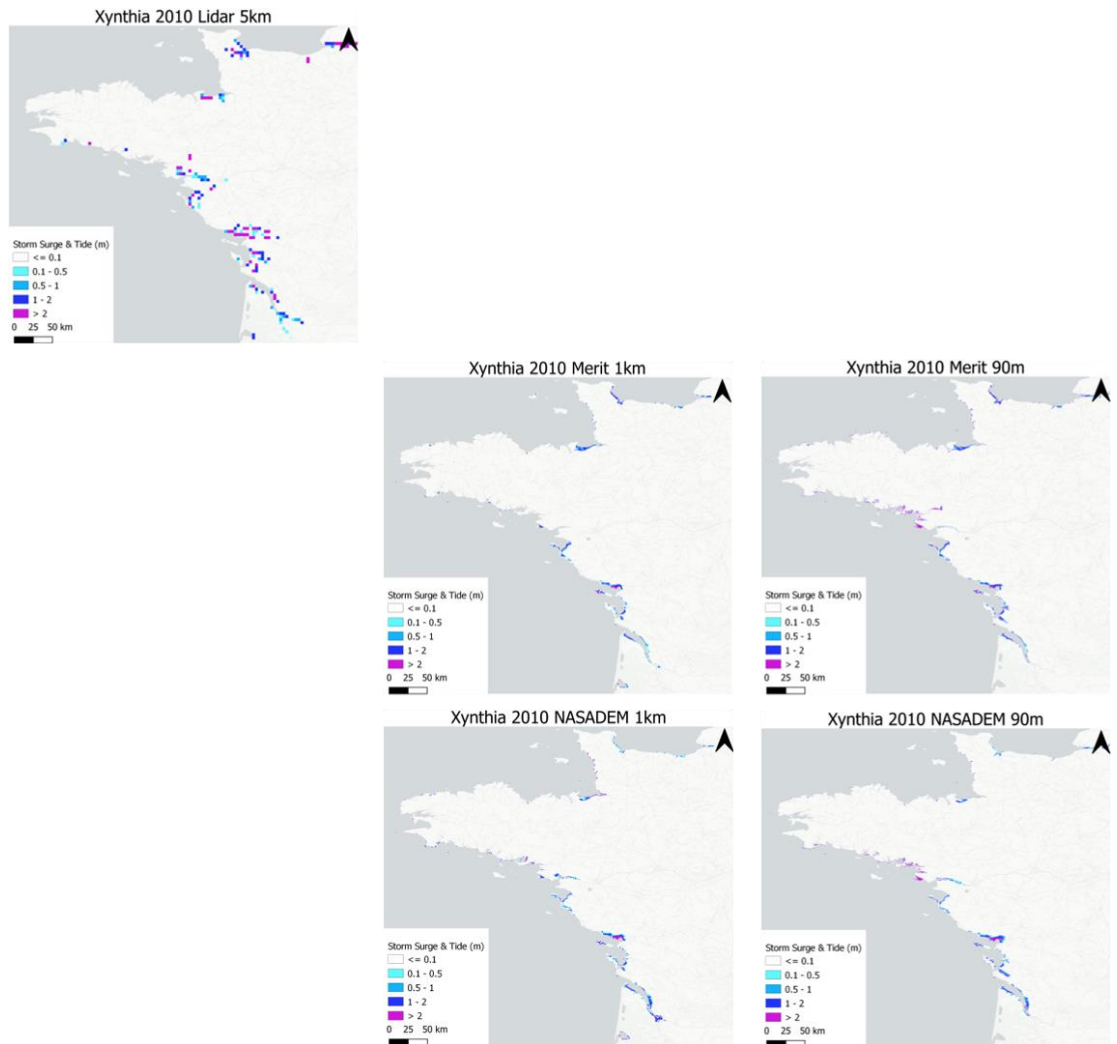


Figure 5-7 Inundation depth and extent for the Sidr event in 2007, output of the model runs with three different DEMs. with varying resolution.

5.2

Flood maps with return period

Table 5-1 presents the total flood extent computed with different DEMs. The flood extent is largest with the MERIT DEM at 90m resolution, followed by the NASA DEM at 90m resolution, despite having the same spatial resolution. The 90m resolution results are consistently higher than the 1km results for both DEMs.

It should also be noted that some areas show permanent inundation even under mean sea level (MSL) conditions and in the absence of storm surge and tides. This is most likely due to the fact that existing protective structures are not resolved in the NASA or MERIT DEMs. Low-lying areas below sea level that are hydrodynamically connected to the coast are being inundated. In practice, these areas would not be flooded because they are protected. A prime example of this is the Netherlands where 27% of the country - including the most densely populated areas - are below mean sea level. The Netherlands has invested heavily in flood protection to protect the low-lying areas from storms with a reoccurrence probability of 10^{-4} per year. Our modeling approach does not include protective structures, so they simulate flooding where none would be expected. Other reason for flood overestimation under MSL could be that MSL in GTSM is not the same as for the DEMs, and the correction with the mean dynamic topography (MDT) could still have large errors.

Table 5-1. Total area potentially exposed to flooding globally in 1000 km².

Year	Return Period	NASA1km	MERIT1km	NASA90m	MERIT90m
Present-day (2018)	MSL*	30	18	51	52
	1 in 250 years	317	320	403	456
Mid-century (2050)	MSL*	39	22	64	62
	1 in 250 years	337	344	430	491

* Permanent flood inundation due to mean sea level

Ignoring existing levels of protection, the largest areas per country currently exposed to potential flooding (i.e. more than 50,000 km² in a 100-year event), are countries in Southeast Asia, Australia and Northern America. Mediterranean and African countries are exposed to smaller potential flood extents (Figure 5-8). The largest relative increase in potentially flooded area due to sea-level rise is projection for countries in central America, South Asia and Western and Northern Africa.

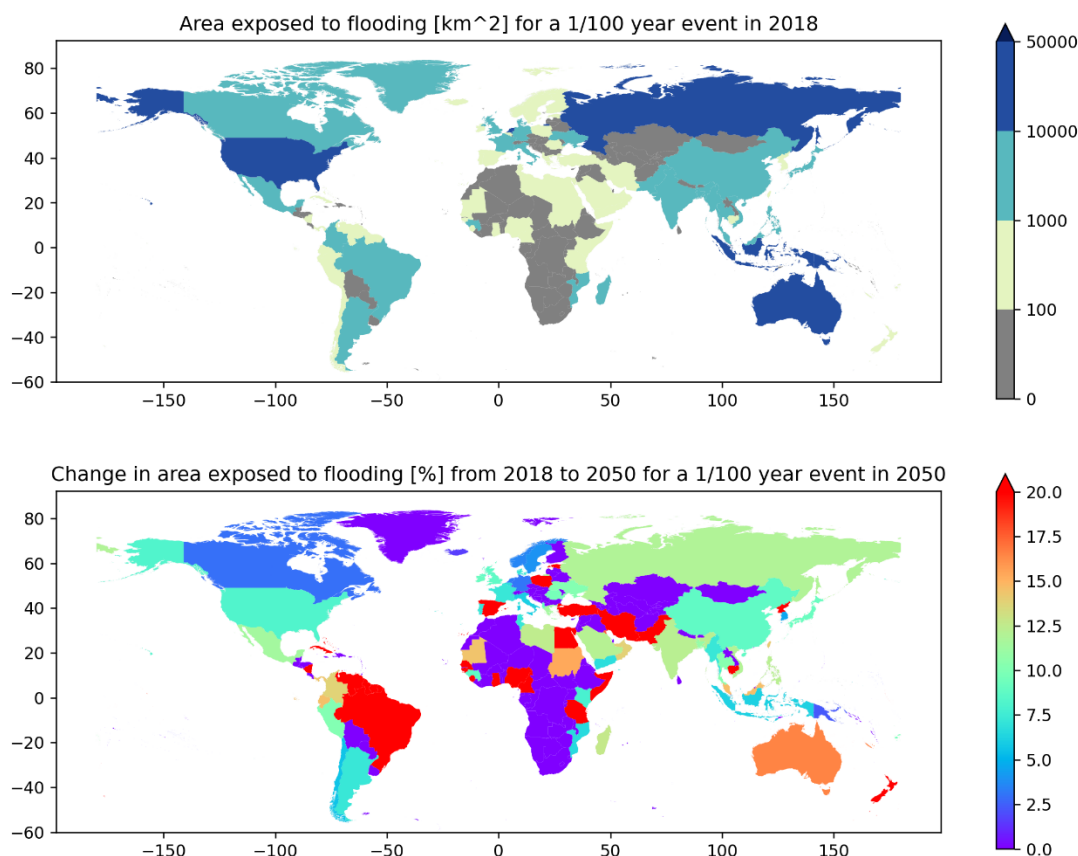


Figure 5-8. Top: Area exposed to potential flooding in a 1/100 year event and current MSL. Bottom: Change (in %) in area exposed to potential flooding in a 1/100 year event and projected mean sea level mid-century.

Figure 5-11 to 5-13 show the results from the inundation modeling along the southern US coastline for the three DEMs. The left column of the figures shows the flood extent based on present-day sea level, whereas the right column shows the flood extent based on projected sea level rise in 2050. The rows in the figures show different return periods, starting at a return period of zero, which represents the permanent inundation due to mean sea level alone.

Differences in inundation depths are a direct result of the differences between the DEMs, which impact inundation depths for all return periods. The inundation depth of DEMs and return periods are yet to be quantified and require further analysis. Results show that extreme sea levels are a more important driver of flooding than sea level rise until 2050. This is because sea level rise by 2050 is rather small. However, sea-level rise is accelerating and as such it may become a more important driver when projecting the flood extents for 2100. Results for other regions around the world are presented in Appendix C.

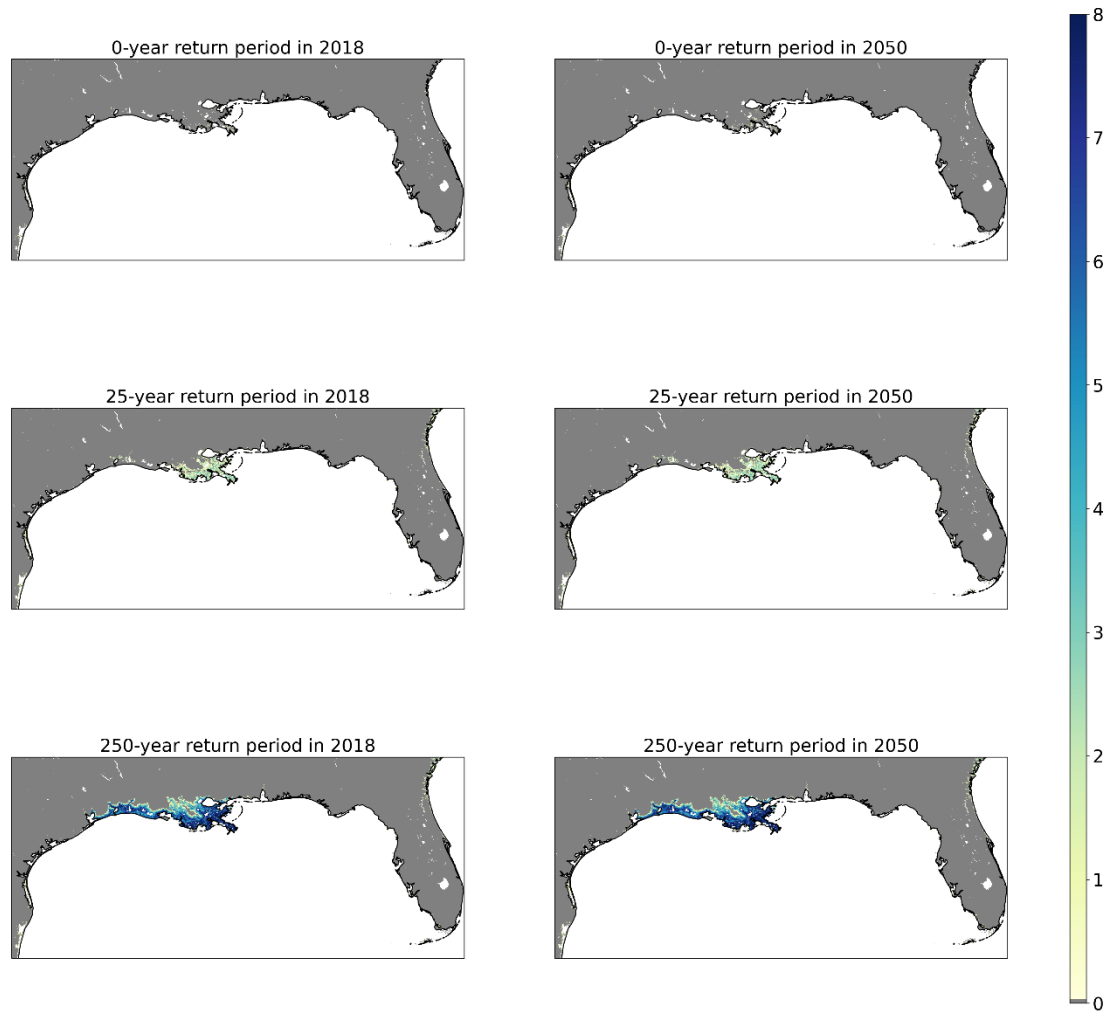


Figure 5-9 Inundation depth and extent along the southern US coast from the global flood maps with the MERIT DEM at a 90m resolution for the present-day sea level and the 2050 sea level rise projection and return periods of 0 (entirely sea level driven), 25 and 250 years

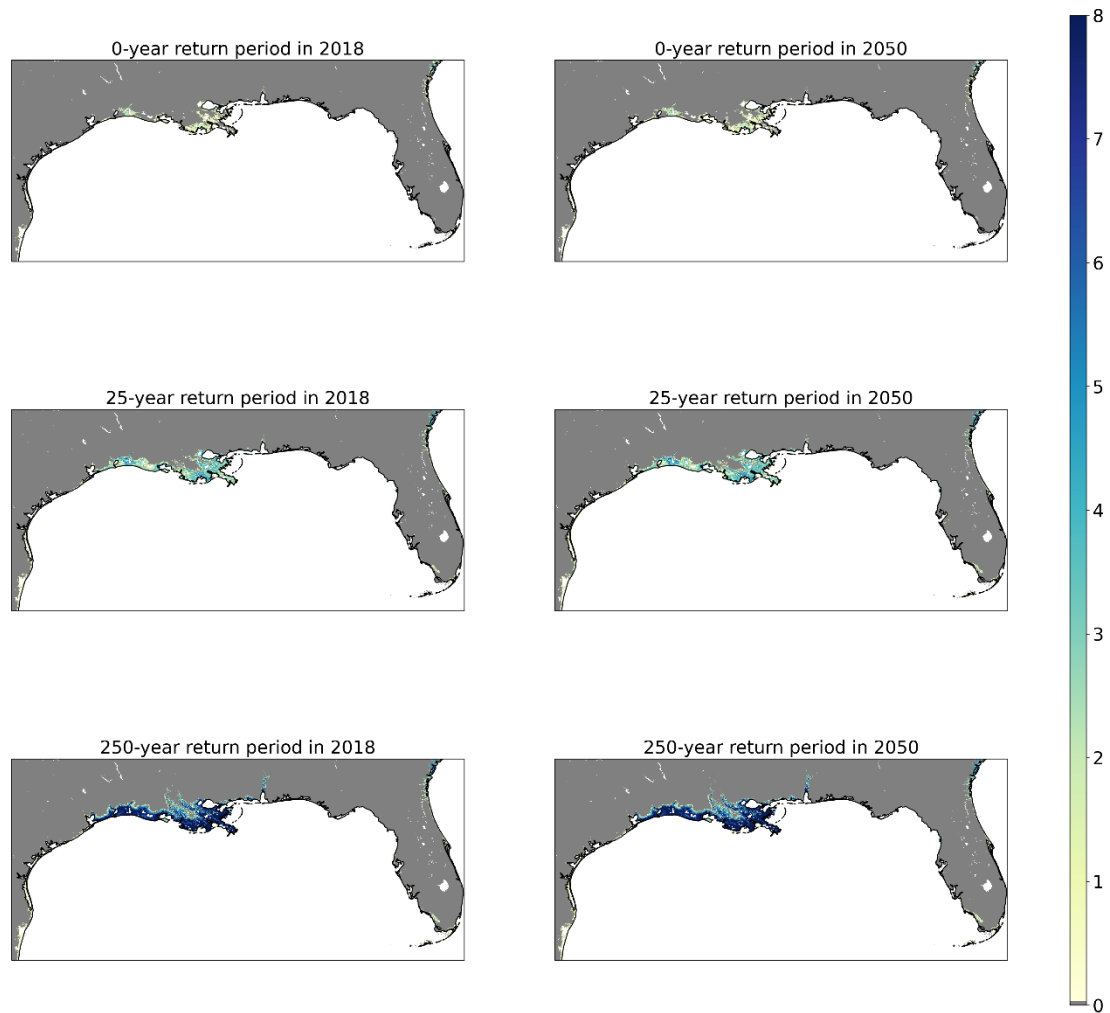


Figure 5-10 Inundation depth and extent along the southern US coast from the global flood maps with the NASA DEM at a 90m resolution for the present-day sea level and the 2050 sea level rise projection and return periods of 0 (entirely sea level driven), 25 and 250 years

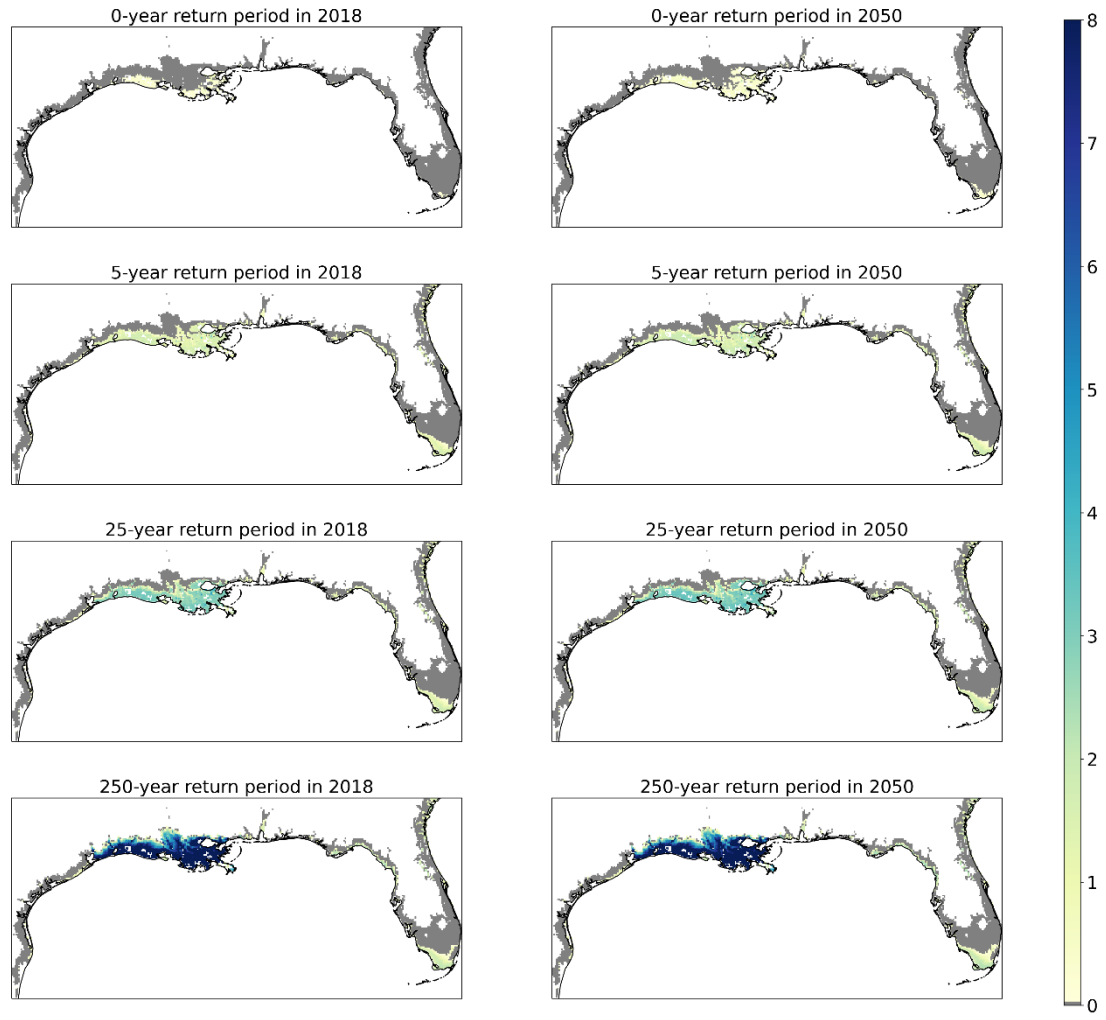


Figure 5-11 Inundation depth and extent along the southern US coast from the global flood maps with the LIDAR DEM at a 5km resolution for the present-day sea level and the 2050 sea level rise projection and return periods of 0 (entirely sea level driven), 5, 25 and 250 years

6 Limitation

This work of global high resolution coastal flood maps is affected by limitations due to uncertainties in input data and methodology adopted. It is important for the users to understand the limitations when use the dataset. Therefore, the limitations are listed below according to the importance and impact (ranked from high to low).

Various sources of uncertainties in the input data and assumptions are underlying the flood modeling. It is worth mentioning that this dataset is created by using the most up to date freely available global datasets, and is presented as is without further manipulation. The flood maps created in this study are unavoidably affected by uncertainties, and it is strongly recommended taking those uncertainties into account when interpreting the results and when applying the flood maps in real life applications, especially in local flood impact studies. The main limitations and uncertainties are detailed below.

The flood maps made in this study are coastal flood maps. The modeling approach accounts for flooding from tide, surge and sea-level rise. It does not resolve all physical processes that contribute to coastal flooding such as the effect of waves and flood duration. Moreover, the model does not account for the compound flooding due to a combination of rainfall and high river discharge in the coastal zone (e.g. estuary and delta). Tropical cyclones in particular often induce high surge levels but also generate extensive rainfall, with associated inland flooding. Consequently, the potential flood extent during historic events is mostly underestimated. In addition, the water masks used in the study are with uniform resistance factor of 0.5m/km (apart from permanent water bodies). In reality, the roughness will vary depending on land use. This adds to the uncertainty of the potential inland inundation extent particularly in low-lying delta regions.

The sea level rise (SLR) forcing used in this study is absolute SLR rather than relative SLR. Local subsidence due to tectonic movements or due to groundwater extraction is not accounted for. Particularly in densely populated delta regions that extract groundwater (e.g. Jakarta), local subsidence can exacerbate the effect of sea level rise considerably. Local subsidence can be combined with sea level rise to derive *relative* sea level rise. As to date there exist no global dataset with reliable estimates of relative sea level rise, this is recommended to consider in the future work.

Existing flood protection is not accounted for in the global DEMs, resulting in an overestimation of flooding in protected areas. This particularly affects the results for developed countries with high flood protection standards (e.g. in Europe and Northern America). It is recommended to include coastal flood protections in the flood modelling in the future work.

Due to the fact that observations for model validation are limited, two different options to validate the model (i.e. validation against satellite images and process-based models) were applied, each with their own limitations. Process-based models solve the physical equations of water flow and can thus more accurately simulate the flooding during a storm event. Some process-based models may also include the effects of waves and the compound flooding due to rainfall, surge and tide. These models are, however, computationally expensive. Furthermore, uncertainties exist that are related to the quality of the input data, model structure, numerical schemes, and model parameter estimation. For satellite images, peak flood extent can only be mapped if a satellite passed over the area at the peak of the event and if it was cloud free. These limitations make it feasible to conduct an extensive quantitative validation of the produced flood maps.

The results are based on coastal water levels that have been computed using the GTSM model. The GTSM model is a global 2D hydrodynamic model that is forced by large scale wind and pressure fields.

The main input to the model is meteorological forcing, provided by the ERA5 climate reanalysis. While ERA5 has a relatively high spatial resolution and good performance in general, the intensity of tropical cyclones is often underestimated in the resulting global climate model. Moreover, the global coastal resolution of 2.5km of GTSM (1.25 in European coasts) may be insufficient in areas with complex coastlines, such as semi-enclosed bays and barrier islands. Although the GTSM is calibrated and validated against historical measurements, the inherent uncertainties will propagate to the coastal water levels and then to the flood maps.

The global DEMs used as topographic data in this study have limited vertical accuracy. The vertical accuracy in low-lying coastal areas appears to be better than in mountain areas with steep slopes. However, the flood extent in the coastal areas are highly sensitive to the topography. The vertical accuracy of the DEM therefore has a major influence on the computed flood maps in coastal areas.

This dataset of calculated flood maps can be used as an indication of coastal flood extent due to extreme sea level on a large scale. This can be useful especially in data scarce areas where measurements and more detailed information about flooding is unavailable (e.g. developing countries, small island states). However, this dataset is not suitable for local studies such as flood mapping of a coastal city or for the design of coastal dykes despite high spatial resolution, due to the limitations and uncertainties mentioned above.

7 Future work

The current study has produced a global coastal flood extent dataset with return periods based on current climate and a mid-century sea level rise projection. Historical flood maps have been produced based on three DEMs with various resolutions down to 90m resolution. It is recommended that this dataset will be further improved in the future study.

First, we want to emphasize that, to add value to the current data and for potential users of this dataset it is highly important that the dataset remains up to date and maintained. Future updates of the dataset should also reflect new developments in the modeling and other new innovations in the field with regard to input data, such as meteorological forcing (ERA5), DEMs and water masks:

- The flood maps for the historical events should be kept up to date and include recent events (e.g. with ERA5 near real time updates). This can be achieved by simulating global extreme events in GTSM + flood model once ERA5 data become available.
- New flood maps should be produced when new return levels become available.
- The global datasets developed have a 90m spatial resolution for MERIT and NASA DEM, whereas the global LiDAR DTM has resolution of 5km. The LiDAR DTM can, for example, be further improved to 1km resolution, which would allow coastal flood maps to be produced based on high resolution LiDAR for the first time. In addition, modularization and parallelization of the script on Azure environment could improve the performance, making it more efficient to produce higher resolution datasets.
- The water mask file used in the current flood model accounts for uniform roughness over land and permanent water bodies such as rivers and lakes. To further refine the bathtub model, the attenuation factor could be linearly scaled to account for spatial variation in roughness based on the proportion of permanent water features in each model grid cell (Haer, 2018).

Another major priority with regard to adding more value to the current data is the inclusion of coastal flood protections. Moreover, the analysis can be extended to also investigate societal impacts:

- The bathtub model could be extended to include the effect of coastal protection. Although there is no global register of existing coastal protection infrastructure and their footprint is too small to be resolved in digital elevation/terrain models, a database exists that estimates the coastal protection standard per sub-country region (FLOPROS, Tiggeloven et al. 2020). The flood protection standards are expressed in return periods that the sub-country region is protected against. It is computed-based on the country's expected annual damage from flooding and the GDP of the country. This provides an indication of the country's incentive to protect against flooding and the financial resources of the country to build coastal defense structures. The database has been validated against known protection standards.

Second, the dataset can be updated by inclusion of more climate change and SLR scenarios.

- As the current dataset only accounts for the effect of sea level rise in the year 2050, this may not be useful for all users and purposes. Some users might be interested in long term impact and planning activities in e.g. 2100. The choice of the scenario will depend on user feedback.
- The next dataset could present how future coastal flood inundation will change due to *both* sea level rise and climate change (i.e. changes in wind and pressure fields). In addition, the dynamic interaction between sea level rise and tide/surge should be included. Flood maps based on baseline simulations (without sea level rise) could be compared to simulations based on future climate scenario runs (with sea level rise).

- Based on recently published data on global subsidence estimates (Herrera-García, et al. 2021), relative sea level rise (includes land subsidence) may also be considered in future model versions.
- The extreme sea levels used for the forcing at boundaries of the global flood model, have been computed in the GTSM with five high resolution CIMP6 climate models. A decision should be made to either select a single climate model or to use the median of all models. Bias correction will need to be applied to remove the spatial bias in the selected climate scenario run for future study.

Third, the flood maps can be provided in real time forecasting, which allows prediction of flood extent in real time with maximum lead time of 10 days. The forecasting flood maps can be updated every 6 to 12 hours at the global scale. These flood maps are important information for coastal early warning, disaster preparedness and prevention. The Global Storm Surge Information System (GLOSSIS), developed based on Delft-FEWS forecasting platform, can be updated with GTSM v4.0, which has higher spatial resolution and more output locations compared to its old version. GLOSSIS can be deployed with the latest cloud technology (e.g. docker/container) in Azure cloud.

Last, in addition to flooding driven by coastal process, the future dataset should represent the compound flooding by including processes such as rainfall and river discharge. For this reason the bathtub model probably need to be replaced by process-based flood models. Deltares has recently developed the SFINCS (Super-Fast INundation of CoastS) model, which is a computationally very efficient model that can be used to rapidly simulate compound flooding from storm surge and river discharge (Leijnse et al. 2020). The model has already been applied in regional coastal flood assessments, but it has not yet been applied at global scales. In order to better simulate the flood process, the extreme value statistics (e.g. return period) need to be expanded to time series-based hydrographs, for both river discharges and coastal water levels.

Reference

- Charnock, H. (1955) Wind Stress on a Water Surface. *Quarterly Journal of the Royal Meteorological Society*, 81, 639-640. <http://dx.doi.org/10.1002/qj.49708135027>
- Church, J. A., Clark, P. U., Cazenave, A., Gregory, J. M., Jevrejeva, S., Levermann, A., ... Unnikrishnan, A. S. (2013). *Sea Level Change. In: Climate Change 2013: The Physical Science Basis. Contribution of Working Group I to the Fifth Assessment Report of the Intergovernmental Panel on Climate Change [Stocker, T.F., D. Qin, G.-K. Plattner, M. Tignor, S.K. Allen, J. Bosch, Cambridge University Press, Cambridge, United Kingdom and New York, NY, USA.*
- Egbert and Ray (2001)
- Fritz, Hermann M, Jose C Borrero, Costas E Synolakis, Emile A Okal, Robert Weiss, Vasily V Titov, Bruce E Jaffe, et al. 2011. "Insights on the 2009 South Pacific Tsunami in Samoa and Tonga from Field Surveys and Numerical Simulations." *Earth-Science Reviews* 107 (1): 66–75. <https://doi.org/https://doi.org/10.1016/j.earscirev.2011.03.004>.
- Fritz, Hermann M, Chris Blount, Swe Thwin, Moe Kyaw Thu, and Nyein Chan. 2010. "Cyclone Nargis Storm Surge Flooding in Myanmar's Ayeyarwady River Delta BT - Indian Ocean Tropical Cyclones and Climate Change." In , edited by Yassine Charabi, 295–303. Dordrecht: Springer Netherlands. https://doi.org/10.1007/978-90-481-3109-9_34. Haarsma et al., 2016
- Haer, Toon, W J Wouter Botzen, Vincent van Roomen, Harry Connor, Jorge Zavala-Hidalgo, Dirk M Eilander, and Philip J Ward. 2018. "Coastal and River Flood Risk Analyses for Guiding Economically Optimal Flood Adaptation Policies: A Country-Scale Study for Mexico." *Philosophical Transactions of the Royal Society A: Mathematical, Physical and Engineering Sciences* 376 (2121): 20170329. <https://doi.org/10.1098/rsta.2017.0329>
- Hawker, L., Bates, P., Neal, J., & Rougier, J. (2018). Perspectives on digital elevation model (DEM) simulation for flood modeling in the absence of a high-accuracy open access global DEM. *Frontiers in Earth Science*, 6, 233.
- Herrera-García, Gerardo, Pablo Ezquerro, Roberto Tomás, Marta Béjar-Pizarro, Juan López-Vinyelles, Mauro Rossi, Rosa M Mateos, et al. 2021. "Mapping the Global Threat of Land Subsidence." *Science* 371 (6524): 34 LP – 36. <https://doi.org/10.1126/science.abb8549>.
- Hinkel, Jochen, Daniel Lincke, Athanasios T Vafeidis, Mahé Perrette, Robert James Nicholls, Richard S J Tol, Ben Marzeion, Xavier Fettweis, Cezar Ionescu, and Anders Levermann. 2014. "Coastal Flood Damage and Adaptation Costs under 21st Century Sea-Level Rise." *Proceedings of the National Academy of Sciences* 111 (9): 3292 LP – 3297. <https://doi.org/10.1073/pnas.1222469111>.
- Hope, M. E., Westerink, J. J., Kennedy, A. B., Kerr, P. C., Dietrich, J. C., Dawson, C., ... & Westerink, L. G. (2013). Hindcast and validation of Hurricane Ike (2008) waves, forerunner, and storm surge. *Journal of Geophysical Research: Oceans*, 118(9), 4424-4460.
- Kernkamp, H.W.J., Van Dam, A., Stelling, G.S. et al. Efficient scheme for the shallow water equations on unstructured grids with application to the Continental Shelf. *Ocean Dynamics* 61, 1175–1188 (2011). <https://doi.org/10.1007/s10236-011-0423-6>
- Kirezci, Ebru, Ian R Young, Roshanka Ranasinghe, Sanne Muis, Robert J Nicholls, Daniel Lincke, and Jochen Hinkel. 2020. "Projections of Global-Scale Extreme Sea Levels and

Resulting Episodic Coastal Flooding over the 21st Century." *Scientific Reports* 10 (1): 11629. <https://doi.org/10.1038/s41598-020-67736-6>.

Kolen, B., Slomp, R., Van Balen, W., Terpstra, T., Bottema, M., & Nieuwenhuis, S. (2010). Learning from French experiences with storm Xynthia; damages after a flood. *ISBN 978-90-77051-77-1*.

Leijnse, T., M. van Ormondt, K. Nederhoff, and A.R. van Dongeren. n.d. "Modeling Compound Flooding in Coastal Systems Using a Computationally Efficient Reduced-Physics Solver: Including Fluvial, Pluvial, Tidal, Wind- and Wave-Driven Processes." *Coastal Engineering*.

LP DAAC. (2020, February 13). Release of NASADEM Data Products. Earthdata. <https://lpdaac.usgs.gov/news/release-nasadem-data-products/>

Muis S, Irazoqui Apecechea M, Dullaart J, de Lima Rego J, Madsen KS, Su J, Yan K and Verlaan M (2020) A High-Resolution Global Dataset of Extreme Sea Levels, Tides, and Storm Surges, Including Future Projections. *Front. Mar. Sci.* 7:263. doi: 10.3389/fmars.2020.00263

National Hurricane Center and Central Pacific Hurricane Center. (n.d.). Historical SLOSH Simulations. https://www.nhc.noaa.gov/surge/HistoricalRuns/?large&parm=2008_ike#contents

National Weather Service. (n.d.). Hurricane Irma Local Report/Summary. Retrieved March 19, 2021, from <https://www.weather.gov/mfl/hurricaneirma>

National Weather Service. (n.d.-a). Hurricane Ike - September 2008. https://www.weather.gov/hgx/projects_ike08

NASA's Jet Propulsion Laboratory. (n.d.). NASADEM: Creating a New NASA Digital Elevation Model and Associated Products. Earthdata. Retrieved March 18, 2021, from <https://earthdata.nasa.gov/esds/competitive-programs/measures/nasadem>

Needham, H. F., Keim, B. D., Sathiaraj, D., & Shafer, M. (2013). A global database of tropical storm surges. *Eos, Transactions American Geophysical Union*, 94(24), 213-214.

Kirezci, Ebru, Ian R Young, Roshanka Ranasinghe, Sanne Muis, Robert J Nicholls, Daniel Lincke, and Jochen Hinkel. 2020. "Projections of Global-Scale Extreme Sea Levels and Resulting Episodic Coastal Flooding over the 21st Century." *Scientific Reports* 10 (1): 11629. <https://doi.org/10.1038/s41598-020-67736-6>.

Roberts, M., Camp, J., Seddon, J., & Ullrich. Paul (2020) Impact of Model Resolution on Tropical Cyclone Simulation Using the HighResMIP–PRIMAVERA Multimodel Ensemble. <https://doi.org/10.1175/JCLI-D-19-0639.1>

Tiggeloven, T, H de Moel, H C Winsemius, D Eilander, G Erkens, E Gebremedhin, A Diaz Loaiza, et al. 2020. "Global-Scale Benefit--Cost Analysis of Coastal Flood Adaptation to Different Flood Risk Drivers Using Structural Measures." *Natural Hazards and Earth System Sciences* 20 (4): 1025–44. <https://doi.org/10.5194/nhess-20-1025-2020>.

Uuemaa, E., Ahi, S., Montibeller, B., Muru, M., & Kmoch, A. (2020). Vertical Accuracy of Freely Available Global Digital Elevation Models (ASTER, AW3D30, MERIT, TanDEM-X, SRTM, and NASADEM). *Remote Sensing*, 12(21), 3482.

Vafeidis, Athanasios T, Mark Schuerch, Claudia Wolff, Tom Spencer, Jan L Merkens, Jochen Hinkel, Daniel Lincke, Sally Brown, and Robert J Nicholls. 2017. "Water-Level Attenuation in Broad-Scale Assessments of Exposure to Coastal Flooding: A Sensitivity Analysis." *Natural Hazards and Earth System Sciences Discussions*, 1–18.

Vernimmen, R.; Hooijer, A.; Pronk, M. New ICESat-2 Satellite LiDAR Data Allow First Global Lowland DTM Suitable for Accurate Coastal Flood Risk Assessment. *Remote Sens.* **2020**, *12*, 2827. <https://doi.org/10.3390/rs12172827>

Ward, P. J., Winsemius, H. C., Kuzma, S., Bierkens, M. F., Bouwman, A., De Moel, H., ... & Luo, T. (2020), Aqueduct Floods Methodology, Technical Note, World Resource Institute, URL: <https://files.wri.org/s3fs-public/aqueduct-floods-methodology.pdf>

Yamazaki, D., Ikeshima, D., Tawatari, R., Yamaguchi, T., O'Loughlin, F., Neal, J. C., ... & Bates, P. D. (2017). A high - accuracy map of global terrain elevations. *Geophysical Research Letters*, *44*(11), 5844-5853.

Yamazaki, D., Ikeshima, D., Sosa, J., Bates, P. D., Allen, G. H., & Pavelsky, T. M. (2019). MERIT Hydro: a high - resolution global hydrography map based on latest topography dataset. *Water Resources Research*, *55*(6), 5053-5073.

Annex

A List of historical events

Table 0-1. List of simulated historic surge events and their country, date and location of major impact and the peak storm surge level as simulated by the GTSM. The events have been sourced from the Surgedat database¹ and were amended with other high impact events.

Year	Name	Country	Date	Lat	Lon	Peak water level (from GTSM)
1980	Allen	US	11/08/1980	26.56	-97.42	2.72
1980	Danielle	US	07/09/1980	29.68	-93.84	0.79
1980	Jeanne	US	16/11/1980	26.47	-97.24	0.75
1981	Eddie	AU	13/08/1981	-16.99	139.08	2.34
1981	Thad	JP	25/08/1981	41.77	140.72	1.17
1981	Unnamed	BD	07/08/1981	20.94	87.46	2.28
1982	Chris	US	12/09/1982	29.76	-93.56	0.77
1982	Orissa Cyclone	IN	03/06/1983	20.82	86.97	2.48
1983	Alicia	US	21/04/1983	29.09	-95.12	0.88
1983	Barry	MX	29/04/1983	25.98	-97.15	0.84
1983	Oscar	FJ	06/03/1983	-18.41	178.10	1.37
1983	Veena	FR	14/04/1983	-14.93	-148.22	0.55
1984	Diana	US	16/09/1984	34.03	-77.89	1.25
1984	Jim	AU	09/03/1984	-14.88	135.42	4.04
1984	Kathy	AU	24/03/1984	-15.69	137.08	2.69
1984	Unnamed	IN	01/08/1984	20.28	86.67	2.55
1985	Bob	US	26/07/1985	32.78	-79.93	1.19
1985	Danny	US	20/08/1985	29.59	-92.15	1.64
1985	Elena	US	04/09/1985	29.72	-85.07	1.78
1985	Gloria	US	02/10/1985	40.70	-74.01	1.45
1985	Hina	FJ	20/03/1985	-18.18	177.59	1.29
1985	Juan	US	31/10/1985	30.00	-89.86	1.88
1985	Kate	US	26/11/1985	29.67	-85.33	1.95
1985	Sandy	AU	24/03/1985	-15.69	136.78	3.12
1985	Unnamed	BD	25/05/1985	21.74	91.29	4.46

¹ <http://surge.srcc.lsu.edu/>

1986	Bonnie	US	28/06/1986	29.68	-94.03	0.66
1986	Charley	US	30/08/1986	41.29	-70.10	2.93
1986	Unnamed	IN	12/08/1986	17.62	83.23	2.42
1987	Connie	AU	20/01/1987	-20.31	118.58	5.99
1987	Floyd	US	14/10/1987	24.65	-81.42	1.07
1987	Sally	CK	05/01/1987	-21.21	-159.77	0.86
1988	Beryl	US	10/08/1988	30.00	-89.86	1.12
1988	Chris	US	29/08/1988	32.03	-80.90	1.27
1988	Florence	US	11/09/1988	30.00	-89.86	1.39
1988	Gilbert	JM	20/09/1988	22.16	-87.17	1.59
1988	Herbie	AU	19/05/1988	-25.93	113.53	2.47
1988	Keith	US	24/11/1988	28.36	-81.80	1.77
1989	Allison	US	30/06/1989	29.87	-93.94	0.80
1989	Chantal	US	03/08/1989	29.55	-94.39	0.99
1989	Felicity	AU	15/12/1989	-16.48	141.31	2.40
1989	Hugo	FR	17/09/1989	24.64	-70.59	3.54
1989	Jerry	US	16/10/1989	29.72	-95.01	1.13
1989	Kavali Cyclone	IN	09/11/1989	15.43	80.17	1.05
1989	Orson	AU	24/04/1989	-20.66	116.70	6.45
1990	Andhra	IN	09/05/1990	15.88	80.72	1.17
1990	Marco	US	13/10/1990	26.44	-82.04	1.14
1991	9119 (Mireille)	JP	27/09/1991	34.01	131.15	2.94
1991	Bob	US	29/08/1991	41.39	-71.48	2.35
1991	Chittagong	BD	01/04/1991	21.60	90.00	2.39
1991	Chittagong Cyclone - Cyclone Gorky	BD	19/04/1991	22.35	91.76	2.39
1992	Andrew	BS	26/08/1992	27.36	-83.65	1.50
1992	Danielle	US	26/09/1992	35.24	-75.53	1.49
1992	Fran	AU	16/03/1992	-24.78	152.42	3.57
1992	Ian	AU	03/03/1992	-20.71	115.46	6.34
1992	Iniki	US	13/09/1992	21.88	-159.46	0.57
1992	Tuticorin Cyclone	IN	17/11/1992	8.96	78.21	0.93
1993	Arlene	US	21/06/1993	28.70	-96.22	1.04

1993	China No. 9315	CN	14/09/1993	31.86	121.24	4.55
1993	China No. 9316	CN	17/09/1993	22.75	113.61	2.53
1993	Emily	US	01/09/1993	35.27	-75.54	1.37
1993	Karaikal Cyclone	IN	04/12/1993	11.00	79.85	0.73
1994	Alberto	US	07/07/1994	30.39	-86.55	0.98
1994	Annette	AU	19/12/1994	-19.70	120.81	7.82
1994	Beryl	US	19/08/1994	29.73	-84.98	1.34
1994	China No. 9417 (Fred)	CN	23/08/1994	27.84	120.85	3.45
1994	Doug	CN	12/08/1994	25.10	121.92	3.45
1994	Gordon	US	21/11/1994	24.78	-81.14	1.38
1995	Allison	US	11/06/1995	29.98	-83.81	1.76
1995	Bobby	AU	27/02/1995	-20.78	116.67	5.91
1995	Erin	US	06/08/1995	30.38	-86.86	1.28
1995	Jerry	US	28/08/1995	28.75	-82.64	1.39
1995	Opal	US	06/10/1995	30.26	-85.97	2.04
1995	Roxanne	MX	21/10/1995	20.08	-87.48	1.16
1995	Warren	AU	06/03/1995	-17.46	140.83	2.10
1996	Arthur	US	21/06/1996	34.61	-76.54	1.28
1996	Barry	AU	07/01/1996	-16.19	141.37	2.19
1996	Bertha	US	14/07/1996	34.37	-77.63	1.32
1996	Edouard	US	06/09/1996	41.24	-69.99	3.95
1996	Ethel	AU	13/03/1996	-12.67	141.86	2.40
1996	Josephine	US	08/10/1996	29.32	-83.14	1.92
1996	Kakinada Cyclone	IN	07/11/1996	16.95	82.27	2.06
1996	Lili	US	29/10/1996	24.56	-81.68	1.92
1997	Danny	US	26/07/1997	33.09	-83.16	1.22
1997	Rachel	AU	08/01/1997	-20.31	118.57	5.85
1997	Winnie	CN	18/08/1997	31.00	122.00	4.50
1998	Bonnie	US	30/08/1998	33.97	-77.91	1.98
1998	Charley	US	24/08/1998	29.29	-94.79	0.73
1998	Earl	US	08/09/1998	29.81	-84.73	2.25
1998	Frances	US	13/09/1998	28.68	-95.98	1.85

1998	Georges	PR	30/09/1998	24.36	-77.30	2.25
1998	Mitch	HN	05/11/1998	22.42	-82.21	2.29
1998	Thelma	AU	14/12/1998	-11.42	130.67	5.20
1999	Bart	JP	30/09/1999	32.64	130.65	4.77
1999	Bret	US	25/08/1999	26.56	-97.28	1.35
1999	Dennis	US	08/09/1999	35.03	-76.69	1.71
1999	Floyd	BS	19/09/1999	30.30	-78.18	1.71
1999	Harvey	US	22/09/1999	26.88	-82.06	1.50
1999	Irene	US	19/10/1999	27.69	-81.29	1.17
1999	John	AU	16/12/1999	-20.31	118.58	5.75
1999	Odisha	IN	04/11/1999	20.28	86.67	2.17
1999	Vance	AU	24/03/1999	-21.80	114.74	6.20
2000	Gordon	US	21/09/2000	27.92	-82.84	1.19
2000	Helene	US	25/09/2000	30.40	-86.47	1.14
2000	Keith	BZ	06/10/2000	17.74	-88.02	2.12
2000	Rosita	AU	21/04/2000	-18.20	122.26	8.42
2000	Suptrob 13	CA	29/10/2000	47.05	-64.83	4.02
2001	Allison	US	19/06/2001	29.18	-94.97	1.03
2001	Barry	US	08/08/2001	30.33	-86.19	1.01
2001	Gabrielle	US	21/09/2001	26.77	-82.06	1.55
2001	Iris	BZ	09/10/2001	16.52	-88.37	2.31
2001	Michelle	US	06/11/2001	24.66	-81.36	1.19
2002	Bertha	US	09/08/2002	30.33	-89.33	0.66
2002	Chris	AU	07/02/2002	-19.85	120.41	8.19
2002	Fay	US	11/09/2002	28.83	-95.50	1.07
2002	Gustav	CA	12/09/2002	40.90	-69.30	4.08
2002	Hanna	US	15/09/2002	30.36	-89.09	1.83
2002	Isidore	US	27/09/2002	30.17	-89.73	1.83
2002	Kenna	MX	26/10/2002	21.53	-105.24	1.04
2002	Kyle	US	12/10/2002	32.78	-79.93	1.22
2002	Lili	US	04/10/2002	29.57	-91.42	2.27
2003	Bill	US	03/07/2003	30.00	-89.86	1.71

2003	Claudette	US	17/07/2006	28.92	-95.39	1.71
2003	Craig	AU	12/03/2003	-11.46	132.24	5.22
2003	Grace	US	02/09/2003	29.29	-94.79	0.69
2003	Isabel	US	25/09/2003	36.05	-75.68	2.24
2003	Juan	CA	29/09/2003	44.63	-63.58	4.12
2004	Alex	US	06/08/2004	35.27	-75.54	1.25
2004	Bonnie	US	14/08/2004	29.14	-83.03	1.35
2004	Chaba	JP	30/08/2005	34.78	134.67	3.05
2004	Charley	US	15/08/2004	30.18	-80.05	1.35
2004	Frances	US	10/09/2004	30.41	-81.12	2.67
2004	Gaston	US	01/09/2004	33.00	-76.58	1.55
2004	Ivan	US	24/09/2004	30.06	-90.33	2.67
2004	Jeanne	US	29/09/2004	29.14	-83.04	2.67
2004	Matthew	US	11/10/2004	30.11	-90.43	0.99
2005	Arlene	US	14/06/2005	30.33	-86.19	1.47
2005	China No. 0518 (Damrey)	CN	28/09/2005	19.54	110.82	2.53
2005	Cindy	US	11/07/2005	30.23	-87.95	2.43
2005	Dennis	US	18/07/2005	29.14	-84.38	2.43
2005	Emily	US	21/07/2005	26.02	-97.15	1.55
2005	Ingrid	AU	17/03/2005	-12.78	135.29	8.42
2005	Katrina	US	29/08/2005	27.70	-85.21	6.09
2005	Matsa	CN	06/08/2005	31.00	122.00	3.75
2005	Ophelia	US	17/09/2005	30.40	-81.43	1.30
2005	Percy	NZ	26/02/2021	-9.20	-171.85	0.99
2005	Rita	US	26/09/2005	27.17	-87.47	3.28
2005	Tammy	US	06/10/2005	32.03	-80.90	1.34
2005	Wilma	US	26/10/2005	25.08	-81.13	2.77
2006	Alberto	US	14/06/2006	30.41	-81.76	1.56
2006	Ernesto	US	01/09/2006	28.37	-81.00	1.19
2006	Glenda	AU	31/03/2006	-20.76	116.62	6.38
2006	Larry	AU	20/03/2006	-17.83	146.10	3.72
2006	Mala	MM	29/04/2006	17.39	94.57	5.17

2006	Monica	AU	25/08/2006	-12.59	138.72	5.21
2007	Andrea	US	05/11/2007	31.13	-81.40	1.34
2007	Dean	MX	13/08/2007	19.60	-87.75	1.22
2007	Erin	US	19/08/2007	29.18	-94.97	0.75
2007	Felix	NI	06/09/2007	14.77	-83.32	2.39
2007	Gonu	OM	07/06/2007	22.53	59.80	1.87
2007	Humberto	US	14/09/2007	29.68	-93.84	0.72
2007	Sidr	BD	15/11/2007	21.72	89.40	2.47
2008	Dolly	US	27/07/2008	26.35	-97.21	1.14
2008	Fay	US	28/08/2008	25.85	-81.39	1.40
2008	Gustav	US	05/09/2008	27.15	-85.36	4.84
2008	Hanna	US	08/09/2008	34.16	-77.88	1.45
2008	Ike	US	15/09/2008	27.72	-87.32	4.84
2008	Nargis	MM	03/05/2008	15.82	94.81	4.84
2008	Omar	AG	21/10/2008	17.19	-61.87	0.53
2008	Paloma	KY	14/11/2008	19.71	-79.80	0.85
2009	Claudette	US	16/08/2009	29.68	-85.23	0.00
2009	Ida	US	10/11/2010	29.60	-89.62	0.00
2010	Alex	US	02/07/2010	28.62	-96.62	0.89
2010	Earl	US	06/09/2010	35.55	-75.61	1.43
2010	Hermine	US	09/09/2010	28.62	-96.62	0.85
2010	Paul	AU	10/04/2010	-13.86	136.42	3.24
2010	Xynthia	FR	28/02/2010	46.30	-1.40	7.87
2011	Bingiza	MG	14/02/2011	-16.03	49.68	3.27
2011	Don	US	30/07/2011	27.58	-97.22	0.65
2011	Irene	US	27/08/2011	40.58	-73.66	2.31
2011	Lee	US	05/09/2011	30.03	-90.04	1.36
2011	Thane	IN	30/11/2011	11.94	79.84	0.90
2011	Yasi	AU	02/02/2011	-18.26	146.03	3.82
2012	Debby	US	27/06/2012	29.14	-83.03	1.51
2012	Evan	WS	19/12/2012	-13.83	-171.77	0.97
2012	Isaac	US	01/09/2012	29.57	-89.77	0.75

2012	Sandy	US	29/10/2012	40.54	-73.77	2.92
2013	Haiyan	PH	18/11/2013	11.21	125.01	2.71
2017	Irma	US	10/09/2017	24.00	-86.00	

B

Flooded area for each historic event

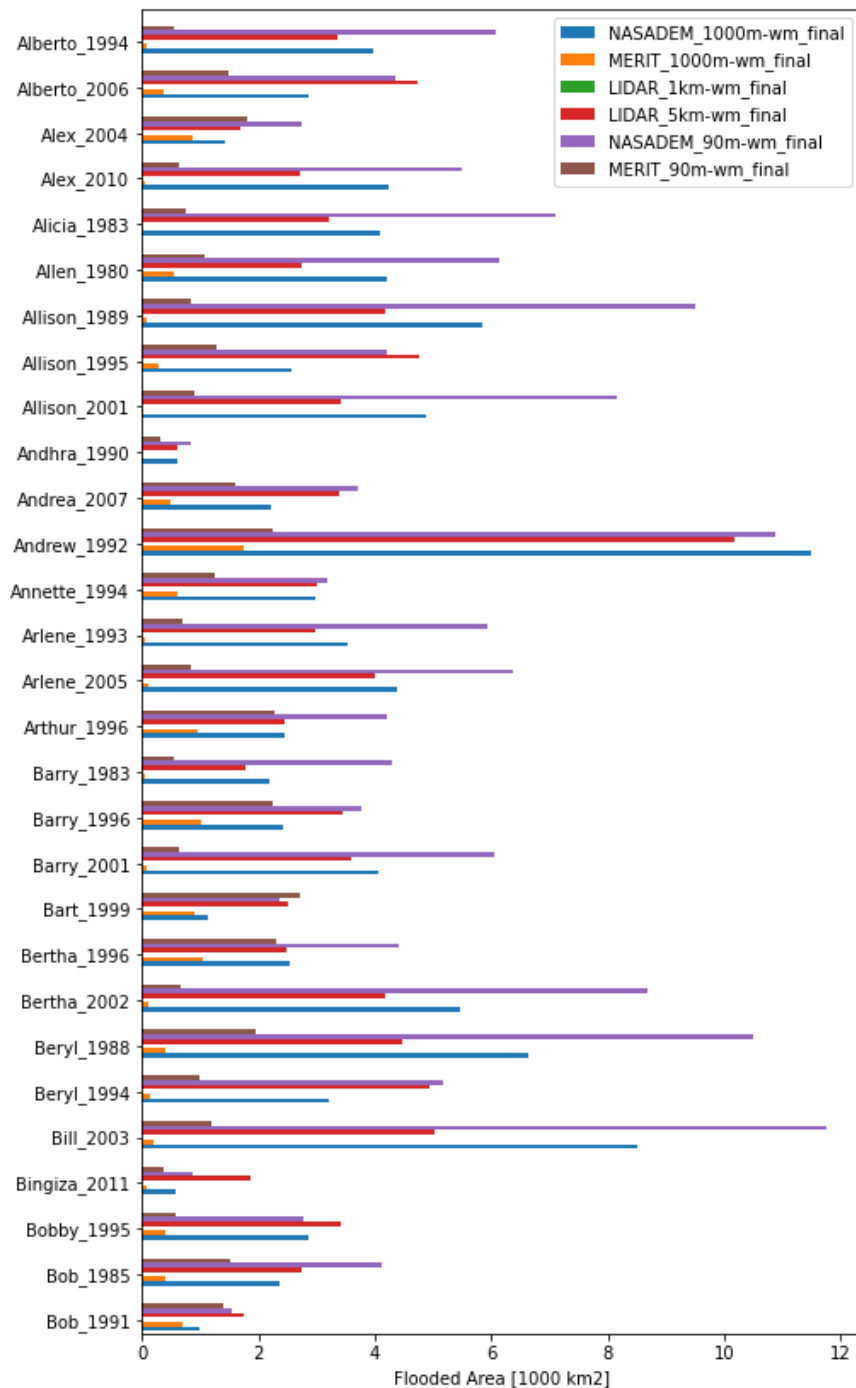


Figure 0-1. Flooded Area simulated for each event with the different DEMs. Note that LIDAR at 1km resolution was only available for selected regions: Part 1/6. This overview continues on the following pages.

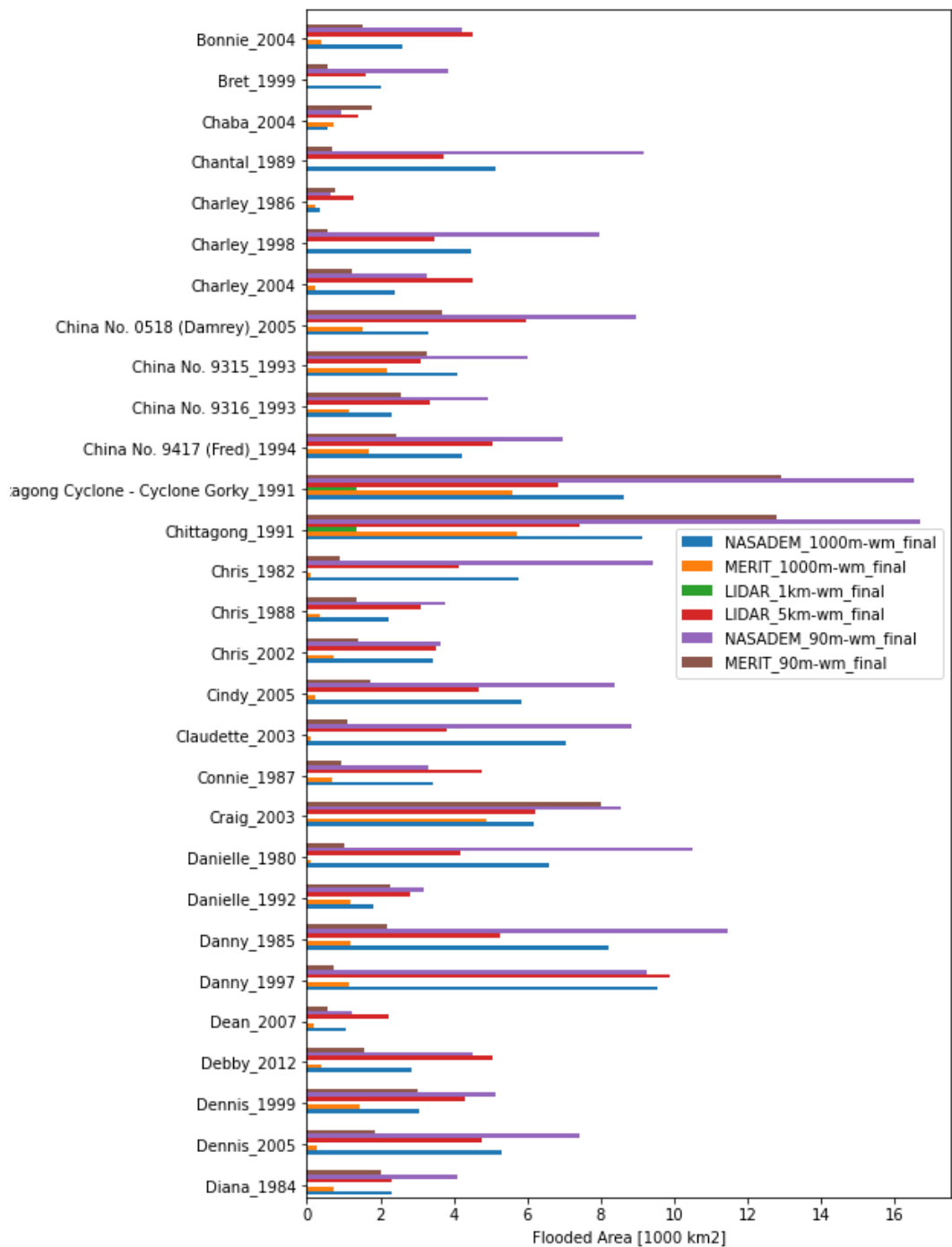


Figure 0-2. Flooded Area simulated for each event with the different DEMs. Note that LIDAR at 1km resolution was only available for selected regions: Part 2/6. This overview continues on the following pages.

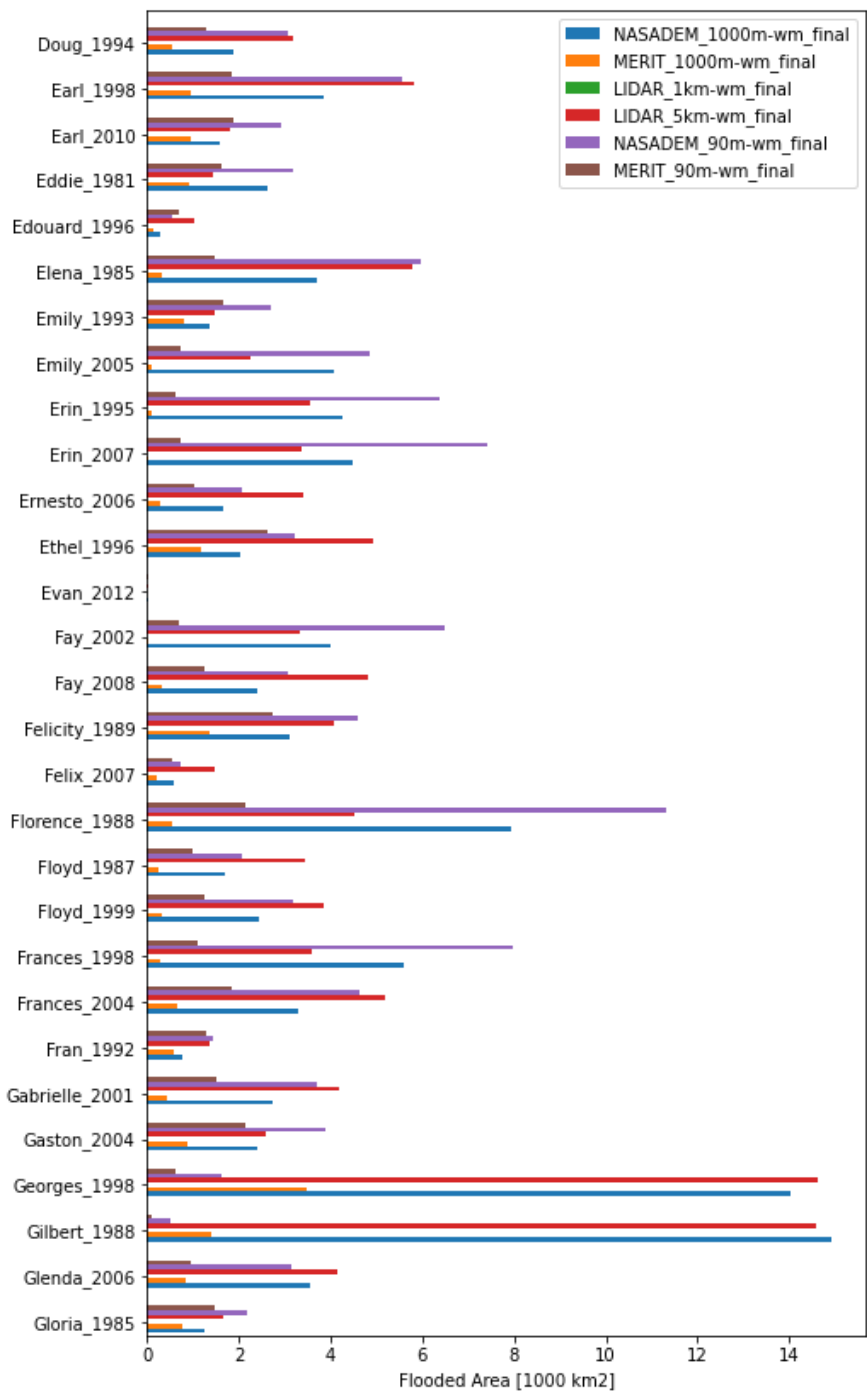


Figure 0-3. Flooded Area simulated for each event with the different DEMs. Note that LIDAR at 1km resolution was only available for selected regions: Part 3/6. This overview continues on the following pages.

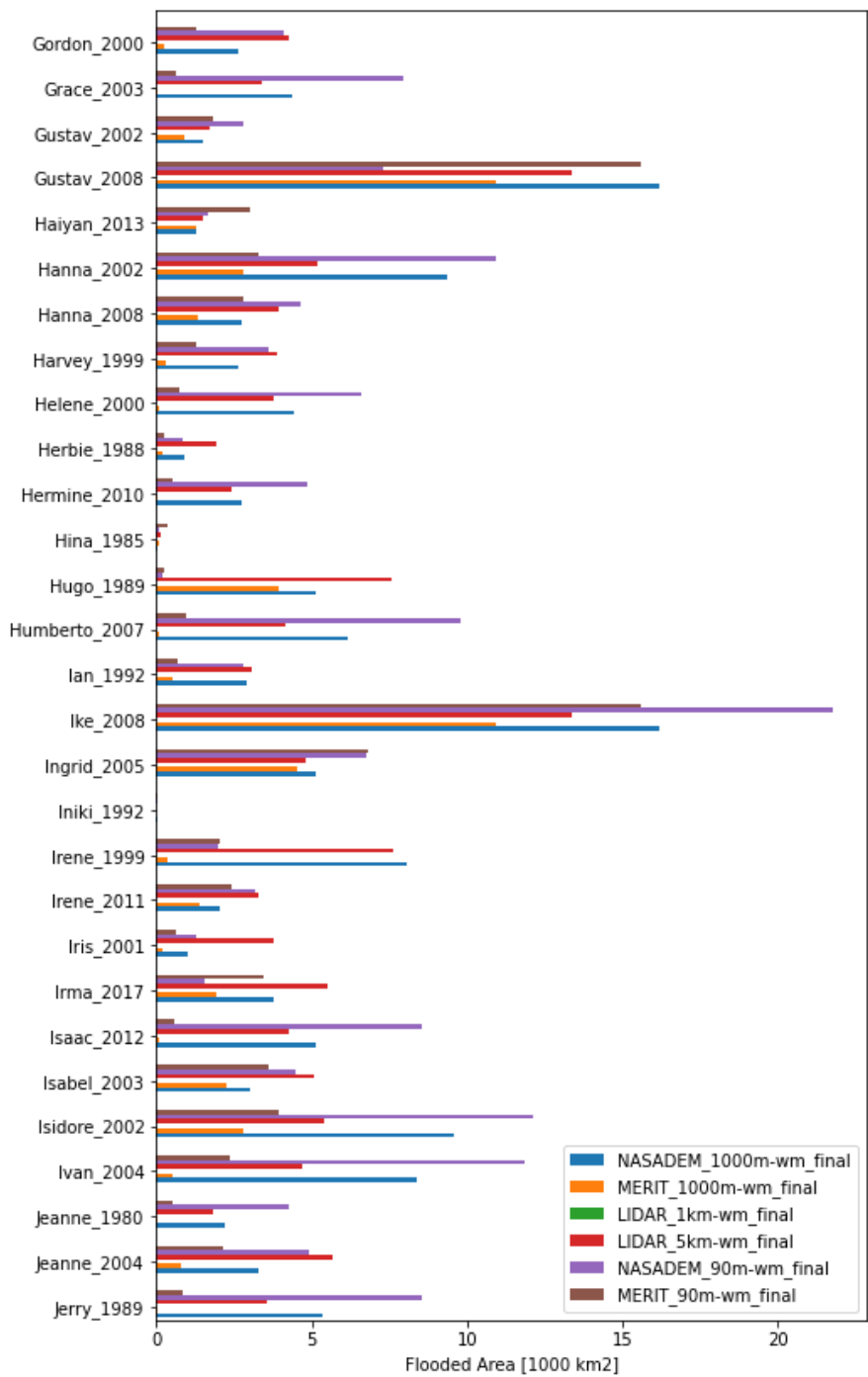


Figure 0-4. Flooded Area simulated for each event with the different DEMs. Note that LIDAR at 1km resolution was only available for selected regions: Part 4/6. This overview continues on the following pages.

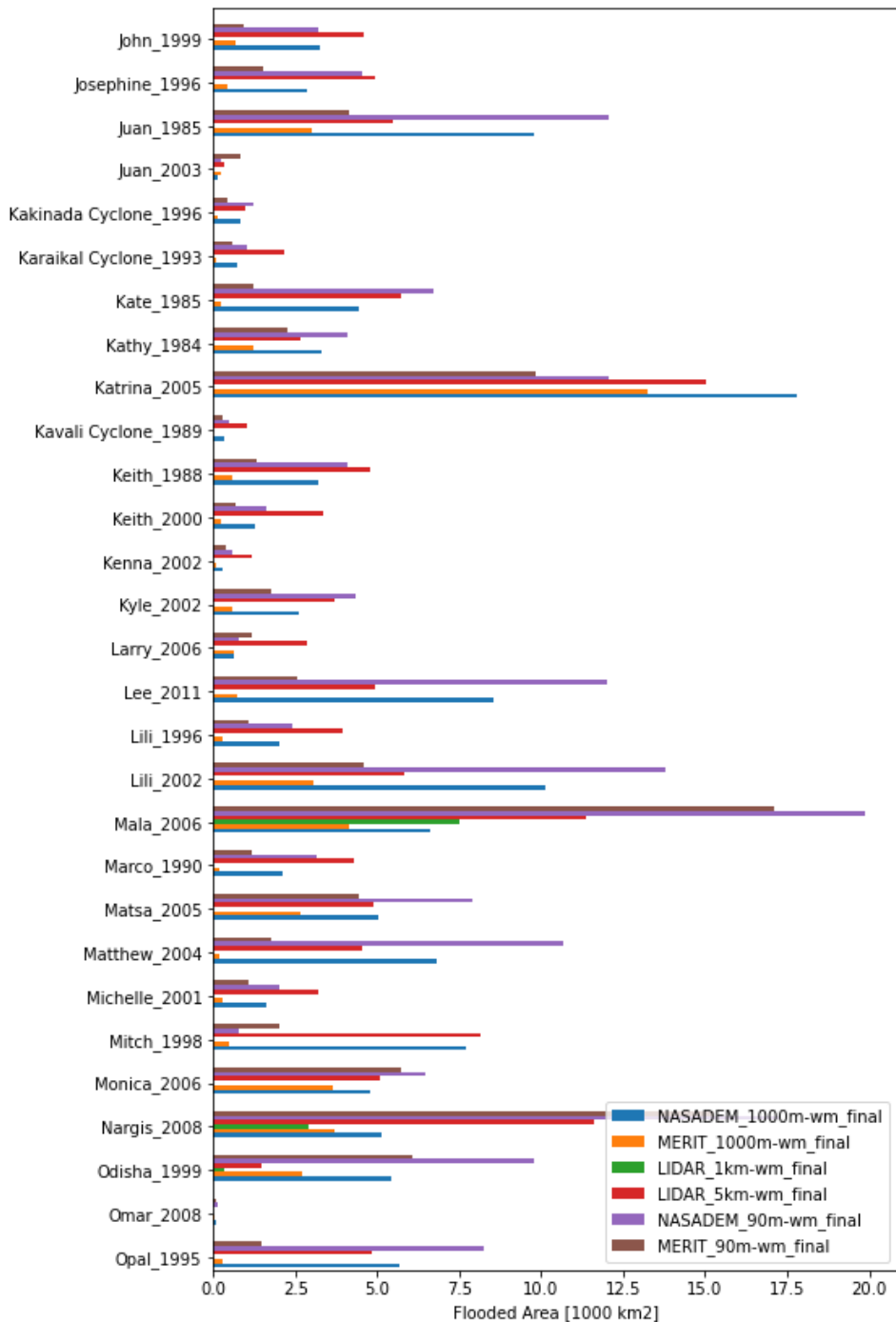


Figure 0-5. Flooded Area simulated for each event with the different DEMs. Note that LIDAR at 1km resolution was only available for selected regions: Part 5/6. This overview continues on the following pages.

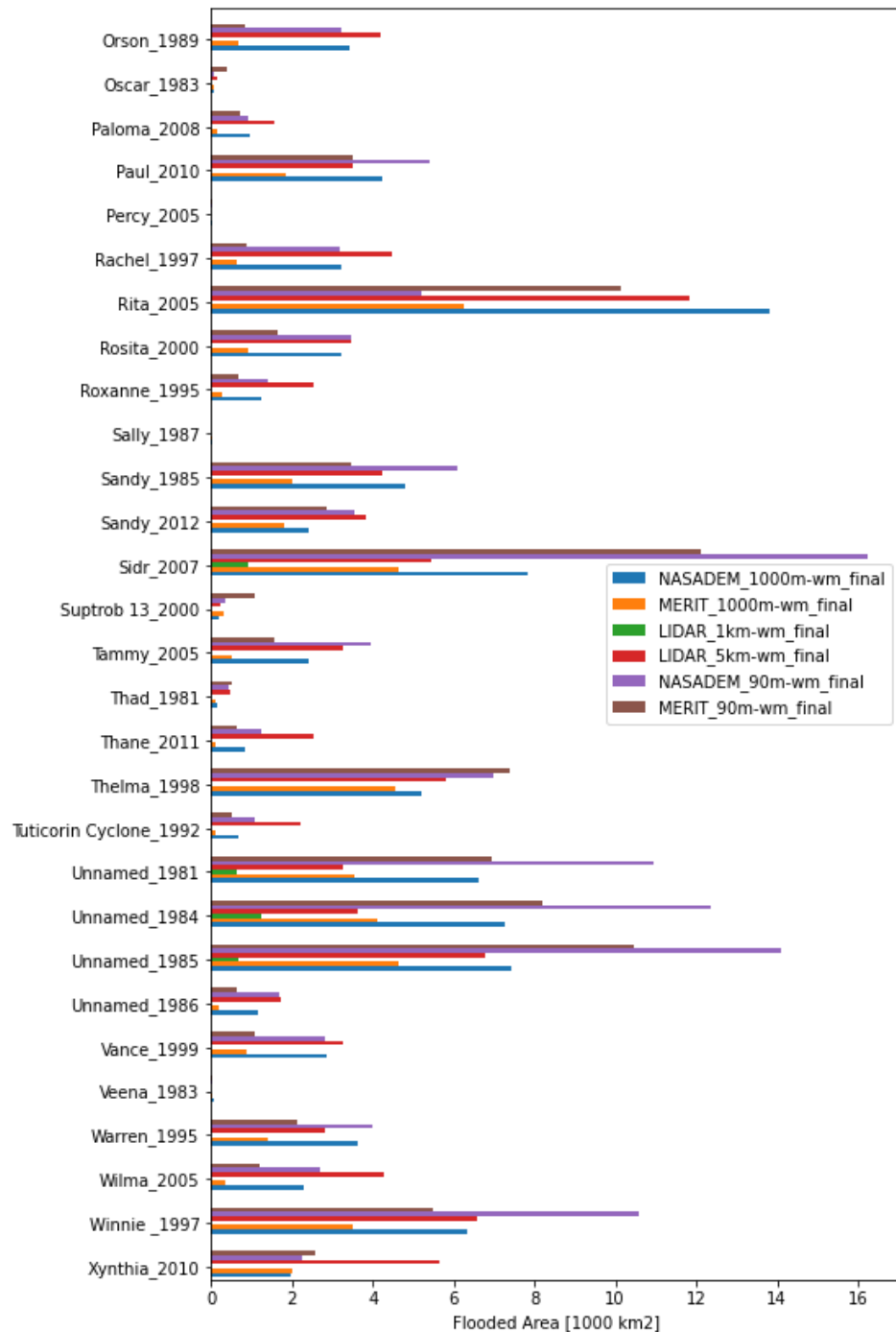


Figure 0-6. Flooded Area simulated for each event with the different DEMs. Note that LIDAR at 1km resolution was only available for selected regions: Part 6/6.

C Additional global flood map results

C.1 Northwestern Europe

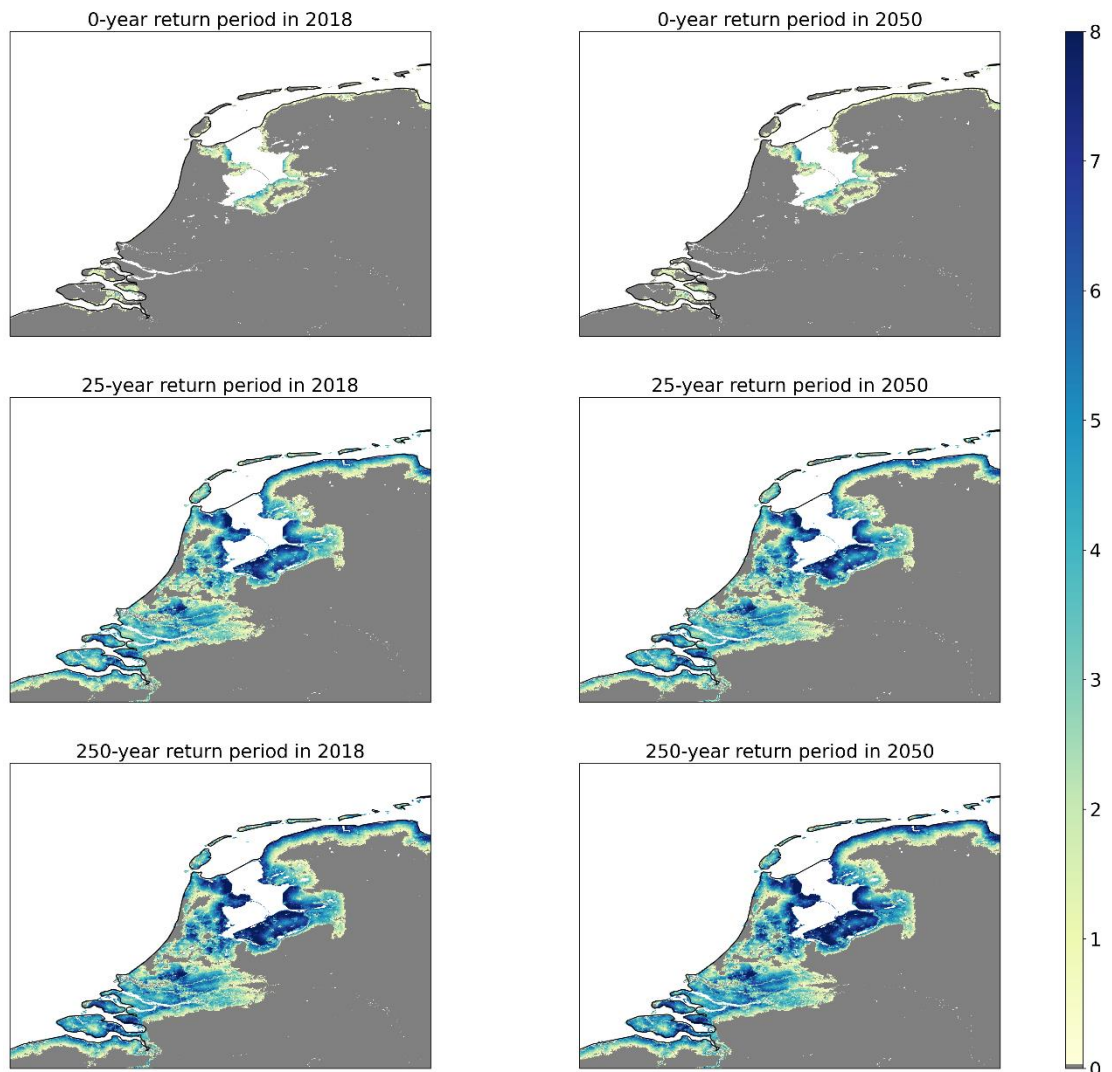


Figure 0-0-7 Inundation depth and extent in the Netherlands with the MERIT DEM at 90m resolution

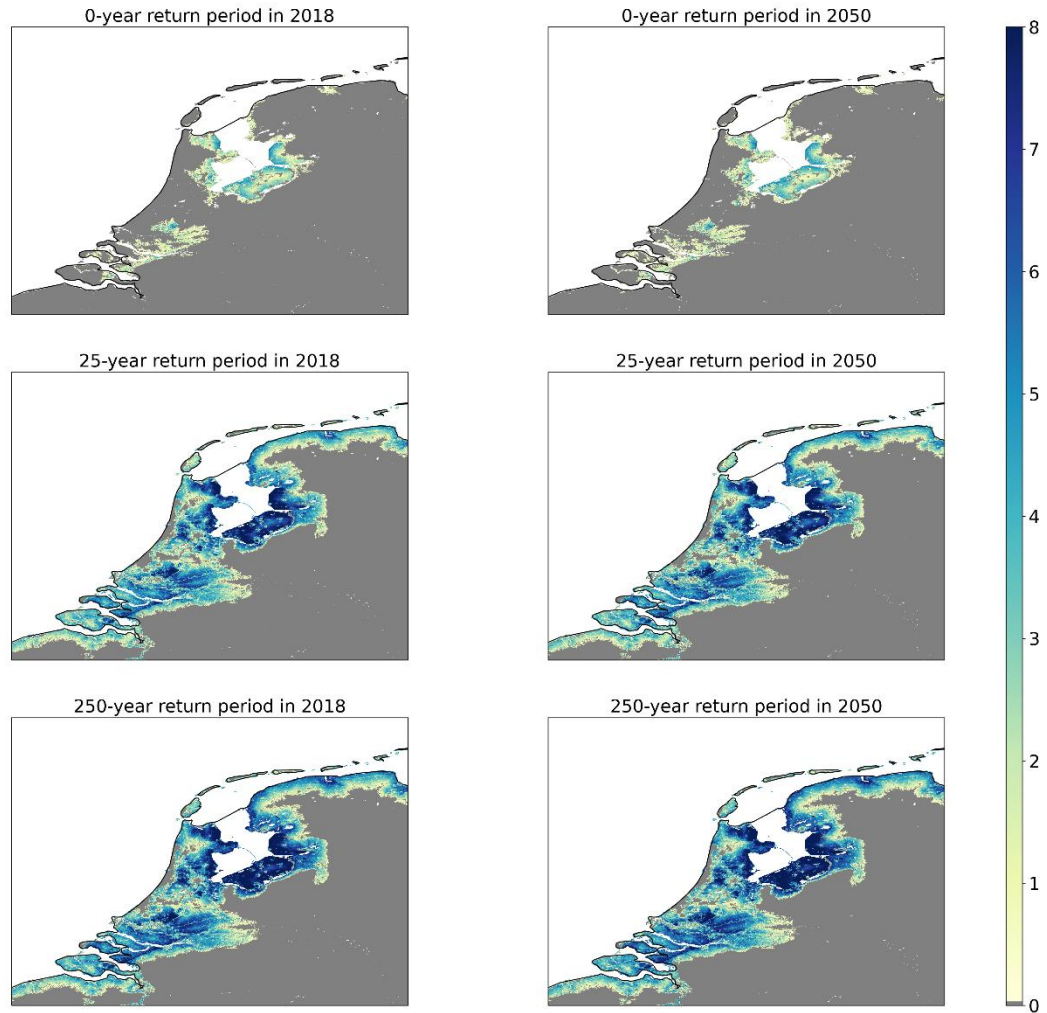


Figure 0-0-8 Inundation depth and extent in the Netherlands with the NASA DEM at 90m resolution

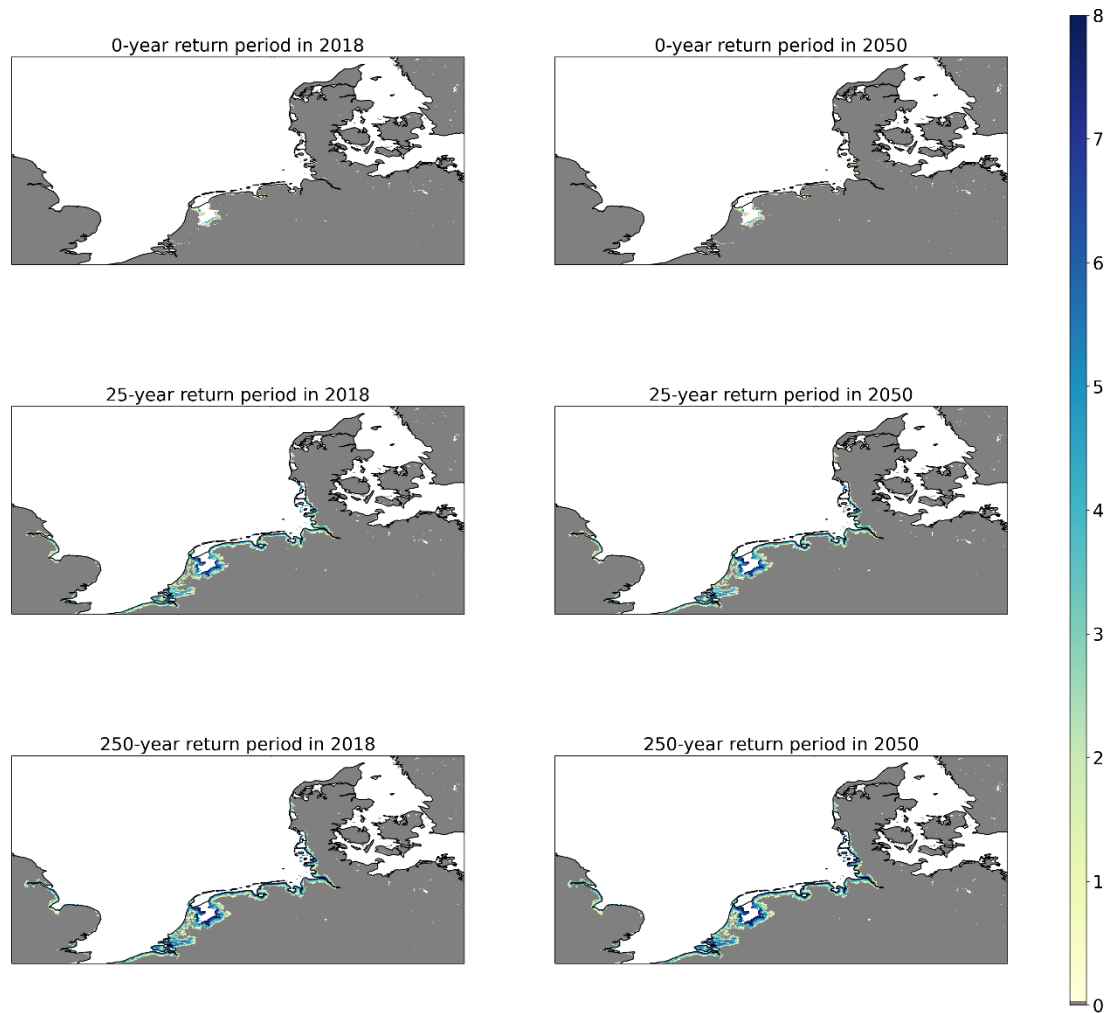


Figure 0-0-9 Inundation depth and extent in Northwestern Europe with the MERIT DEM at 1km resolution

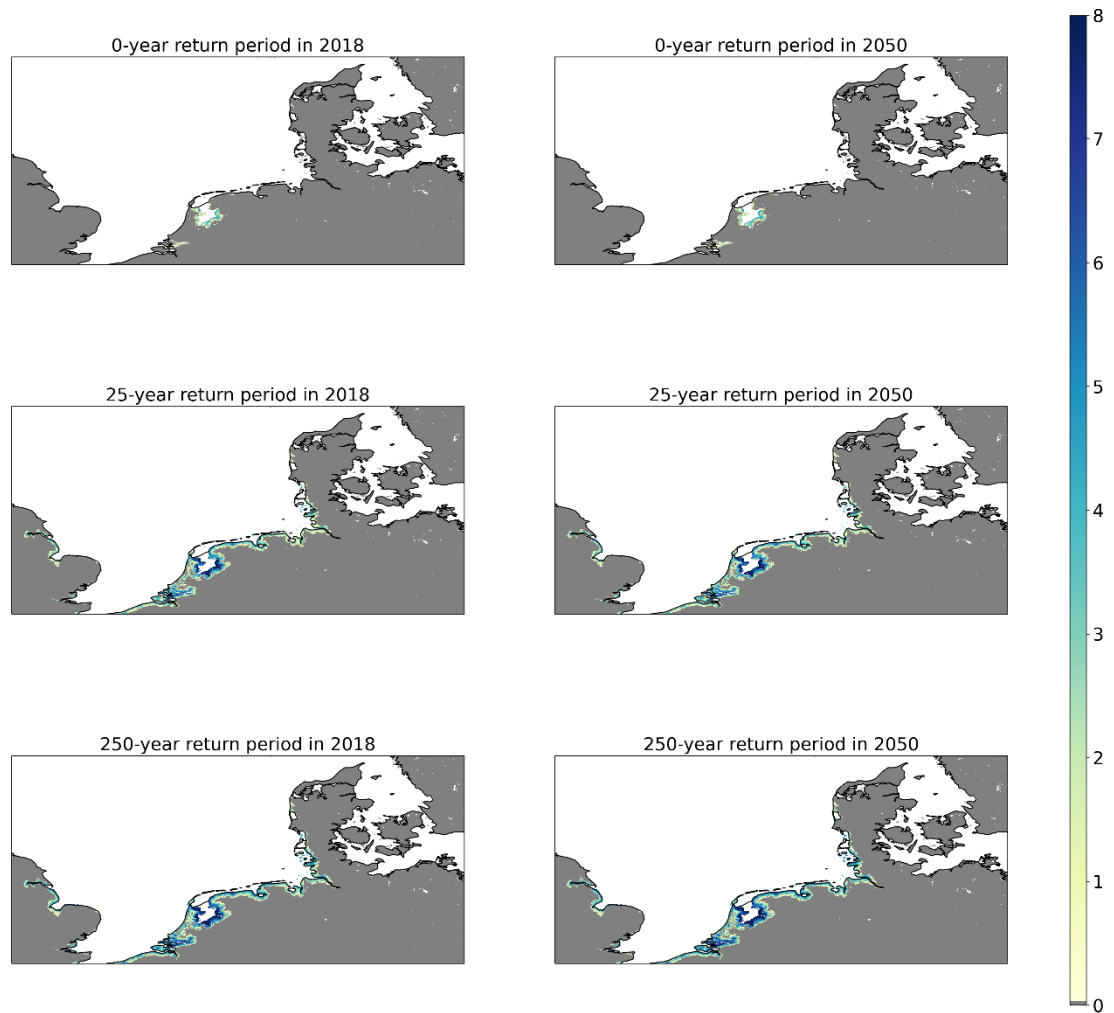


Figure 0-0-10 Inundation depth and extent in Northwestern Europe with the NASA DEM at 1km resolution

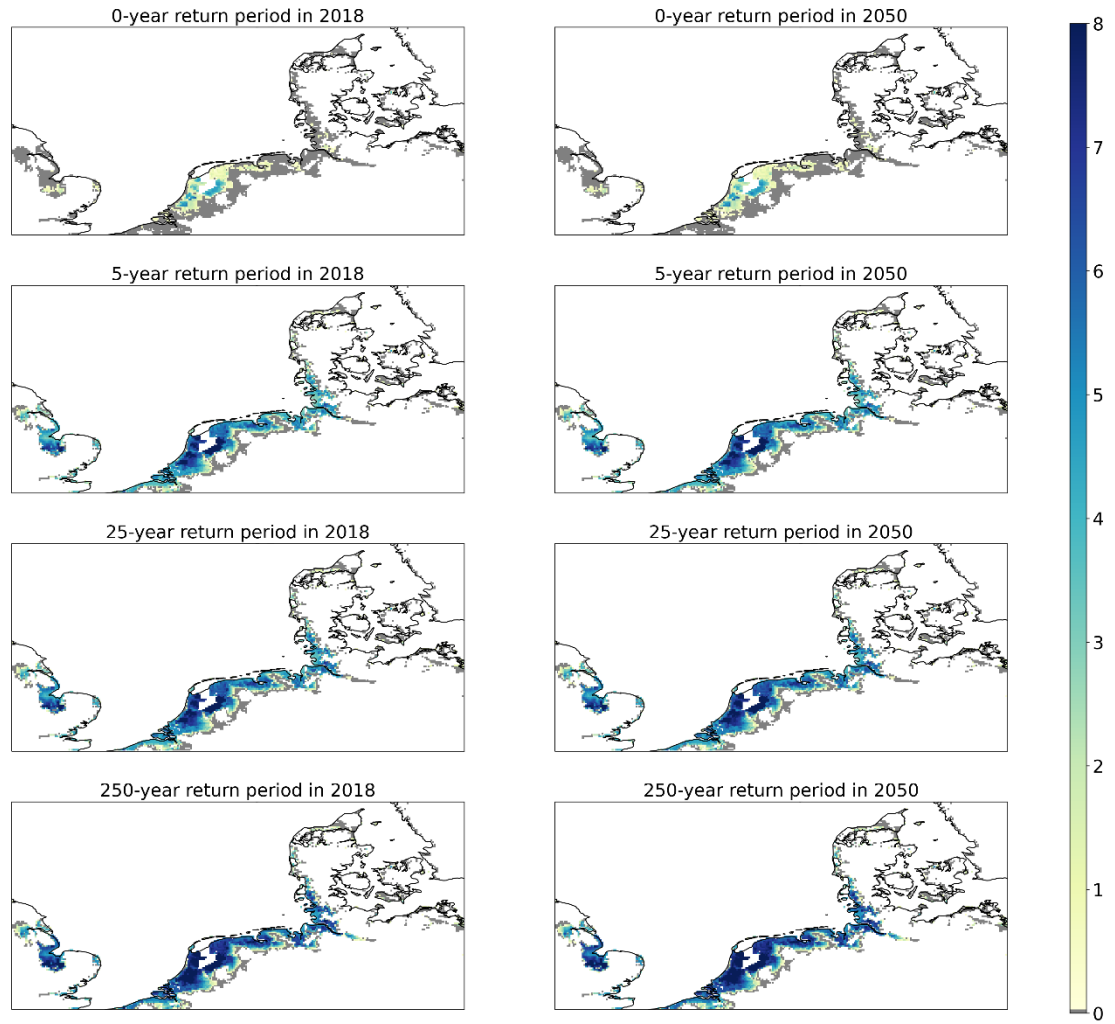


Figure 0-0-11 Inundation depth and extent in Northwestern Europe with the LIDAR DEM at 5km resolution

C.2 Gulf of Thailand

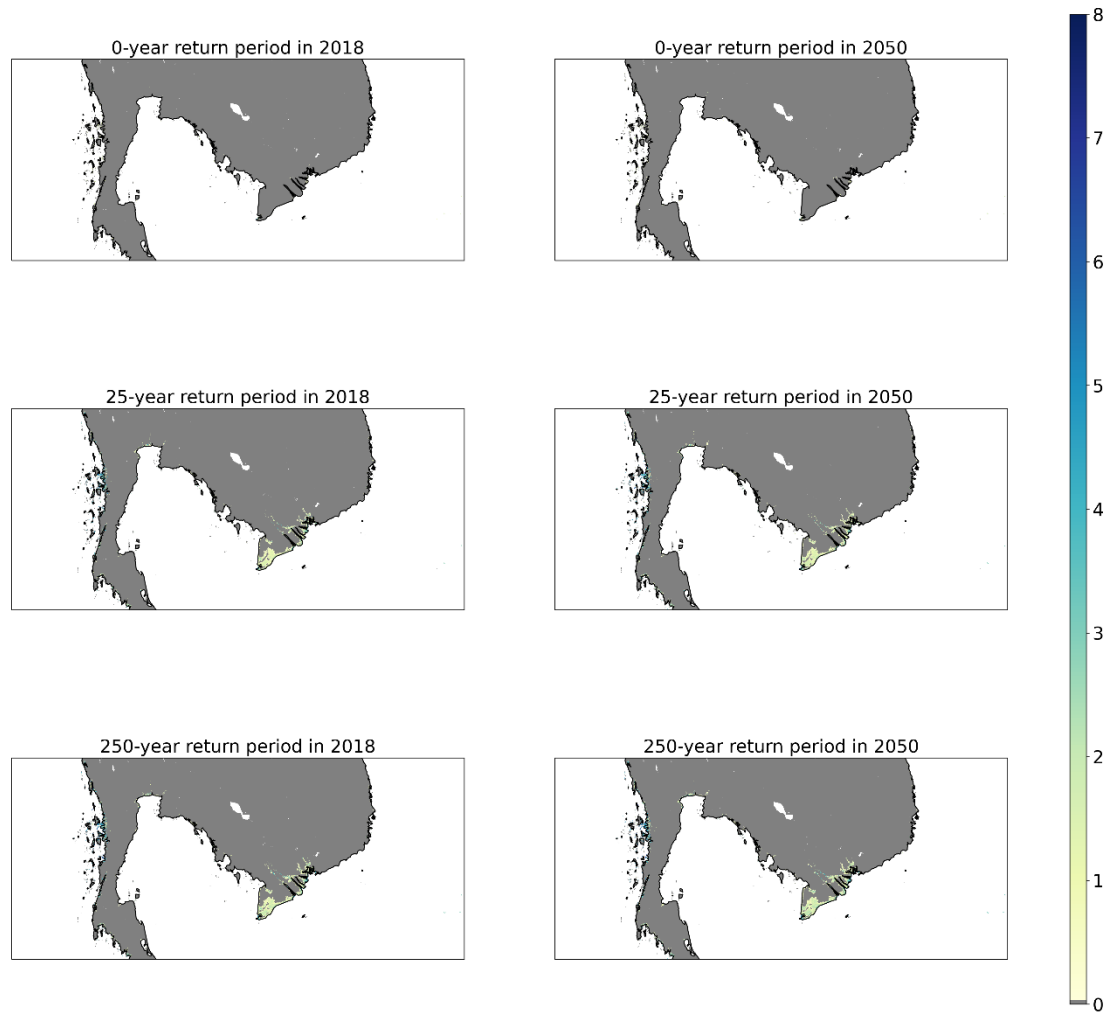


Figure 0.-0-12 Inundation depth and extent in the Gulf of Thailand with the MERIT DEM at 90m resolution

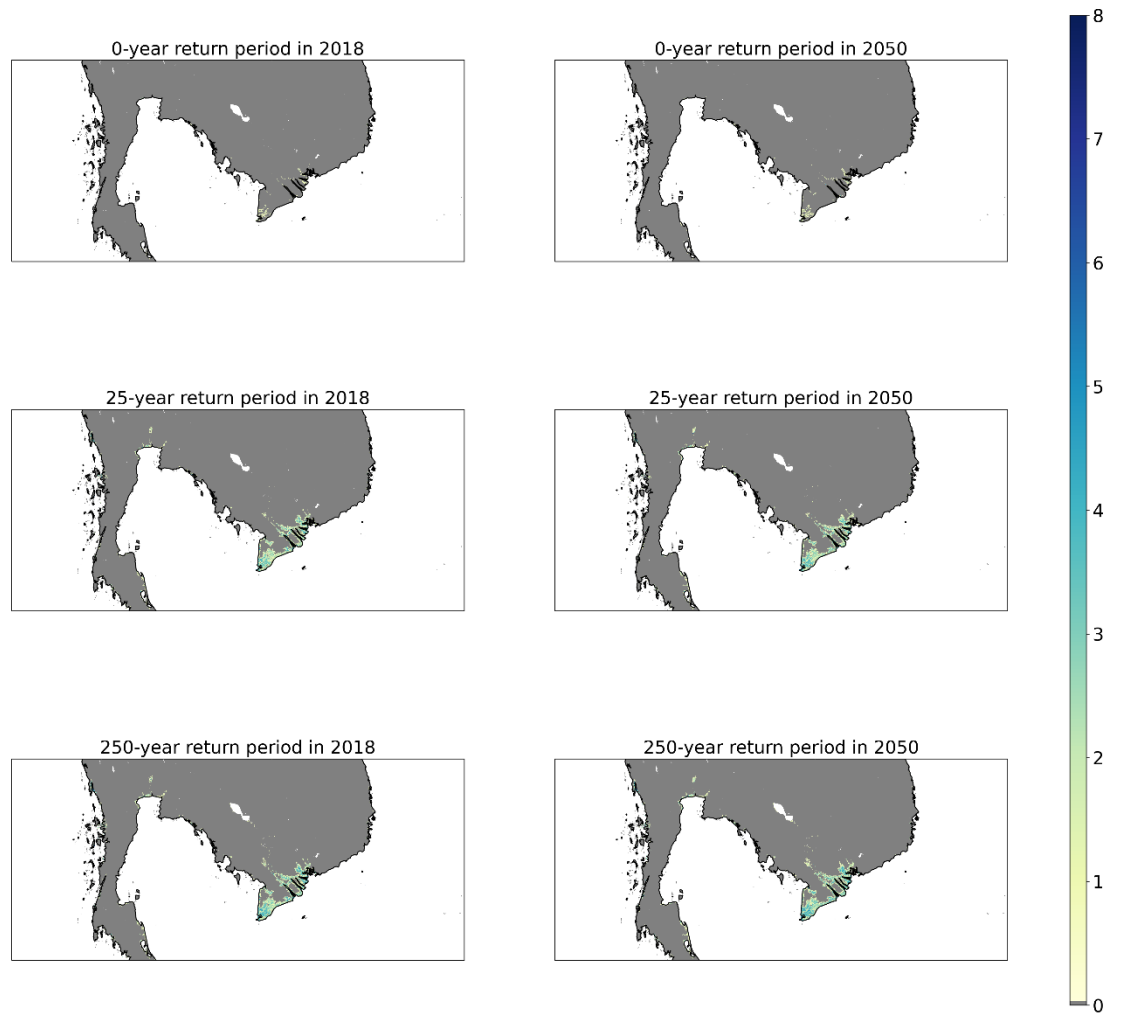


Figure 0-0-13 Inundation depth and extent in the Gulf of Thailand with the NASA DEM at 90m resolution

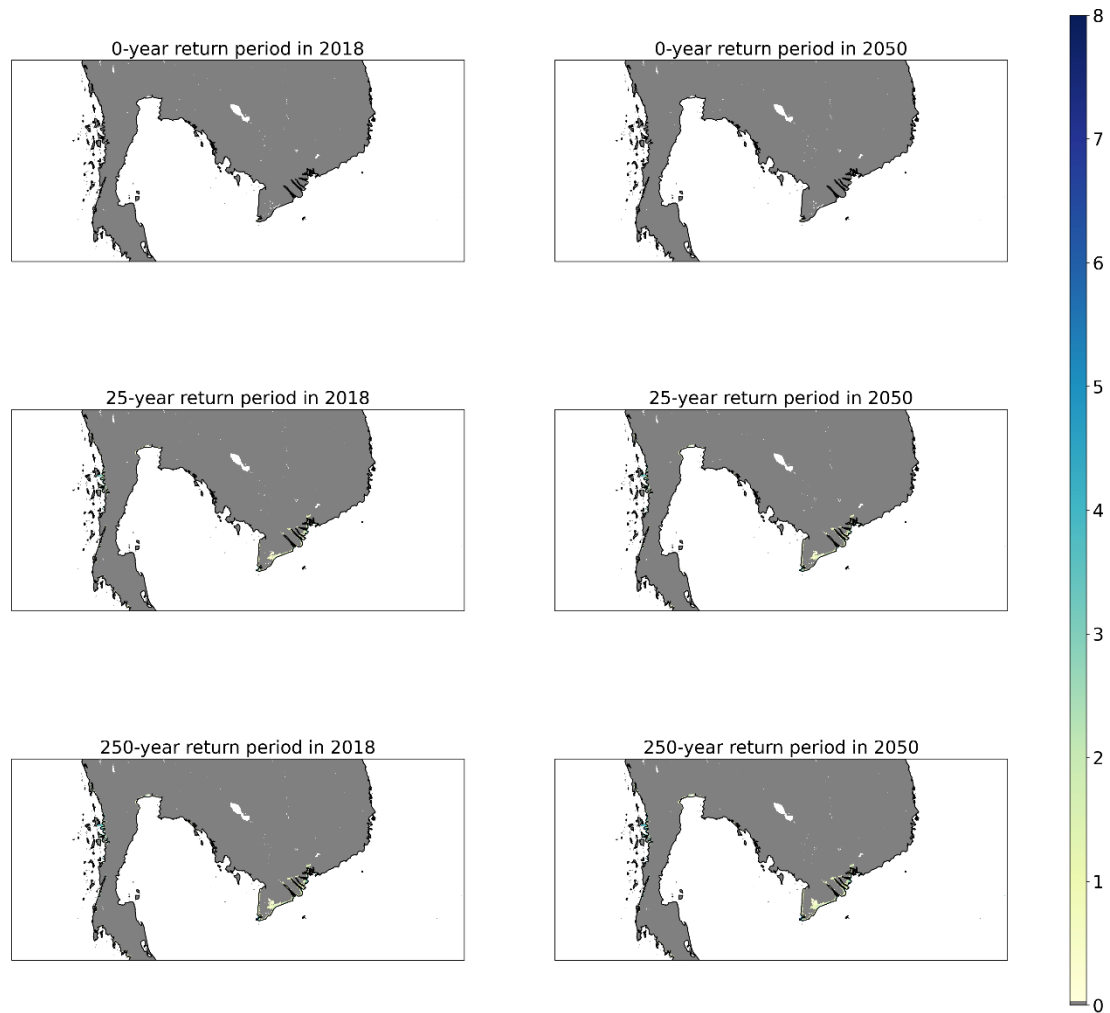


Figure 0-0-14 Inundation depth and extent in the Gulf of Thailand with the MERIT DEM at 1km resolution

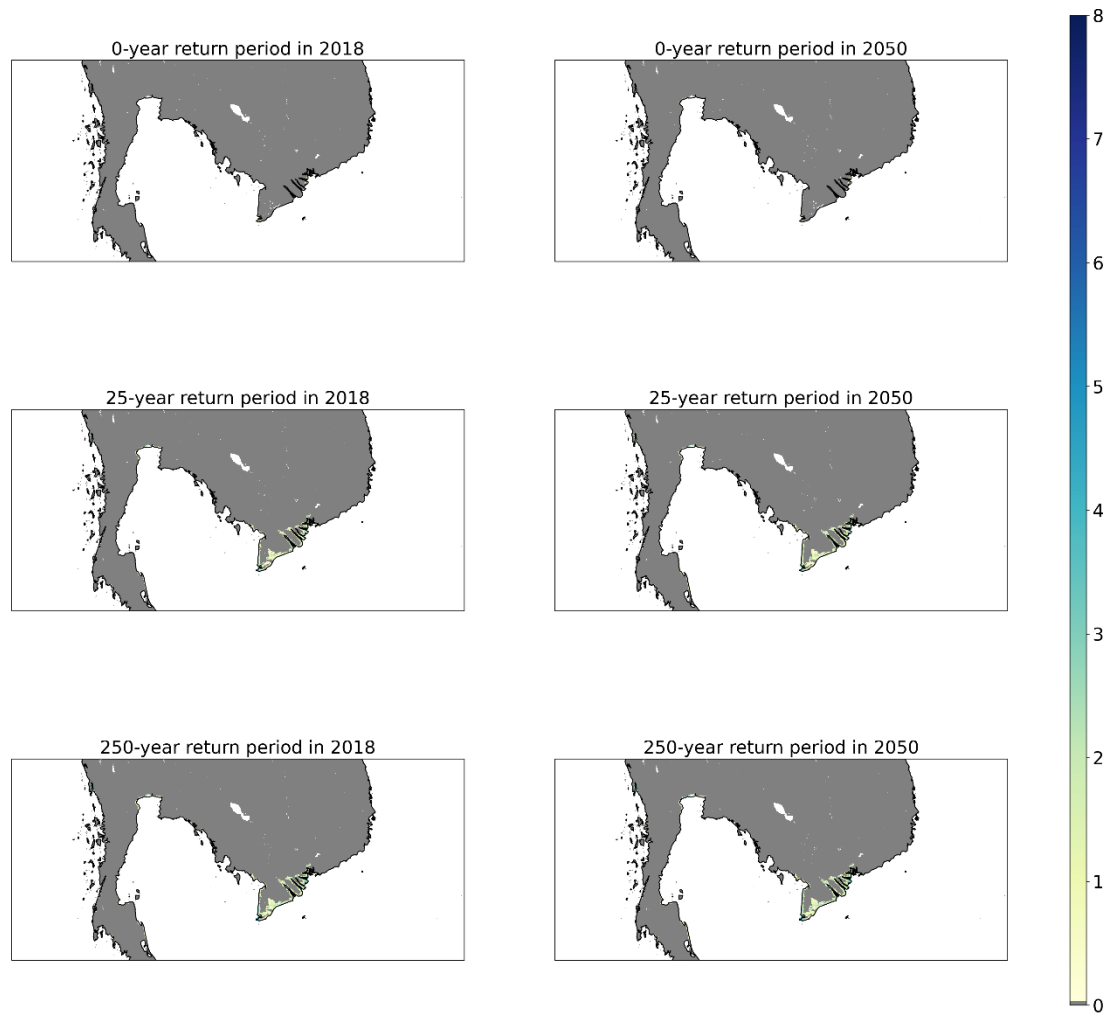


Figure 0.-0-15 Inundation depth and extent in the Gulf of Thailand with the NASA DEM at 1km resolution

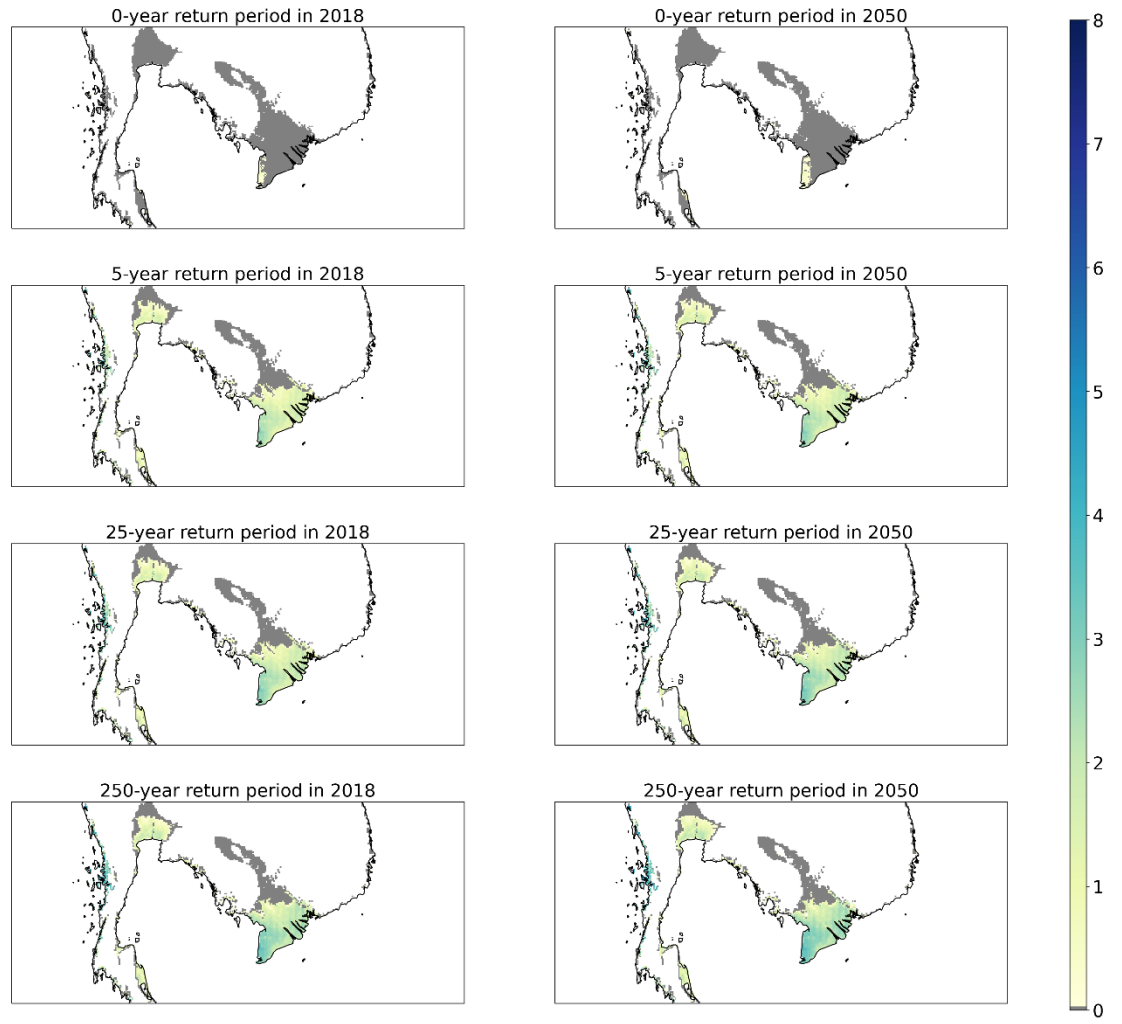


Figure 0-0-16 Inundation depth and extent in the Gulf of Thailand with the LIDAR DEM at 5km resolution

C.3 Bay of Bengal

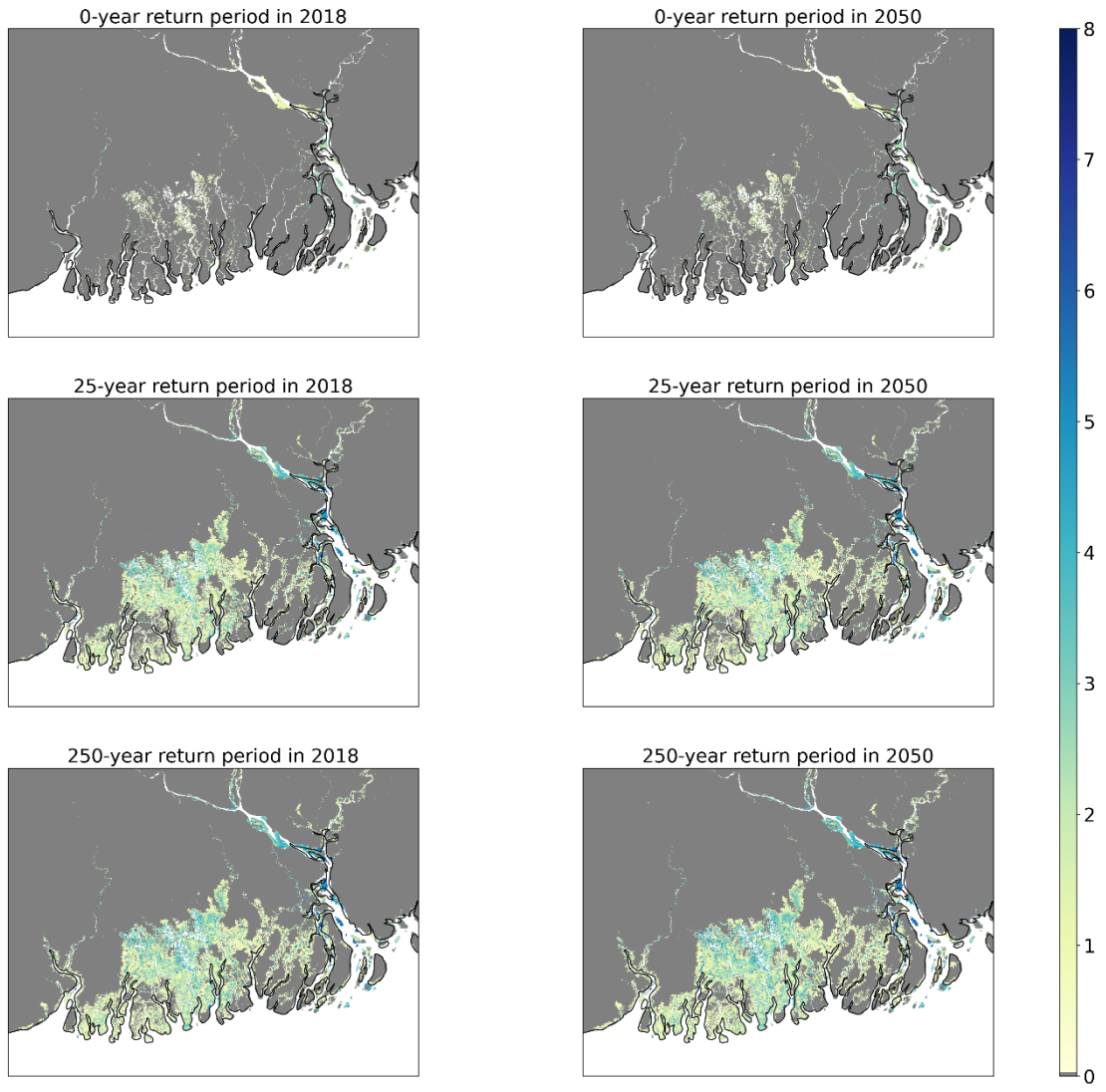


Figure 0-17 Inundation depth and extent in Bangladesh with the MERIT DEM at 90m resolution

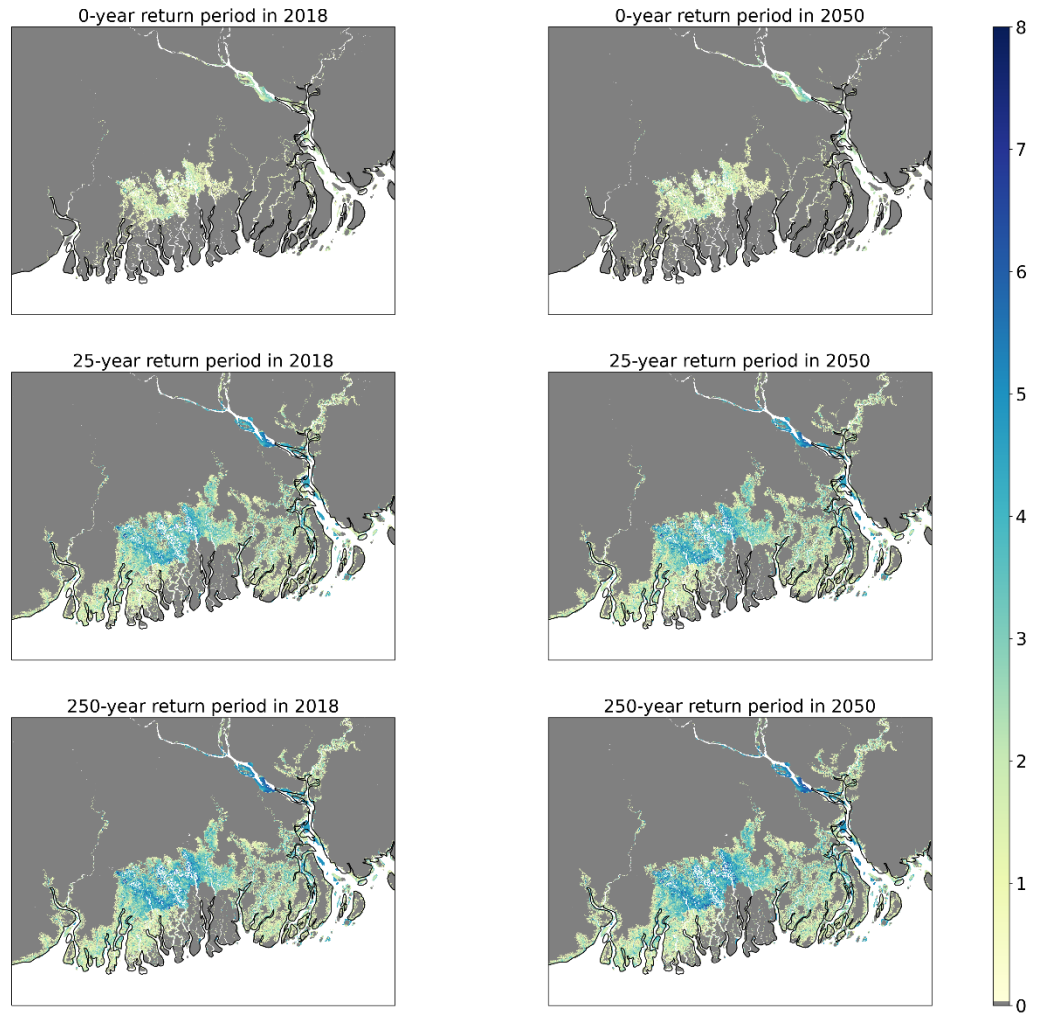


Figure 0-18 Inundation depth and extent in Bangladesh with the NASA DEM at 90m resolution

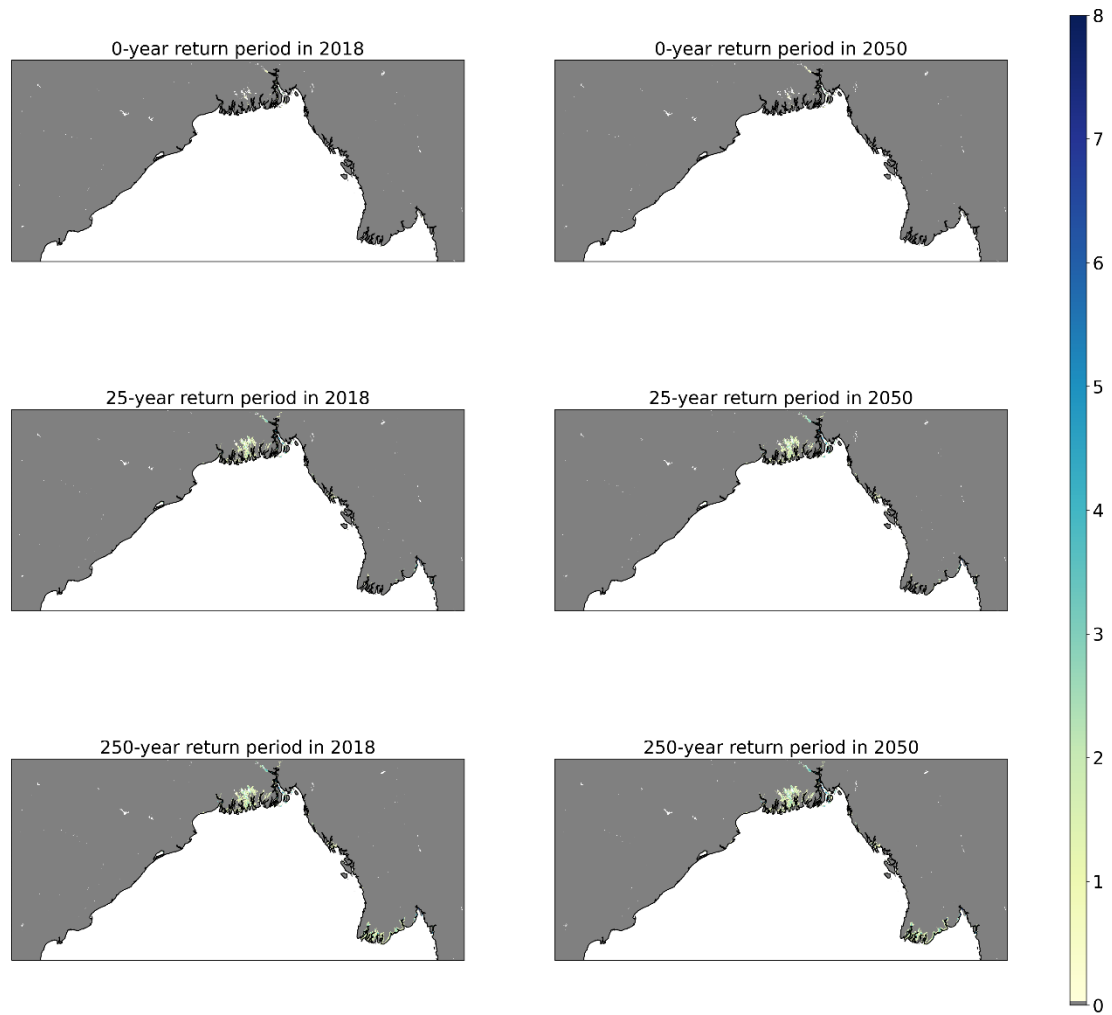


Figure 0-19 Inundation depth and extent in the Bay of Bengal with the MERIT DEM at 1km resolution

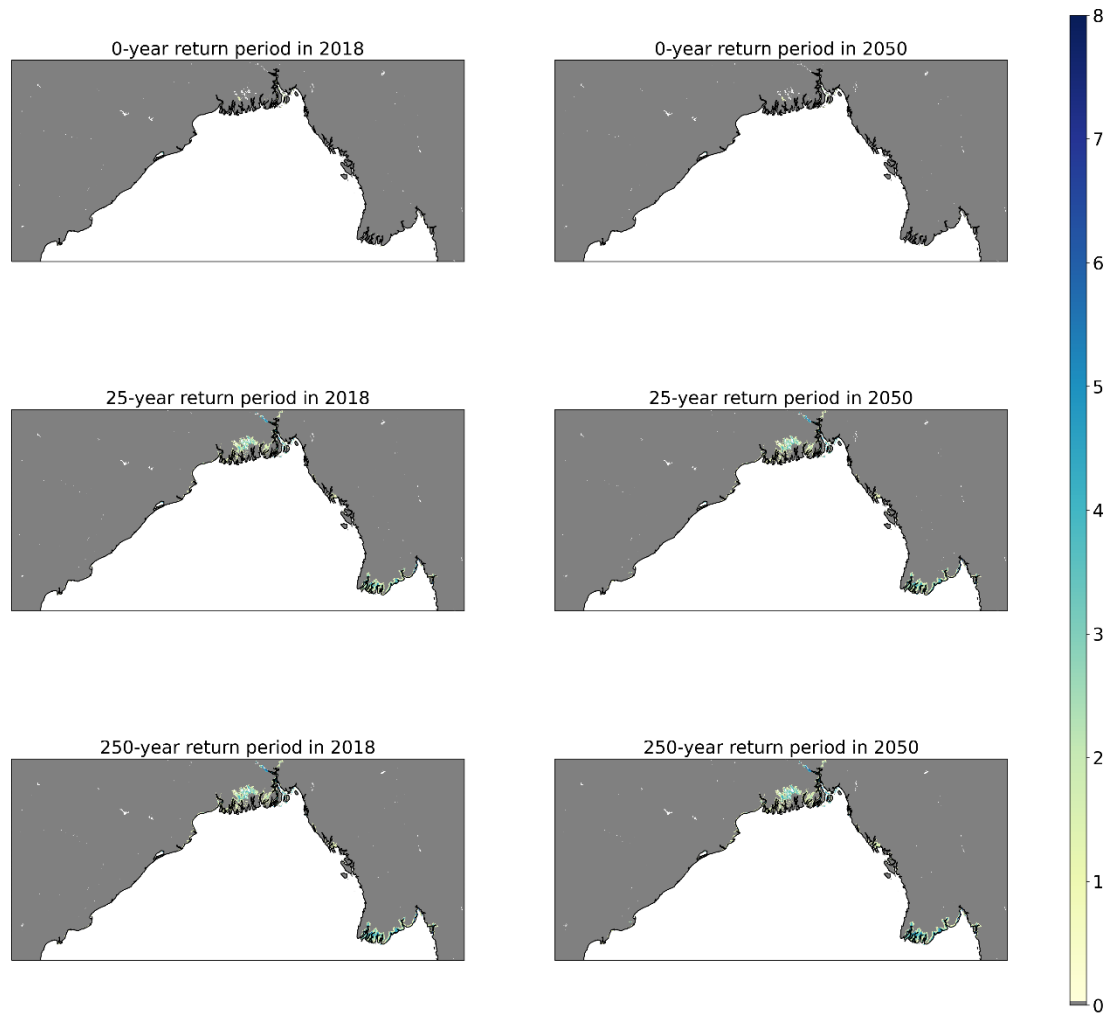


Figure 0-0-20 Inundation depth and extent in the Bay of Bengal with the NASA DEM at 1km resolution

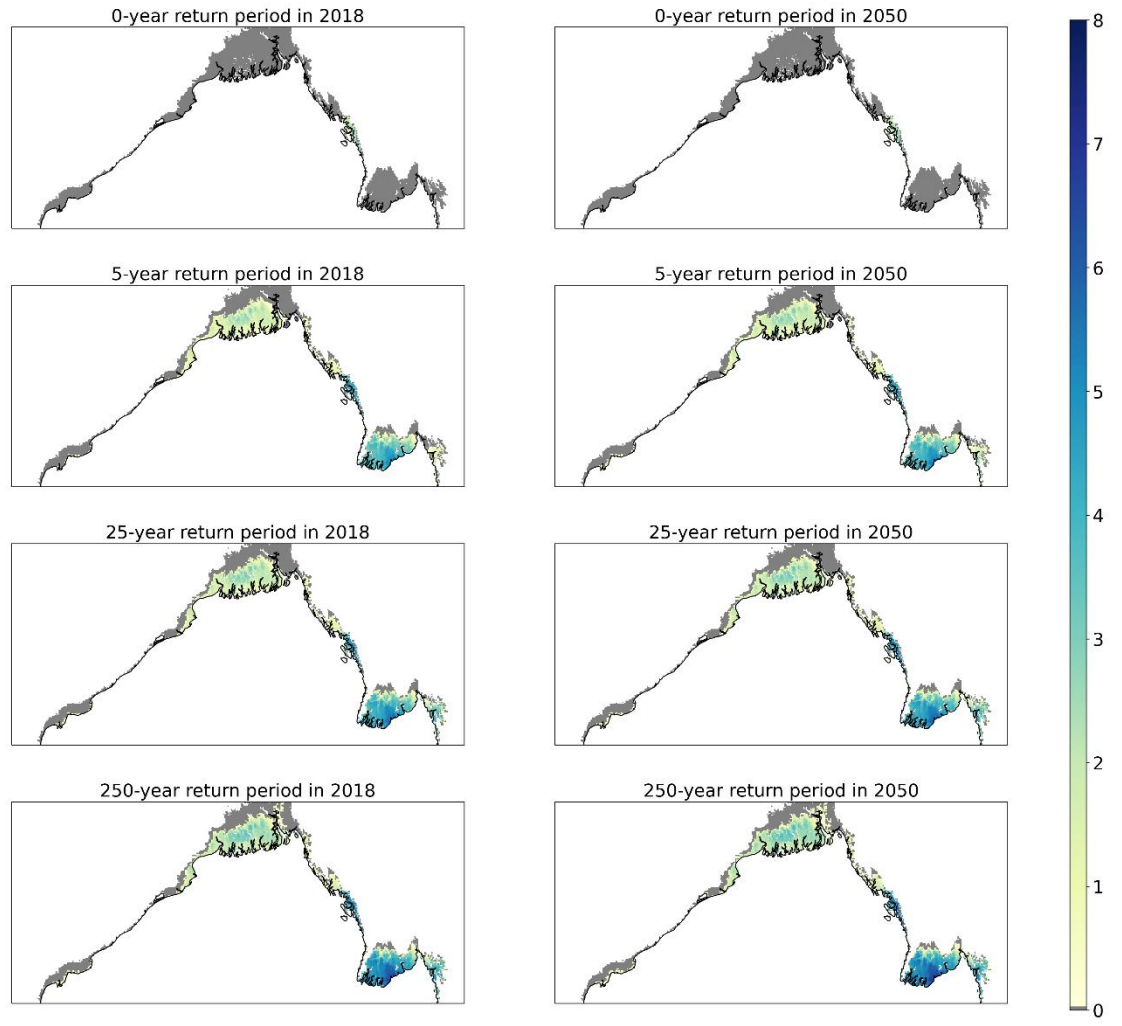
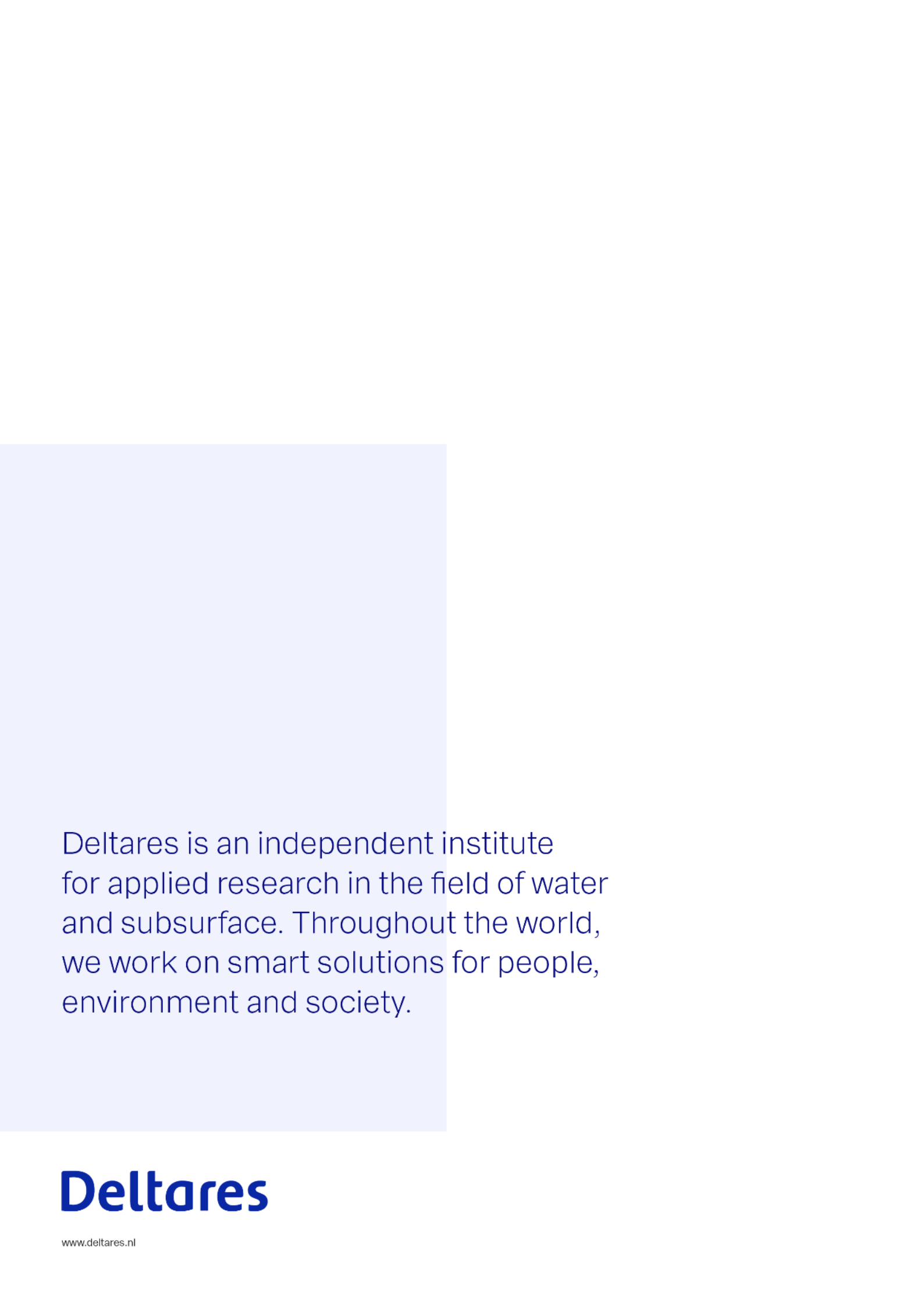


Figure 0-0-21 Inundation depth and extent in the Bay of Bengal with the LIDAR DEM at 5km resolution



Deltares is an independent institute
for applied research in the field of water
and subsurface. Throughout the world,
we work on smart solutions for people,
environment and society.

Deltares